UNIVERSITY OF BIRMINGHAM

Novel Metal-organic Frameworks with Naphthalene-diimide Based Linkers

by

MUSA MUHAMMAD MAHMUD

A thesis submitted to the University of Birmingham for the degree of

DOCTOR OF PHILOSOPHY

School of Chemistry

College of Engineering and Physical

Science University of Birmingham

January 2024

Dedication

To my dearly departed parents, Mallam Muhammad Mahmud and Hajja Maryam Ahmad, who are no longer with us. My success has been built on your everlasting love, support and direction. I dedicate this thesis to you with eternal gratitude and love. Your memory continues to inspire and motivate me every day.

Abstract

A naphthalene diimide-based ligand (DNNDI) was used to create novel lanthanide metal-organic frameworks (MOFs). The lanthanide metals used were Yb(III), Y(III), Lu(III), Er(III), and Sm(III). A simple solvothermal technique was used to create each MOF, and FTIR, SCXRD, PXRD, TGA, SEM, and UV-Vis spectroscopy were used to characterize them. All the frameworks crystalised in a similar tetragonal crystal system $I4_1/a$ space group or monoclinic space group and are isostructural being built from similar rod SBUs linked by the naphthalene-diimide-based ligand. The secondary building units (SBUs) consist of M-O-C rods and MO_8 polyhedra. The pyridyl nitrogen of the nicotinic acid moiety was found to be uncoordinated, providing opportunities for post-synthetic alteration of the MOFs. Host-guest studies encapsulating molecules of phenothiazine and ferrocene were synthesized, characterized and reported. Additionally, a mixed metal MOF with DNNDI linkers and the first, medium and last member of the lanthanide series (La(III), Gd(III) and Lu(III)) were synthesized and characterized by the same techniques as with the single metal lanthanide MOFs reported.

Acknowledgment

Alhamdu Lillah! Many individuals contributed to the success of this thesis. Above all, I would like to take this opportunity to thank Professor Neil R. Champness for his meticulous supervision of this research as well as for all of his support, encouragement, advice, and understanding over the last four years. Your steadfast assistance has been my driving force in pursuing this field of inquiry that piqued my interest. Special thanks go to my sponsor, the Petroleum Technology Development Fund (PTDF) for funding this work.

It has been a great honour and privilege to work with several excellent scientists, especially Dr. Georgia Orton, for taking the time to teach me working in the Laboratory and a lot more too numerous to mention, Dr. Sarah Griffin, and Dr. Nicholas Pearce, you have been beneficial in countless ways. I appreciate and enjoy the sense of community among our group members back in Nottingham, especially with people like Dr Joseph Ogar and here in Birmingham. My sincere appreciation to Dr Josh, Dr Louise, Mr Trevor and Dr Ludwig for taking me through various analytical techniques useful for this research and beyond.

Finally, to my caring, loving and supportive wife, Aisha and sons, Jawad and Mahdi, I say thank you for your unwavering support, commitment and sacrifice throughout the period of my academic journey.

Abbreviations

PCP	Porous Coordination Polymer
MOFs	Metal-Organic Framework
L-N	Lanthanides
DNNDI	Dinicotinic Naphthalenediimide
DMF	N, N-Dimethylformamide
SEM	Scanning Electron Microscopy
EDX	Energy Dispersive X-ray
NMR	Nuclear Magnetic Resonance
FTIR	Fourier Transform Infrared Spectroscopy
UV-Vis	Ultraviolet-Visible Spectroscopy
PT@MOF	PT@MOFs
Fc@MOF	Ferrocene MOF
LAG	Liquid-Assisted Grinding
EPR	Electron Scanning Microscopy
SBU	Secondary Building Block
PXRD	Powder X-ray Diffraction
SCXRD	Single Crystal X-ray Diffractometer
TGA	Thermal Gravimetric Analysis

BET	Brunauer-Emmett-Teller
NTCDA	1,4,5,8-Naphthalene dianhydride

Table of Contents

Chapter one

1.0 Introduction

1.1 Porous crystalline material

Because of their beneficial applications, porous crystalline materials (pcm) are of great scientific interest. These materials are one of the most extensively used groups of solids for several applications such as separation, adsorption, ion exchange, and catalysis.[1] According to the International Union of Pure and Applied Chemistry (IUPAC), porous materials can be classified into three different groups – microporous having less than 2 nm pore diameters, mesoporous with pore diameters between 2 – 50 nm and macroporous having pores larger than 50 nm.[2–5] Nanoporous materials are, however, those porous materials whose pore diameters are less than 100 nm. Research in this area of porous materials is developing rapidly producing a lot of new different materials, characteristics, and applications that are recognized and improved on a daily basis.[6] Microporous materials are sometimes considered to be crystalline frameworks whose materials possess channels and cavities of molecules in a huge range of sizes with narrow pore sizes.[7] Microporous solid materials can be comprised of a range of components and are generally categorized as porous organic, inorganic or organic/inorganic hybrid materials.[8] One of the most common classes of crystalline porous inorganic solids is zeolites, often referred to as molecular sieves, which are crystalline solid materials or structures made of aluminium, oxygen, and silicon. Zeolites form a framework with channels and cavities, in which small molecules can be accommodated, and zeotype, have pores ranging from 0.4 to 1.3 nm. Zeolites occur usually as natural minerals, but a wide variety of synthetic zeolites have also been reported and used in various applications including for industrial purposes, such as catalysis and xylene isomerization.[9–11] Another property of zeolites is ion exchange which

allows them to be used as detergents and water softeners.[12,13] Different zeolite-like materials have been extensively studied, including materials comprising arsenates, aluminophosphates, or zinc phosphates.[14,15] (Whereas organic porous materials primarily comprise amorphous polymers or fragment, COF or molecular cages.) Porous organic-inorganic hybrid materials include metal-organic frameworks (MOFs) as shown in Fig. 1.1 below:

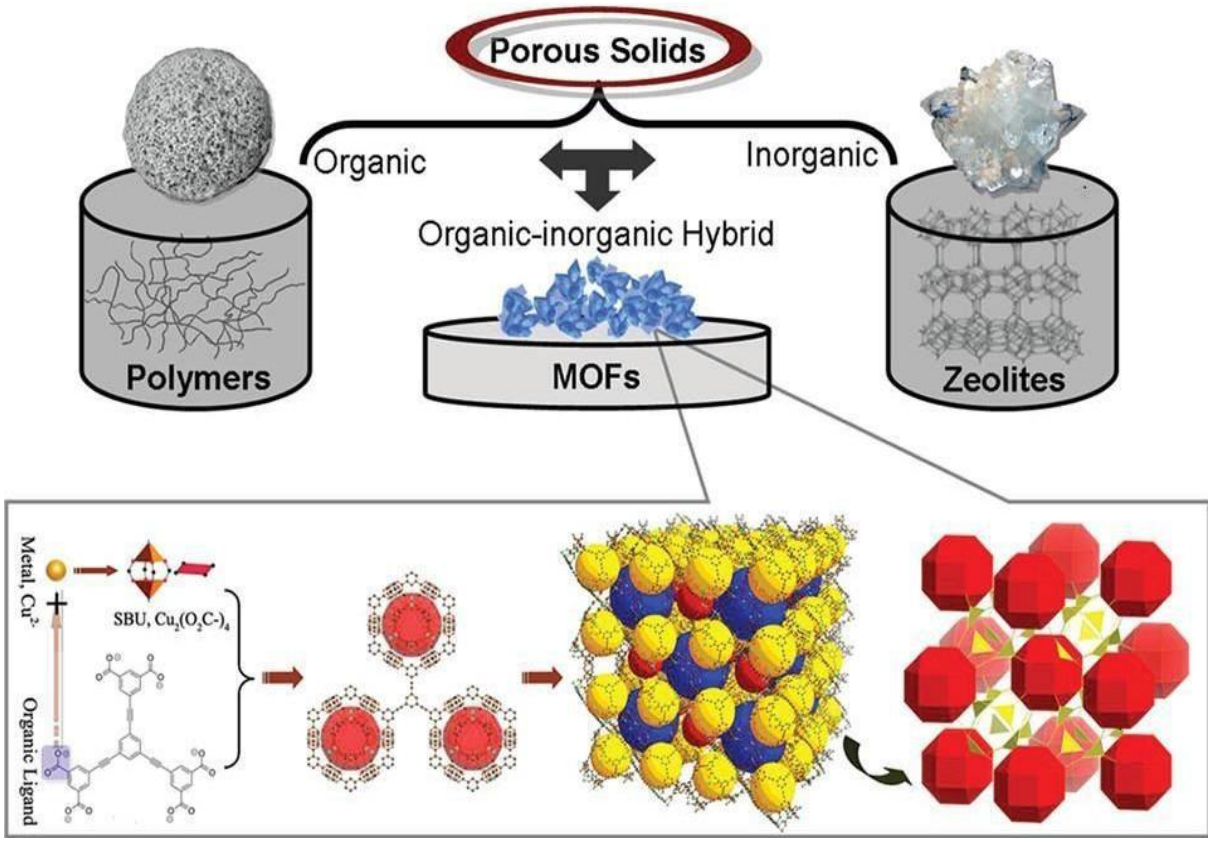

Fig: 1.1 Depiction for General Classification of Porous Solid Materials[16]

1.2 Metal-organic Frameworks (MOFs)

Metal-organic frameworks (MOFs), or porous coordination polymers, (PCPs) are class of porous materials formed through the self-assembly of metal-ligand coordination bonds to create extended networks. These materials are composed of metal atoms or clusters (also known as Secondary Building Units or SBUs) and bridging ligands (also referred to as organic

linkers). MOFs are porous or glassy crystalline materials in which the metal is locked into a position to give highly rigid geometries, joined via different organic groups. MOFs are known to exhibit structural flexibility, large surface areas, and tailorable pore size which allows MOFs to have applications in the fields of gas adsorption and storage, separation, catalysis, sensing, molecular recognition, drug delivery, non-linear optics, luminescence, etc.[17–20] MOFs are useful materials for the storage, separation, or conversion of small molecules due to three-dimensional tunable pores[21,22] and hence much attention is given to this area of study.[23] In terms of gas adsorption, a considerable number of MOFs have been reported that have shown specific selectivity and significant capacity.[24–26] Interestingly, MOFs tend to have the potential for more structural flexibility in terms of rational design via control of the architecture and functionalization of the pores than the conventionally used microporous inorganic materials like zeolites.[27] Different metal ions and oxidation states bring varying structural geometries[28] allowing the construction of a near-infinite library of framework structures and topologies. In addition, the viability for post-synthetic modification of these hybrid materials provides further opportunities to access many other novel architectures.[29–31] Figure 1.2 illustrates the building blocks of metal-organic frameworks whereby metal ions are connected to organic ligands, thus forming the framework structure.[32]

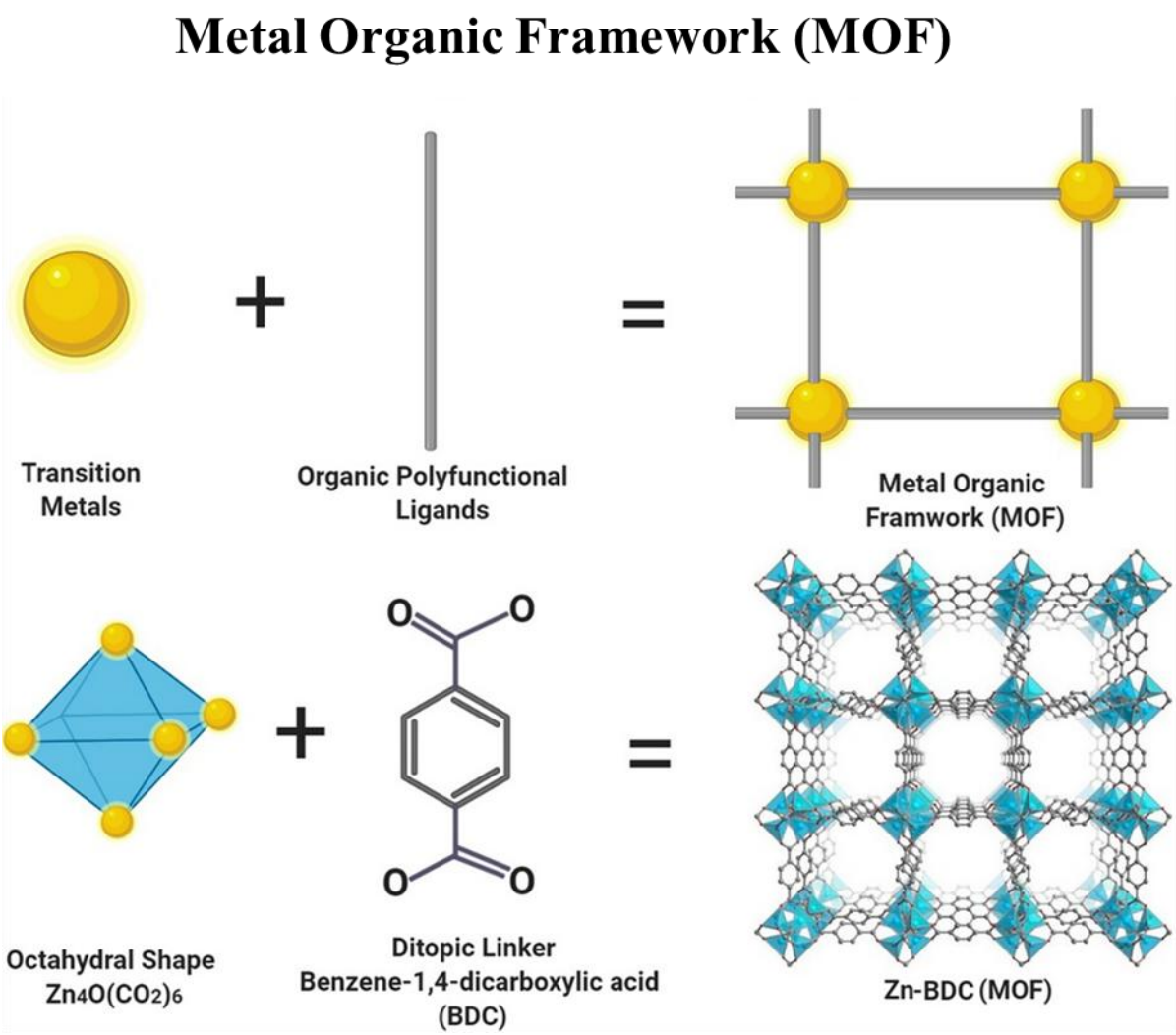

Figure 1.2: Illustrates potential building blocks of Metal-Organic Frameworks.[32]

As far back as 1965, three decades before the advent of what are nowadays categorized as MOFs, Tomic in his first publication on novel solids presented these materials, which he called supramolecular structures or coordination polymers,[33] adding that, these frameworks were formed by bonding bi- to tetravalent aromatic carboxylates with metals like aluminum, iron, nickel, thorium, uranium, and zinc. Features of special interest such as high metal content and thermal stability have also been investigated.[34] In 1989, Hoskin *et al.* proposed this class of inorganic material when they described the synthesis and structure of "the first example of a

deliberately designed and constructed infinite framework". Cu(I) centres were linked with 4,4',4'',4'''-tetracyanotetraphenylmethane (TCTPM), generating a network with a diamondoid topology.[35] A tetrahedral geometry was adopted by both the metal ion and tetratopic organic ligand as shown in Figure 1.3

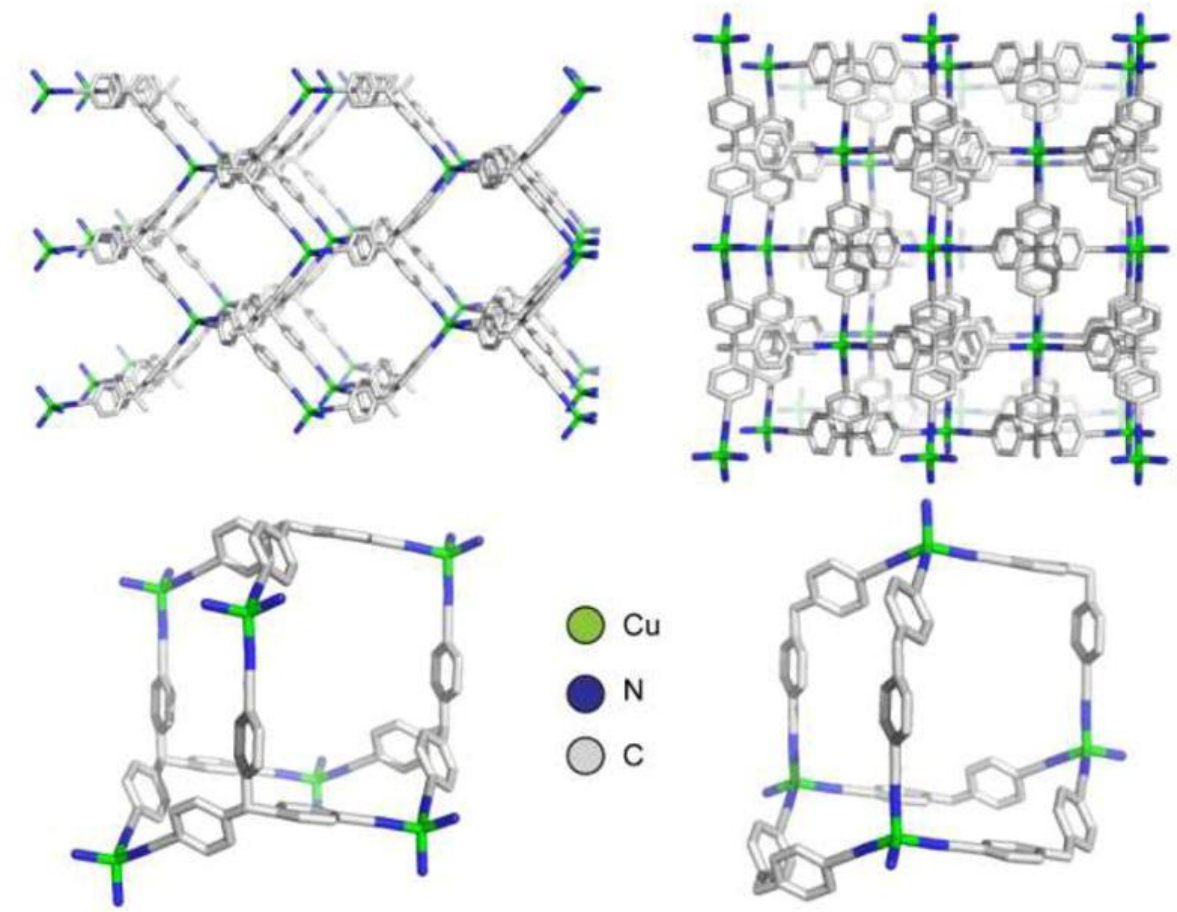

Figure 1.3 Illustrates ''the slow evaporation of a solution of a tetranitrile ligand with a Cu(I) precursor deposits a coordination polymer containing tetrahedral metal nodes with tetrahedral tetratopic spacers. Two views are shown (top) with hydrogen atoms omitted for clarity revealing a diamond-like network comprised of repeating adamantanoid units (bottom).''[36]

Following the seminal works exploring this type of material by Yaghi and co-workers in 1995 at Arizona State University,[37] research in the field of metal-organic frameworks or MOFs has continued to grow with no bounds but a "seemingly ever-increasing level of attention[38] from

different researchers across the globe making prodigious numbers of publications. Much attention has been given to the area of study and yet the field continues to boom, for example in 2010, there were over 30,000 scientific articles on MOFs published that year, this is a watershed for a new field that had started in earnest some 25 years back now.[38] By 2020, this number had surpassed 90,000 reflecting the broad interest and continued innovation in the field.

Since then, this area of research has become a subject of inquiry among active researchers with a huge number of MOFs being widely studied for various applications such as adsorptive removal of numerous toxic environmental contaminants, pollutants, surface charge, pore geometry, and ultra-high porosity are some of the characteristics that have made these applications and uses achievable.[39]

1.2 Definitions

1.2.1 Primary Building Block

The primary building units (coordination spheres) used in the formation of metal-organic frameworks are the nodes (metal ions) and organic compounds. The former connects, in a self-assembly process, to the organic molecules which also act as linkers. This process can result in the formation of porous three-dimensional structures, MOFs. Thus, in MOF synthesis, the organic compounds and metal ions are the primary building units. The metal ions that serve as connectors in the MOF synthesis are usually the first-row transition series including $Zn^{2+,}$ $Cr^{3+,}$ $Co^{2+,}$ alkali metal ions, alkali earth-metal ions, rare earth-metal ions and lately lanthanides metal ions. However, the precursors for preparing MOFs in many of the synthetic routes are sulfate, acetate, chloride, nitrate and oxides of metals while metal rods are used in the electrochemical synthesis of MOFs. Functional groups that are capable of forming coordination

bonds, such as amines, nitriles, sulfonates, phosphates and carboxylates, are generally contained in the organic linker through which the nodes and the metal ions are connected.[40]

1.2.2 Secondary building block

Secondary building units (SBUs) are complex substructures of MOFs that can be abridged by the classification of their simplest replicating inorganic unit. As an idea, the term was espoused from zeolite chemistry to predict the structure of MOFs. SBUs are termed as polynuclear clusters with defined geometries which are connected by the organic linkers to form a framework.[41] Figure 1.4 illustrates some commonly found SBUs in metal carboxylate MOFs (a) the triangle, (b) the square paddlewheel, (c) the tetrahedron, (d) the octahedral zinc acetate cluster, and (e) the trigonal prismatic oxo-centered trimer. The SBUs are connected to form the MOF by joining the carboxylate carbons with organic units. They could also be linked by the replacement of terminal ligands.

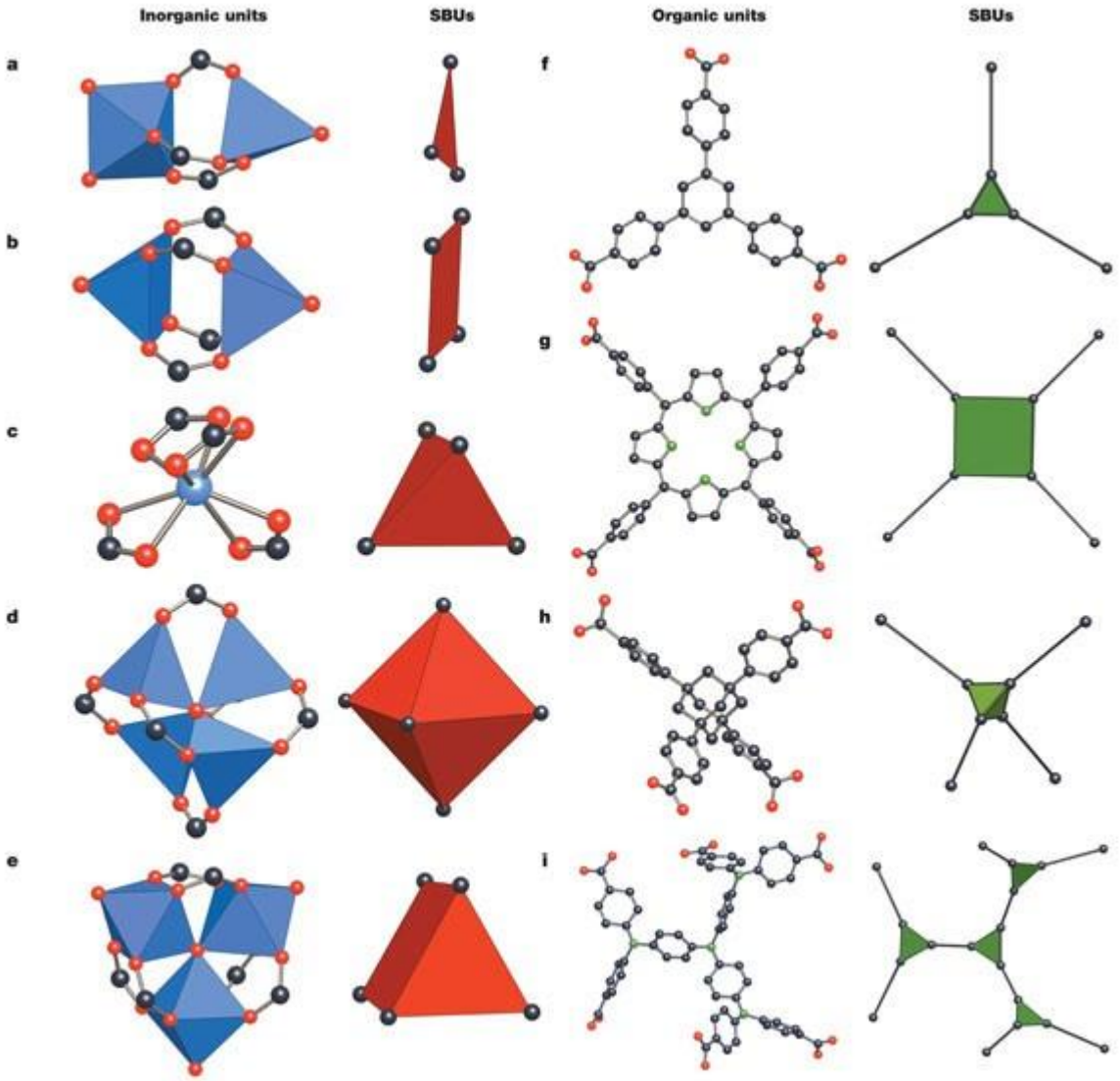

Figure 1.4: Examples of SBUs from carboxylate MOFs. O, red; N, green; C, black in inorganic units, metal-oxygen polyhedra are shown in blue, and the polygon or polyhedron defined by carboxylate carbon atoms (SBUs) are red[42]

1.2.3 Interpenetration

Interpenetration in MOFs is an intriguing, naturally encountered, phenomenon with considerable impact on the structure, porous nature, and functional applications of MOFs.[43] In MOFs, weaving of the multiple lattices with each other is termed interpenetration.[44] Several

techniques may be employed to impede interpenetration as it is conventionally seen as an impediment to permanent porosity. This is because accessibility to the pore of the crystalline material is the major concern when dealing with a porous framework.[45] The system, however, undergoes interpenetration automatically in an attempt to achieve an architecturally stable structure, limiting the much-needed pore space. In contrast, the most common method applied to avert the occurrence of such interpenetration is the construction of steric restrictions by adding bulky moieties or constituents into organic tectons.[45] Furthermore, it is widely reported in many publications that interpenetration is significant in several material properties, principally in the separation of small gas molecules. These types of frameworks have also demonstrated fascinating structural flexibility based on the shearing or movement of the nets.[46] Interpenetration may also be known as entanglement, interlocking, and interweaving. Self-penetration (polyknotting) is another possible phenomenon in coordination polymers. In this process, a single coordination polymer may contain rings through which other components of the same network can pass through. The study of interpenetration in MOF chemistry, with a view to understanding how complex self-assembly processes are designed and predicted, is significant for understanding the properties and application of the corresponding coordination polymer materials. [47–51]

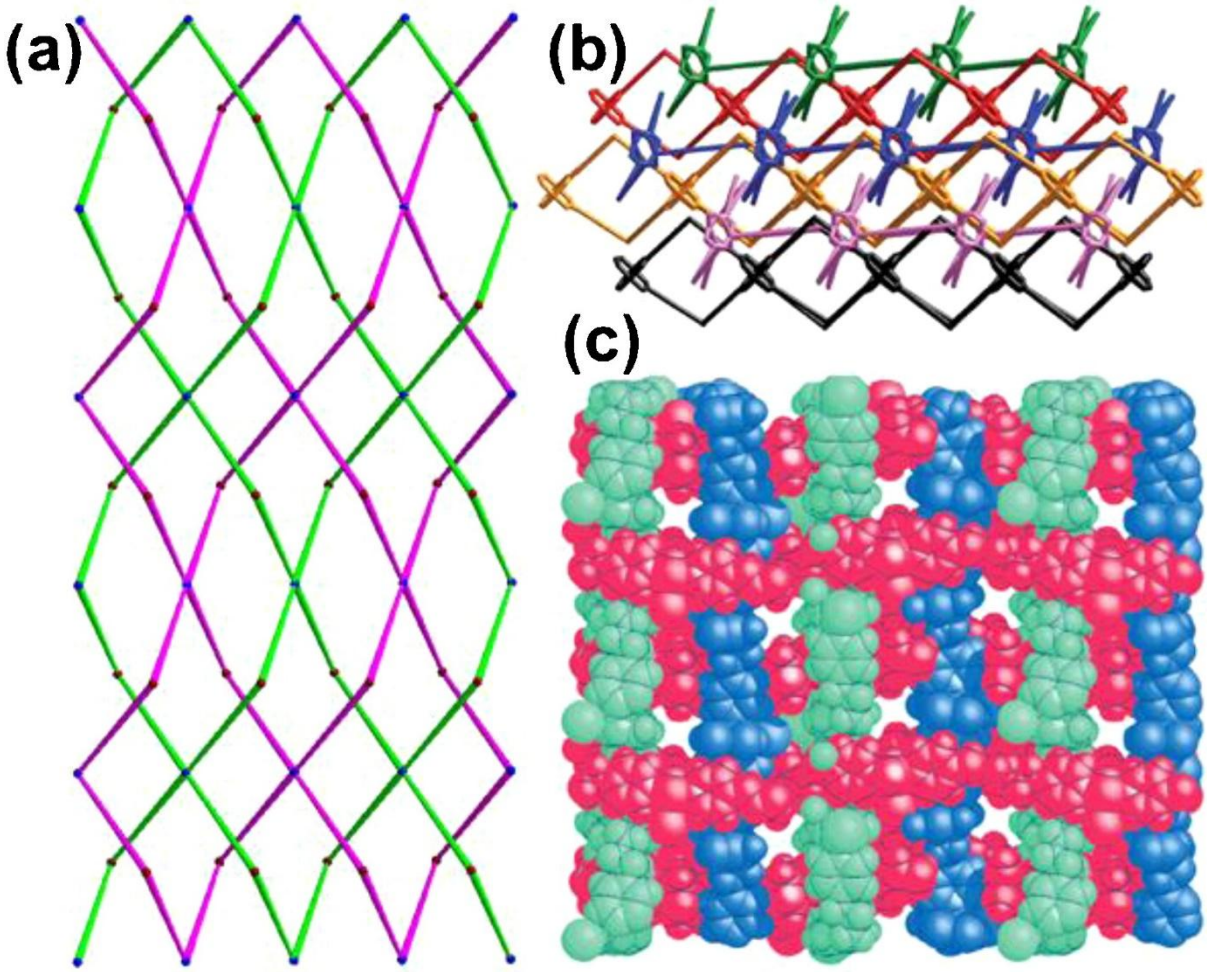

Figure 1.5: (a) Schematic representation of the 2-fold parallel interpenetration between 2D layered structures. (b) Side-on view of the 3-fold parallel interpenetration from 2D to 3D. (c) View of the 3D array fabricated by the interpenetration of the three sets of layers with different colours down the *a*-axis.[52]

1.2.4 Isorecticular MOFs

Isoreticular MOFs are frameworks with the same overall topology but with different organic linkers, varying in length and functionality. The term isoreticular was first introduced into coordination chemistry by Yaghi *et al.*[53] and simply means the theoretical idea of forming a net

by bringing together the building blocks. The first series of MOFs (IRMOFs) prepared using this approach[54] comprised metal-containing octahedral-shaped SBUs linked with various linear ditopic carboxylate linkers to form 16 different MOFs that shared the same cubic topology as IRMOF-1 also known as MOF-5. These 16 IRMOFs, as shown in Figure 1.6, may be expressed as $Zn_4O(linker)_3$. The linkers differ in terms of functionality of the spacer group, i.e. different pendant groups, (IRMOF-1 to IRMOF-7) or in length (IRMOF-8 to IRMOF-16). While the expansion of the links results in an increase in the internal void space (as shown in yellow spheres in Figure 1.6), this expansion, favours the formation of interpenetrated phases (IRMOF-9, IRMOF-11, IRMOF-13 and IRMOF-15). MOF-5 was used to indicate that its 3-D porous framework can be functionalized with IRMOF, -Br (IRMOF-2), $-NH_2$ (IRMOF-3), $-OC_3H_7$, $-OC_5H_{11}$, $-C_2H_4$, and $-C_4H_4$ and that its void space can be further be enlarged by extending the linker with biphenyl: IRMOF-9; tetrahydropyrene: IRMOF-11, pyrene: IRMOF-13 or terphenyl:IRMOF-15.

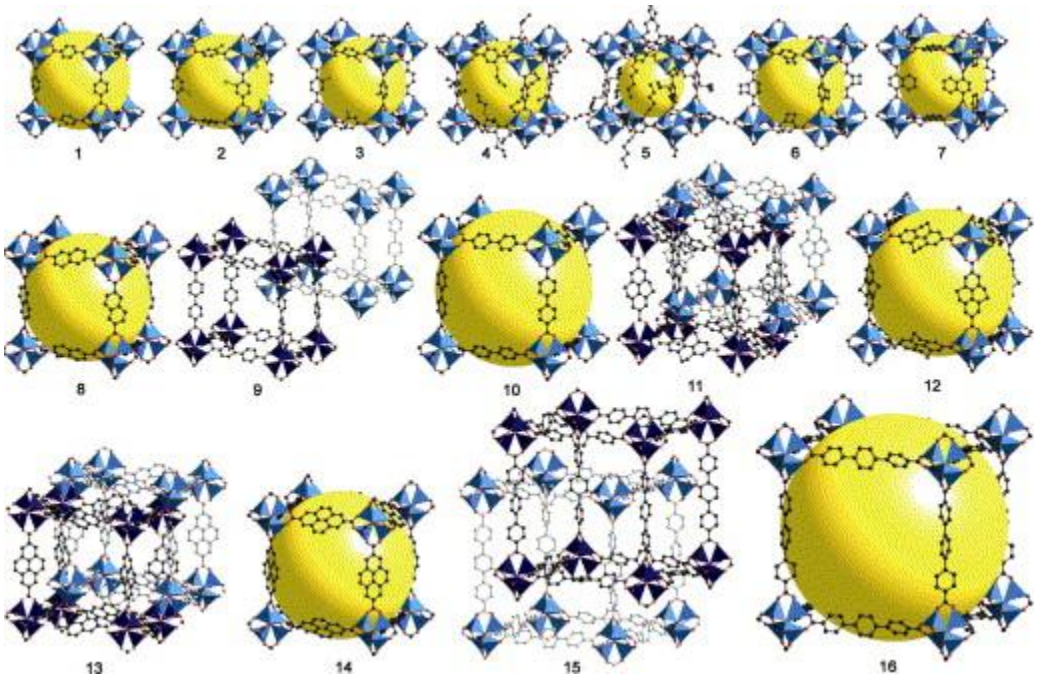

Figure 1.6: Represents a large series of isoreticular metal-organic frameworks (IRMOFs). The internal void is represented by a yellow sphere.[55]

Several other examples of isoreticular expansion for the high surface area were reported in the literature, for example, in 2001, in a review by Yaghi and co-workers on various tritopic carboxylates and Cu_2 paddlewheel units, as illustrated in Figure 1.8, subsequent expansion from btc^{3-} (1,3,5-benzenetricarboxylate) to bbc^{3-} (4,4',4",-benzenetricarboxylate) caused the length of the unit cell to enlarge from 26.34 Å in HKUST-1 (MOF-199) to 68.31 Å in MOF-399 which In turn, has also led to an increase in volume by a factor of 17. Similarly, MOF-399 shows the highest porosity (94 %) and lowest density (0.126 g·cm-3) among all the MOFs recorded by 2011.it remain so until in 2018 when DuT-60 with pore volume of 5.02 cm^3/g and low crystallographic density of 0.187 g/cm^3 was developed.

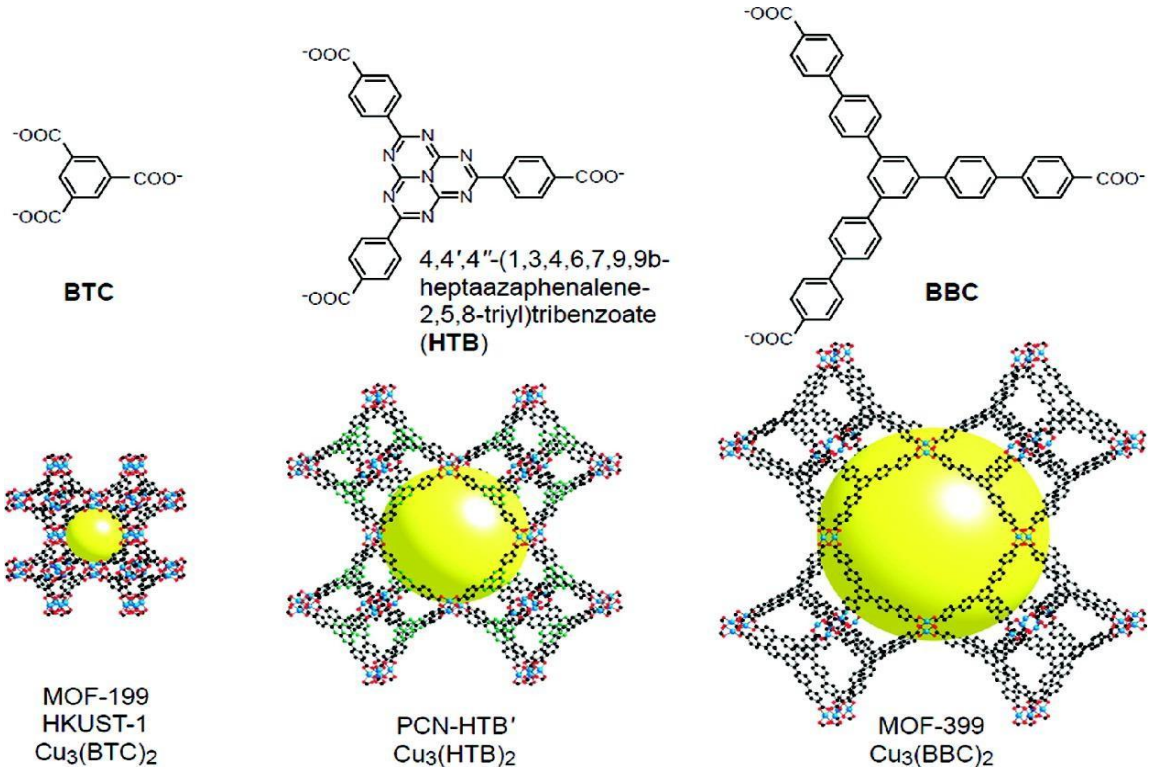

Figure 1.7: Shows molecular structures of organic linkers and the single crystal structures of MOF-199, PCN-HTB', and MOF-399 from the bottom. The internal void space is represented by yellow spheres. Cu, blue; C, black; O, red; and N, green. Hydrogen atoms are omitted for clarity.[56]

1.2.5 Robustness and Flexibility

Among the major challenges encountered from the inception of MOF chemistry was how to preserve the structural stability after any guest molecules were removed. This can be achieved by the addition of multidentate ligands in the MOFs to attain a stable framework.[57,58] Multidentate ligands (two or more coordination sites) were able to produce robust MOFs of high structural stability. In Yaghi and co-workers' IRMOF series, discussed above, some of the organic linkers used were long bridging ligands and hence interpenetration occurred resulting in decreasing the void space. With a view to addressing this issue, Kitagawa and co-workers proposed an idea called ''pillared layer construction'' for the synthesis of MOFs which were termed CPL-*n* compounds (CPL-n means Construction of Pillared Layer Compounds).[59] These types of MOFs tend to show some structural transformations even after they accommodate guest molecules, clearly showing that MOFs can respond to external stimuli. This feature is amongst the characteristics of MOFs that make them attractive and dissimilar in comparison to rigid activated carbons or zeolites. Based on this, MOFs have been classified into the following four generations:[60,61]

- First generation MOFs – the framework collapses irreversibly when the guest molecules are removed.
- Second-generation MOFs – these are non-conformationally changeable frameworks that uphold their rigidity even after the guest molecules are being removed.
- Third-generation MOFs - these frameworks manifest flexibility and dynamic characteristics, leading to guest-responsive adsorption performance.
- Fourth generation MOFs – these frameworks can withstand modification (post-processing of metal (cluster) sites, organic linkers (ligands), or vacant space).

From the above classification, therefore, the second-generation MOFs could be referred to as robust MOFs while the third-generation MOFs are recognized as flexible MOFs. Flexible MOFs experience reversible structural transformations as a result of external stimuli such as guest molecule removal or inclusion, magnetic, heat, and or electric fields, but the robust MOFs on the other hand do not show any further transformations. MOF-5 and HKUST-1 are the prominent examples of robust MOFs while MIL-53 and MIL-88 belong to the category of flexible MOFs.[62–66] In various applications, the two types of MOFs (robust and flexible) tend to have many advantages. For instance, robust MOFs may be used for gas storage owing to their properties like permanent pore size and shape, high porosity, and surface area, whereas flexibility of the framework provides greater advantages for applications in gas separation.[67]

Guest molecules are the major stimuli that affect the structural transformation in flexible MOFs. Given the guest-induced distortion phenomena of flexible MOFs, the guest molecule can either induce crystal-to-crystal transformations or crystal-to-amorphous phase transformations. It has been reported that the lanthanide (III) coordination polymers, $\{[M_2(BDOA)_3(H_2O)]\cdot 6H_2O\}n$ (where M = Tb, Gd and Sm; BDOA= benzene-1,4-dioxylacetate), undergo crystal to crystal structural transformation in which case the crystalline nature of the framework was lost after the guest molecules were removed but the same framework was regained by soaking in water for several minutes.[68,69] This clearly shows a typical example of guest-induced crystal-to-crystal transformation where in each case the crystalline nature of the framework is conserved.

The following factors however can be attributed to the occurrence of guest-induced structural transformation of flexible MOFs:

- Rotation of bridging ligands – here the ligand molecules may partially experience a rotational form of motion especially when there is high void space in MOFs that sterically allows the ligands to move around.
- Shrinking, swelling, and shape-responsive fitting – these normally occur when MOFs accommodate guest molecules. MOF structures are known to be dependent on numerous types of bonding such as hydrogen bonds, coordination bonds, and other weak non-bonding interactions. However, any change in these interactions can ultimately lead to changes such as shrinkage and expansion in the structure of MOFs.
- Interdigitation and interpenetration – here, catenation usually takes place when the resultant framework has a higher void space and collective motion within the frameworks is observed which causes a mutual sliding in such interpenetrated networks.[67,70]

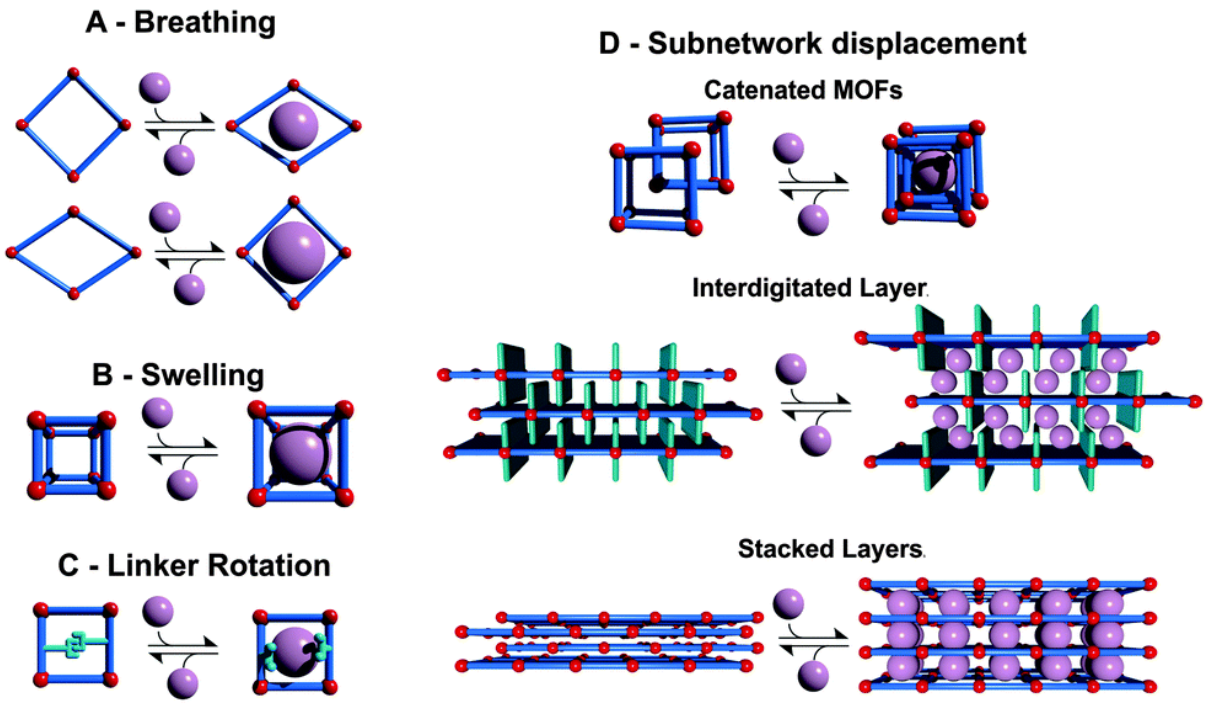

Figure 1.8: Schematic representation of different types of flexibility in MOFs.[71]

1.3 Ligand Used for MOF synthesis.

For the synthesis of MOFs, numerous linkers are available. Multidentate ligands can form distinct structures because they have a wide range of donor atoms or connecting sites that allow them to bind in practically any manner.[72] According to reports, while choosing a ligand potential for network synthesis, certain features like flexibility, ligand length, and bonding site count are crucial.[73] The most frequently mentioned problem with bridging ligands is their flexibility, which allows for the possibility of multiple unanticipated and surprising structures if a ligand possesses a variety of likely conformations. Many studies have been conducted on rigid ligands to eliminate flexibility and unpredictability. For instance, employing a stiff backbone, such as that found in 4,4-bipyridine, can restrict the free rotation of the ligand lone pair and the ligand binding site.[74] Rigid linkers are thus typically used in the assembly of MOFs in order to prevent issues in the anticipated product, typically, multidentate ligands with N or O donors are often used in the construction of these kinds of structures.[75] The most often used organic linkers in the synthesis of metal-organic frameworks (MOFs) have phenyl groups that are connected by carboxylate or pyridyl groups in a way that readily promotes bonding and the ensuing network development. The architecture, functionality, and stability of the resultant MOFs can all be directly impacted by changes to the linker's length, connectivity, and mixture composition.[76–78]

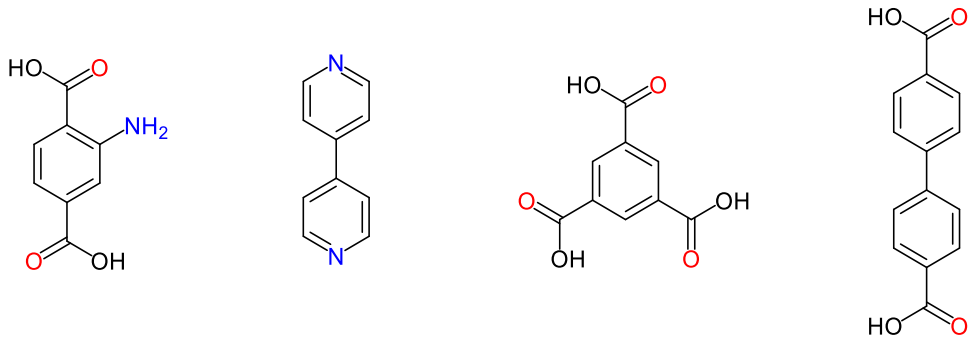

Figure 1.9: Some common linkers used in the synthesis of MOFs (a) Benzene 1,4-dicarboxylic acid (H_2BDC) (b) 2-aminoterephthalic acid ($H_2BDC\text{-}NH_2$) (c) 4,4'- bipyridine (BIPY) (d) Benzene-1,3,5-tricarboxylic acid (BTC) (e) Biphenyl-4,4'- dicarboxylic acid (H_2BPDC)

1.3 MOFs containing mixed ligand

Although it is widely acknowledged that single linkers are sufficient to form high surface area MOFs, multilinkers can also be used to create frameworks for specific applications like catalysis and separation that are difficult to accomplish with single linkers. Numerous researchers have investigated this concept in great detail, and multiple notations for these sorts of MOFs have been reported: mixed-component MOFs (MC-MOFs) by Wang and coworkers,[79] multivariate MOFs (MTV-MOFs) by Smith[80] and MIXMOFs by Chang and coworkers.[81] With these kinds of MOFs, alteration, and modification of properties of the MOFs is possible by binding two or more different organic linkers in connection with the metal nodes. With these kinds of MOFs, alteration, and modification of properties of the MOF is possible by binding two or more different organic linkers in connection with the metal nodes. The strategy of using different organic linkers, connecting 2D MOFs into an extended 3D network is termed 'pillaring' and has been used extensively to construct MOFs.[58,82,83] These pillar linkers are typically inserted gradually[84–87] or used as a "one-pot" method.[88–91] The first coordination networks in which two-dimensional (2D) cyanide-containing layers were connected by

coordinating or non-coordinating axial ligands are known as Hofmann clathrates, and pillar-layered MOFs are a subtype of these networks.[82,92] Figure 1.11 shows a schematic representation of Hofmann clathrate and pillar-layered MOF.

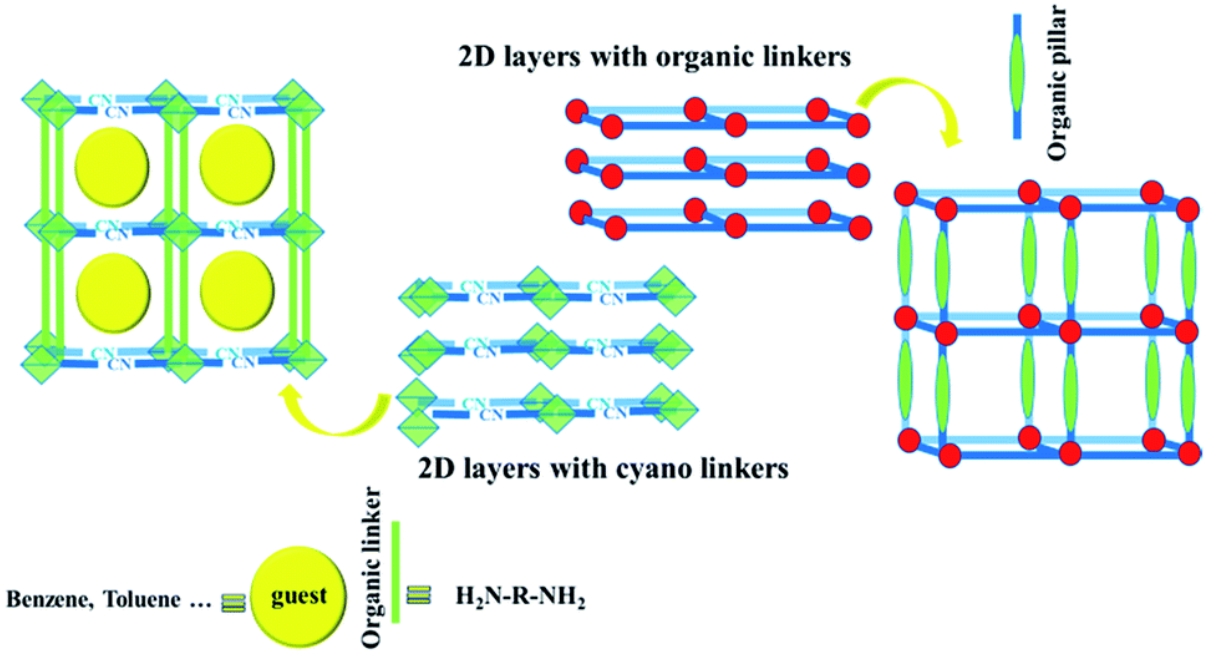

Figure 1.10: Representation of Hofmann clathrate and construction of 3D pillar-layered MOFs.[82]

Due to their capacity to introduce different functionalities at specific points during the development of MOFs, polycarboxylate and bipyridine (which includes isonicotinic and dinicotinic acids) have been the most often used organic linkers in the creation of mixed-ligand MOFs. When attached to metal, the polycarboxylate bridging ligand typically takes on an anionic form that can offer several coordination sites, whereas the neutral character of bipyridine ligands allows them to bind to the metal ions as rod-like bidentate struts.

1.4 Methodology for MOF Synthesis

There have been numerous reports on the approaches and/or paths that can be taken to accomplish MOF synthesis.[93–96] Several synthetic techniques are worth considering, including traditional (solvothermal and non-solvothermal), mechanochemical, microwave-assisted,

sonochemical, and electrochemical which have been widely explored. DMF, which is among the most often used solvents in MOF synthesis, provides for nearly complete dissolution of the starting materials due to its high polarity and boiling point of 153 °C. The reaction factors that influence MOF synthesis are concentration, pH, heating/cooling rates, and reaction time since they all play a key role in the crystallization kinetics of a system. Figure 1.11 depicts the various synthetic approaches, properties, and applications of MOF synthesized in the applied methodologies.

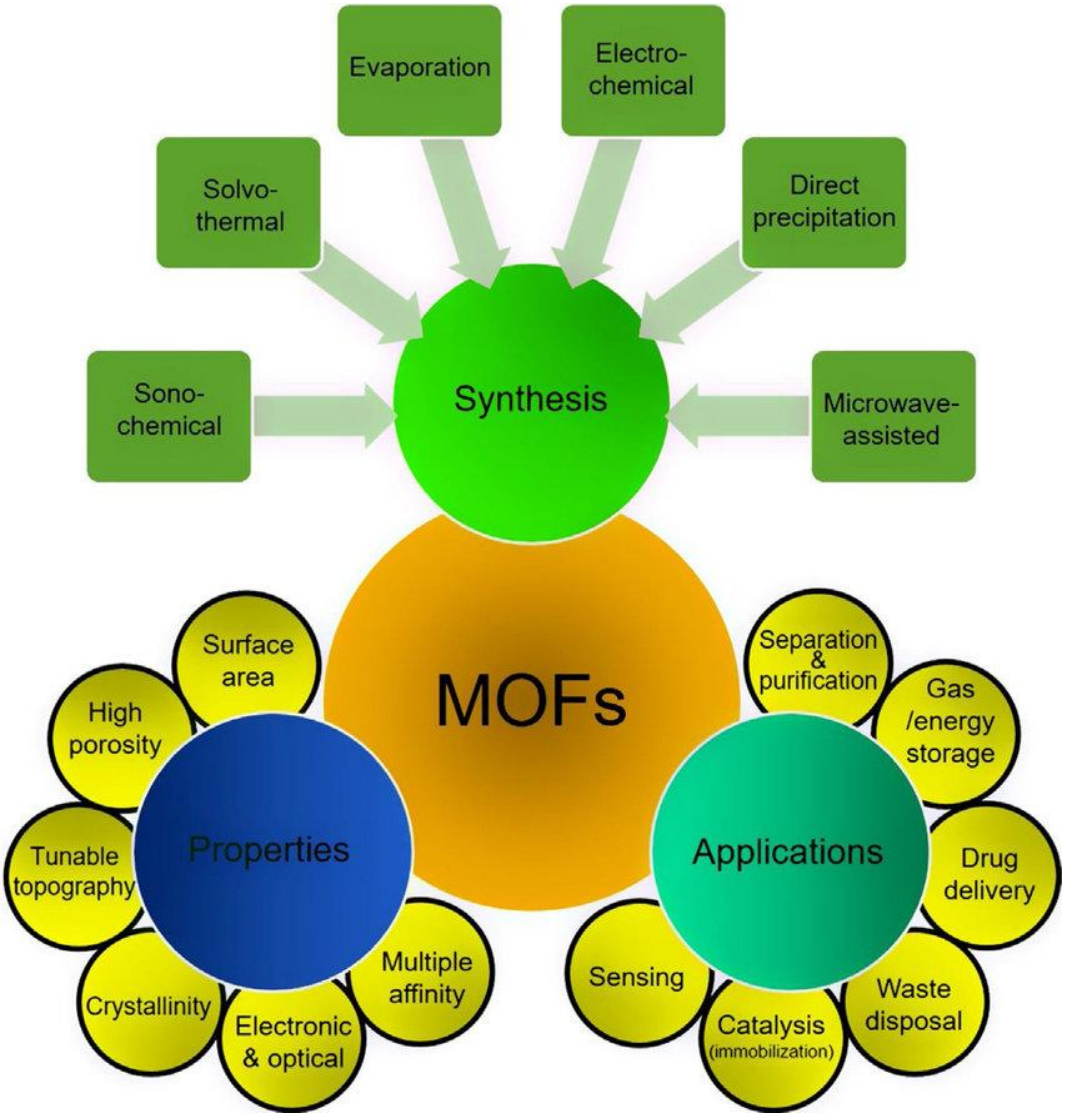

Figure 1.11: A schematic overview of MOF synthesis, properties, and applications.[97]

1.4.1 Traditional Synthesis

Traditional synthesis can be broadly categorized into two classes: solvothermal and non-solvothermal. Using a solvent at high temperature and pressure to speed up the reaction between the metal precursors and organic linkers is known as the solvothermal approach. The procedure is carried out in a solvent that has the ability to dissolve organic ligands as well as metal salts. The reaction mixture is heated to a temperature above the boiling point of the solvent, creating an autogenous pressure within a sealed vessel, typically an autoclave. The temperature range is usually between 100°C to 250°C, but can vary depending on the specific MOF being synthesized. A sealed autoclave is used to contain the reaction mixture, allowing the maintenance of high pressure and temperature conditions necessary for MOF formation. The autoclave is often lined with an inert material like Teflon to prevent reactions with the vessel walls. The reaction time can range from several hours to several days, depending on the desired product and specific synthesis conditions. Under these conditions, the metal ions and organic ligands react to form a crystalline MOF structure. The autoclave may create well-defined MOF crystals if it cools slowly. The technique frequently produces extremely pure and crystalline MOFs, and enables control over the size and shape of the MOF crystals by altering the synthesis conditions. It may be used to synthesize a wide range of MOFs with different metals and ligands.[98–100] Figure 1.12 shows a schematic representation of the solvothermal synthesis of MOFs.

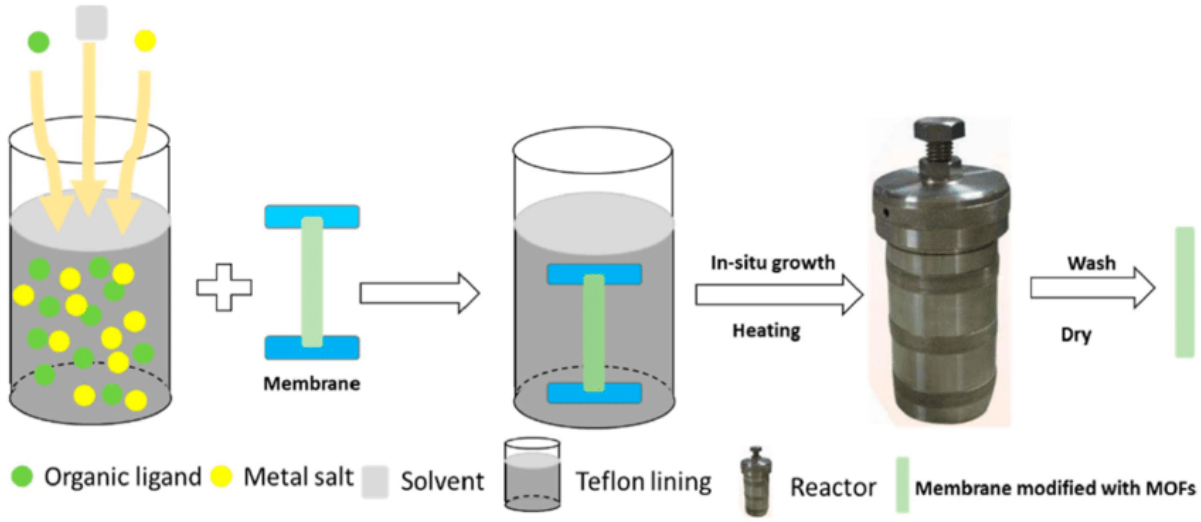

Figure 1.12: Schematic presentation of solvothermal synthesis of MOFs[101]

1.4.2 Microwave-assisted synthesis.

The second most common synthetic method for MOFs is undoubtedly microwave-assisted heating, which enables the rapid synthesis of a wide variety of MOFs in large quantities with favourable crystallographic and physical properties.[102] It is an innovative approach that leverages the unique properties of microwave irradiation to enhance the synthesis process, improve product yield, and often lead to the formation of MOFs with unique properties. In this method, microwaves interact with polar molecules and ions in the reaction mixture, causing rapid heating through dipolar polarization and ionic conduction.[103] When compared to traditional heating techniques, this direct touch produces faster and more uniform heating, usually taking place in a matter of minutes to hours as opposed to days or hours for traditional approaches.[104] Optimal MOF yields are frequently achieved through regulated reaction conditions and effective energy transfer. Compared to MOFs synthesized using traditional techniques, those produced by microwave synthesis can have distinct particle sizes, morphologies, and crystallinities. Figure 1.13 illustrates a reduction in particle size and a

smaller size distribution of nanoparticles using microwave-aided heating.[105] The high uniform heating of the reaction fluid to produce a rapid nucleation rate is observed to have reduced the size of the particle. In contrast to traditional hot MOF synthesis, faster nucleation occurs in large quantities and more reactant is eliminated from the synthesis, which inhibits particle development.[106]

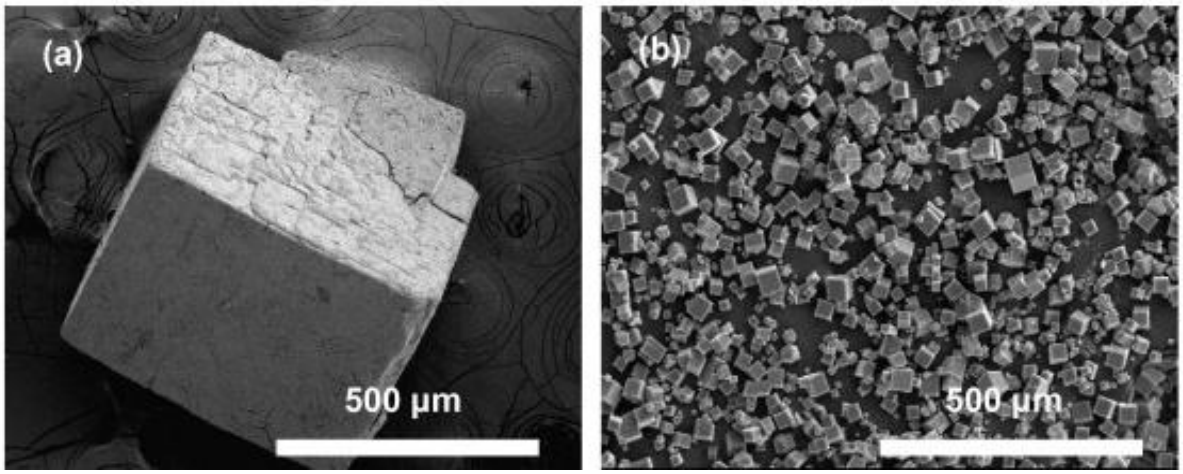

Figure 1.13: SEM images of MOF-5 prepared by solvothermal method (a) and microwave synthesized sample (b), presenting a significant dissimilarity in the size of the particle.[105]

1.4.3 Mechanochemical synthesis

Mechanical energy is used in mechanochemical methods of MOF production to initiate reactions. With little to no solvent, the method can create extremely crystalline structures at ambient temperature. The main principle of this synthesis process is to grind or mill solid starting materials with little or no solvent in order to facilitate chemical reactions. Usually, the liquid phase coordination reaction - which involves dissolving metal salts and organic ligands in the right solvents - is used to synthesize MOFs. However, the use of mechanochemistry opens up a solvent-minimization pathway for the synthesis of MOFs. Large-scale manufacturing and simplicity of handling are two potential benefits of the solid-solid reaction,

which generates compounds directly in powder form with quantitative yields.[107] The scaling up of mechanosynthesis, which is primarily a batch-processing method with very low production rates, is a significant disadvantage. Furthermore, mechanosynthesis is the approach with the least negative environmental impact, and as such, it is anticipated to be a commercially viable technique for producing MOFs. The quick synthesis of MOF materials by mechanochemical syntheses has shown effective when using the liquid-assisted grinding (LAG) technique, which involves adding a small quantity of solvent to a solid reaction mixture.[108–110]

1.4.4 Electrochemical Synthesis

Electrochemical synthesis of Metal-Organic Frameworks (MOFs) is a method that uses electrochemical techniques to produce MOF materials. This method of MOF synthesis has yielded many advantageous conditions, including high yield, low energy consumption, and speedy synthesis with little excess usage of linker and solvent in addition to its straightforward approach such as easy equipment set-up, absence of precursor metal salts, quick reaction time, accumulation of MOFs on the desired substrates and real-time change of MOFs.[111–114] The most alluring aspect of electrochemical synthesis is its gentle reaction conditions, which operate at room temperature and atmospheric pressure but, even with these benefits, this method is not as widely used as it may be, especially when creating functionalized framework materials.[115] Figure 1.14 shows an instrumentation for the electrochemical synthesis of $Zn_3(BTC)_2$-MOF[116]

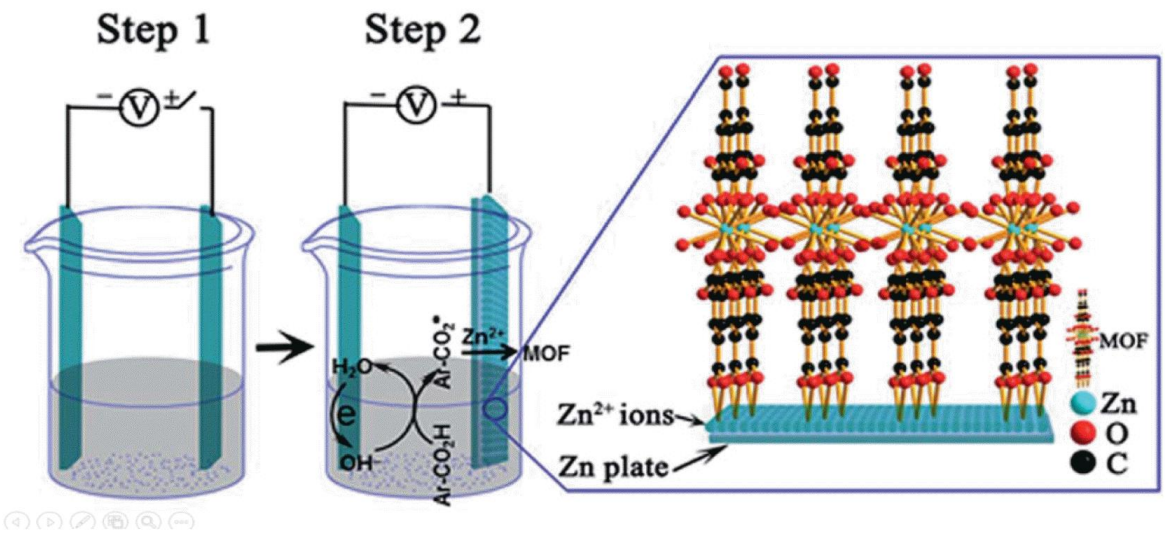

Figure 1.14: Illustrates the instrumentation of electrochemical synthesis of $Zn_3(BTC)_2$-MOF.[116]

1.4.5 Sonochemical Synthesis

As the name suggests, sonochemistry is a branch of chemistry that studies how high-energy ultrasonic radiation (20 KHz–10 MHz) affects chemical reactions. Here, the cavitation process caused by the high-energy ultrasonic radiation results in both physical and chemical changes, such as the growth, production, and rapid breakup of bubbles, which enables the creation of "local hot spots" with increased pressure and temperature over brief periods of time. The reaction's favourable settings promote the quick development of excess crystallization centres. When using sonochemical techniques instead of solvothermal techniques, the material is usually produced with a significantly shorter crystallization time. Although sonochemical techniques are still not commonly used for MOF synthesis, there have been reports of successful synthesis of many MOFs using this method. For instance, 2009 saw the successful ultrasonic synthesis of HKUST-1 by Li *et al.* producing microporous nanoparticles in just five minutes.[117] Subsequent analysis of the substance showed that the process had no effect on its

chemical and physical characteristics and that its surface area, crystallinity, and its capacity to absorb H_2 were all comparable to those of materials made using solvothermal synthesis. The material underwent an unidentified phase shift upon being subjected to a ninety-minute reaction period, suggesting that the decomposition process may not have been fully completed.

1.5 Characterization of MOFs

Diverse analytical methods have been employed to characterize distinct MOF varieties. The properties of the MOFs to be analysed, such as their surface area, sensitivity to air, periodic structure, and high-temperature sensitivity, will determine which of these procedures are best.[118] The two most notable aspects of MOFs are their high surface area and porosity, which provide superior qualities to silica gel, activated carbon, and zeolites. The Brunauer-Emmett-Teller (BET) method of surface area determination is a widely used approach for MOF characterization. Using this method, the entire surface area of the adsorbent is investigated while temperature conditions are measured to determine the experimental dependence of adsorption on high pressure. Materials with a broad range of pore widths are suitable candidates for the application of the BET technique.

X-ray diffraction (XRD), a technique frequently employed for MOF investigation with the goal of obtaining a three-dimensional molecular structure from a crystal, provides the best opportunity for structural identification when applied to periodic structures of MOFs. The non-destructive analytical method known as single crystal x-ray diffraction (SCXRD) provides detailed information about crystalline substances, including the precise location of atoms in three dimensions, which in turn determines the material's molecular structure and reactivity.[119] Powder X-ray diffraction (PXRD) is an alternative method when it is not always possible to create a single crystal of a specific MOF with quality and size appropriate for SCXRD. PXRD

can be used to guarantee synthesis repeatability and provide a clear structural differentiation between samples of a specific MOF prepared using various synthetic techniques and reaction circumstances.[120] However, it is sometimes difficult to determine the MOF structure using PXRD due to the enormous unit cell parameters and variable temperature. Single crystal x-ray diffraction has proven to be a highly effective method for examining the thermal stability of metal-organic frameworks (MOFs) and the impact of guest solvent molecules on their structural composition.[121–123] Another helpful method for ensuring thermal stability in MOFs is thermogravimetric analysis, which calculates an examined sample's mass as a function of temperature over time. The apparatus used in thermogravimetric analysis allows the sample to be heated to a specific temperature, typically between 100 and 1000 ^{o}C, while being exposed to ambient oxygen.[124] Plots of thermogravimetric analysis, which display curves confirming the loss of solvent molecules and organic linkers, have been reported frequently for MOFs.[125] Also, it provides comprehensive details regarding the stability of the MOF. There are many other methods that can be used in addition to a single method for the structural elucidation of MOFs. These methods include x-ray absorption, x-ray absorption near-edge structure (XANES), extended x-ray absorption fine-structure (EXAFS), nuclear magnetic resonance (NMR) spectroscopy, infrared (IR) spectroscopy, scanning electron microscopy (SEM), and elemental analysis for C, H, and N metal. Figure 1.15 shows a thermal gravimetric analysis (TGA) and derivative thermal gravimetric analysis (DTG) for lanthanum-based MOF.

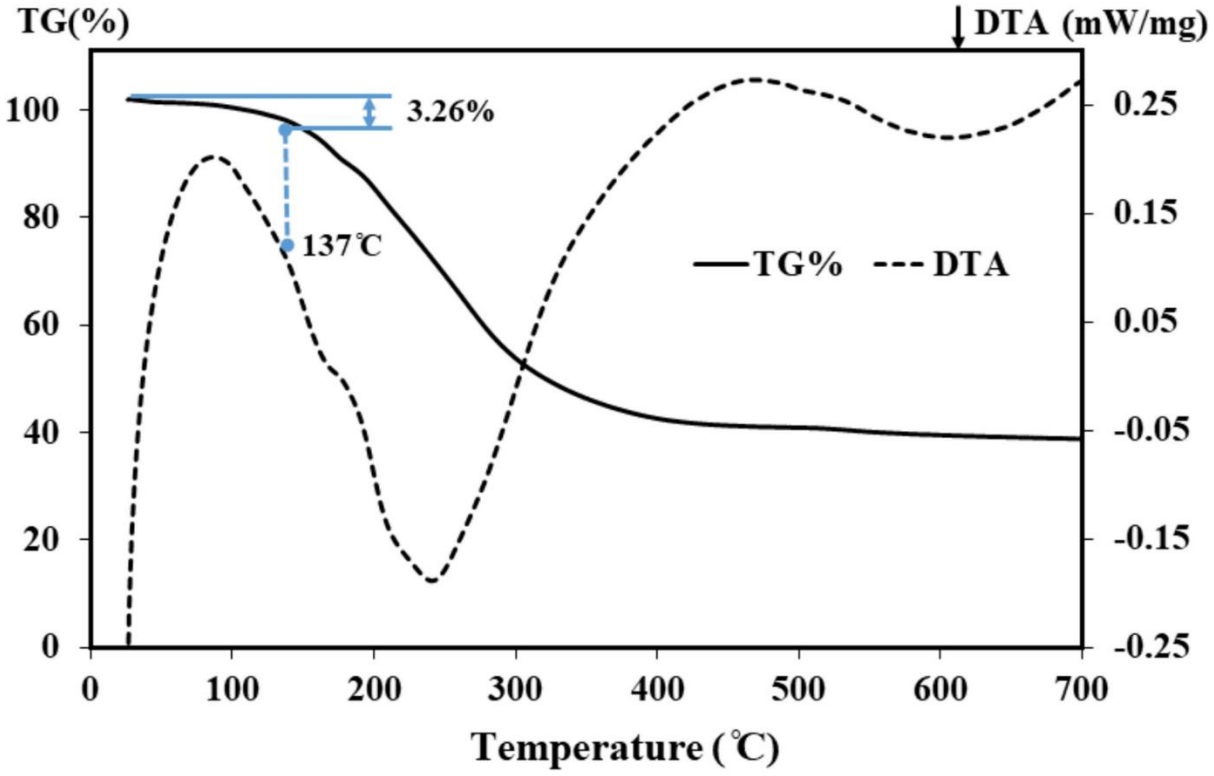

Figure 1.15 Thermal gravimetric analysis (TGA) and derivative thermogravimetric analysis (DTG) curves of La-based MOF.[126]

1.6 Application of MOFs

As previously indicated, reticular chemistry has made it possible to create MOFs with appealing characteristics because of their chemical makeup and structure, which are appropriate for a range of uses in the fields of molecular sensing, biomedicine, hydrogen storage, gas separation, catalysis, and fuel cell membranes. In the following paragraphs, a handful of these extensively researched MOF applications will be covered.

1.6.1 Gas storage and separation

One of the first MOFs uses to be studied was gas storage.[127–131] There are several ways to store gases, but there are significant drawbacks to these conventional techniques, necessitating the development of a less expensive and safer plan. To do this, porous materials, such as zeolites

and activated porous carbons, have been thoroughly researched for this purpose; however, MOFs have been found to be more effective than other materials due to their high surface areas, tuneable pore structures, and functionalization opportunities. Additionally, studies have demonstrated that doping MOFs with metal ions increases their ability to absorb H_2.[132,133] About 500,000 MOFs have been investigated for their ability to store hydrogen,[134] but MOF-177, which was made up from Zn_4O and 1,3,5-triyltribenzoate (BTB) and 4,4',4"-benzene, is the most well-known.[135] It exhibits a gravimetric H_2 uptake of 7.5 wt% at 70 pressure and 77 K because of its huge pore volume (1.59 cm^3 g^{-1}) and high BET surface area (~5000 m^2 g^{-1}). MOF-5 (IRMOF-1), a well-known zinc carboxylate-based MOF, with a BET surface area of 3800 m^2 g^{-1} and can absorb 7.1 wt% of H_2 at 40 bar and 77 K.[136] Several MOFs, including MOF-210, MIL-101, HKUST-1, NU-100, PCN-12, NOTT-102, and MOF-205, are also excellent for storing H_2.[137–139] At 80 pressure and 77 K, MOF-210 has a total H_2 uptake capacity of 176 mmg-^{1}, although NU-100 has the highest H_2 surplus storage. To sum up, MOFs with exposed metal sites are useful materials for absorbing H_2. A few of the MOFs used to store gas are shown in Figure 1.16

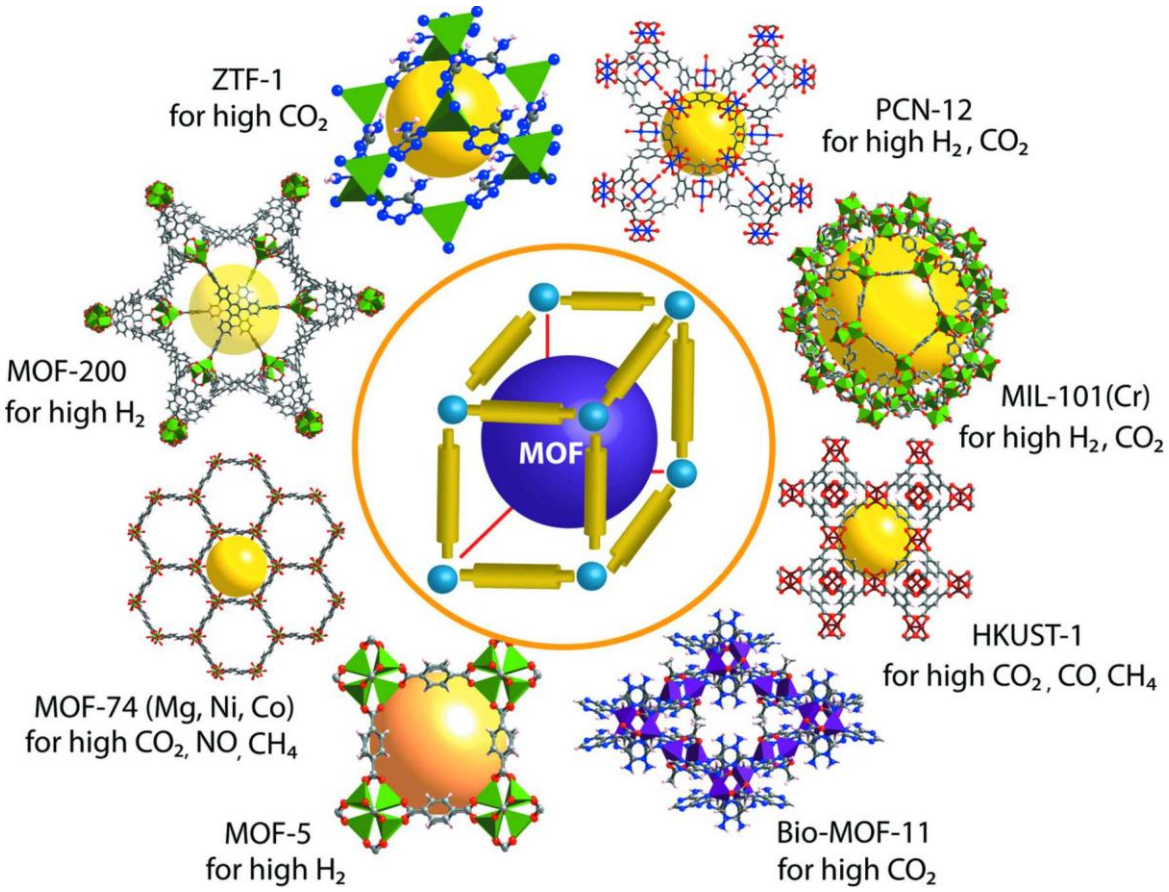

Figure 1.16 Illustration of MOFs recognized for their high gas storage capacity.[140]

1.6.2 MOF as a Molecular Sensor

Metal-organic frameworks can act as a sensing material which is simply the capacity of the MOFs to identify and react to particular compounds or ambient conditions.[141–143] The potential of MOFs to be used in small-molecule and pH sensors, antennae in highly sensitive bioinorganic, light concentrators for solar systems, and advanced optical technologies have drawn a lot of attention to research into their usage as luminous materials. The hybrid nature of MOF which combines organic linkers, inorganic metal ions, and guest molecules, makes it particularly useful in sensing applications. [144–147] Due to their electronic transitions from the d to the f shell, which are accompanied by photon emission, metal ions belonging to the

lanthanide class are frequently used in the creation of luminous MOFs.[148,149] The two lanthanide cations that have drawn the most attention are terbium (Tb) and europium (Eu), because of their appealing narrow emission lumophores and by bonding the lanthanide metal ions with ligands that absorb substantially, increase the luminescence of MOFs.[150,151] Dy, Sm, Nd, Gd, Er, and Yb are further lanthanide series members that have been employed as luminous metal ions. The utilization of organic linkers with considerable conjugation via the expanded π-system is the reason behind the strong absorption and emission, and these electronic transitions π–π* and n–π* are exclusively seen in organic ligands.[152,153] Similarly, in transition metal MOF, only the linkers give their luminous characteristics.[154] Additional factors giving MOFs their luminescence characteristic include charge transfer from metal to ligand (MLCT), ligand to metal (LMCT), ligand to ligand (LLCT), and ligand center.[155]

1.6.3 Magnetic Properties

The use of MOFs as luminous materials has gained attention due to its potential for small-molecule sensor applications.[156,157] Lanthanide MOFs exhibit paramagnetic behaviour due to the presence of unpaired electrons in the metal ions. These unpaired electrons respond to external magnetic fields but do not retain magnetization in the absence of the field.[158] Researchers refer to these types of MOFs as magnetic metal-organic frameworks (MMOFs). Transition metals in the first row such as Fe, Mn, Co, and Ni are common sources of paramagnetism in MOFs and have made significant contributions to the creation of porous molecular magnets.[159–161] The porosity and magnetic characteristics of MMOFs make them suitable for air separation applications.[162,163] The type of organic linkers used in magnetic MOF synthesis have a crucial role in establishing the magnetism of the MOF formed.[164]

1.7 Conclusion

Lanthanide Metal-Organic Frameworks (MOFs) are a subclass of metal-organic frameworks that incorporate lanthanide ions as the metal nodes. MOFs are crystalline materials composed of metal ions or clusters coordinated to organic ligands, forming porous structures with high surface areas. The inclusion of lanthanide ions in MOFs introduces unique properties due to the distinct electronic configurations and luminescent characteristics of lanthanides. They generally exhibit stability in various chemical environments, although this can vary depending on the specific lanthanide and organic ligands used. Developing efficient and scalable synthesis methods for lanthanide MOFs remains a challenge. Functionalizing the ligands or the framework itself to introduce additional properties or improve existing ones is an active area of research. This can lead to multifunctional MOFs with tailored properties for specific applications. lanthanide MOFs are a fascinating class of materials with a wide range of potential applications due to their unique luminescent, magnetic, and catalytic properties.

1.8 Aim Objectives of the study

This project aims to synthesize and characterize self-assembled lanthanide metal-organic frameworks incorporating naphthalene diimide ligand for use in the detection and removal of environmental contaminants. The project will explore post synthetic modifications, including encapsulation of ferrocene and phenothiazine as well as the development of mixed metal MOFs.

1.9 References

1 L. Kong, M. Zhong, W. Shuang, Y. Xu and X.-H. Bu, *Chem Soc Rev*, 2020, **49**, 2378–2407.

2 M. G. Mohamed, Ahmed. F. M. EL-Mahdy, M. G. Kotp and S.-W. Kuo, *Mater Adv*, 2022, **3**, 707–733.

3 K. Lan and D. Zhao, *Nano Lett*, 2022, **22**, 3177–3179.

4 M. T. Colomer, *Int J Mol Sci*, 2024, **25**, 7127.

5 V. Chaudhary and S. Sharma, *Journal of Porous Materials*, 2017, **24**, 741–749.

6 Y. Meng, X. Lin, J. Huang and L. Zhang, *Molecules*, 2024, **29**, 3916.

7 L. Frentzel-Beyme, P. Kolodzeiski, K. Terlinden and S. Henke, *Adv Funct Mater*, 2023, **33**, 202302033.

8 M. Ejaz, M. M. Samy, Y. Ye, S.-W. Kuo and M. Gamal Mohamed, *Int J Mol Sci*, 2023, **24**, 2501.

9 A. El Fadaly, M. A. Sayed, A. O. Abo El Naga, M. El Saied, S. A. Shaban and F. I. Elhosiny, *Bulletin of Chemical Reaction Engineering & Catalysis*, 2023, **18**, 407–419.

10 P. Feng, C. Kang, X. Yue, Z. Zhou, Z. Liu, Y. Gai, J. Shi and B. Zong, *RSC Adv*, 2024, **14**, 19264–19270.

11 W. Liu, Y. Wang, X. Zhang, F. Chen, S. Xie, L. Xu, X. Li and X. Zhu, *Mol Syst Des Eng*, 2024, **9**, 1000–1016.

12 E. Kusrini, N. M. Mualim, A. Rahman and A. Usman, *AIP. Conf*. 2020, **2255**. 060012.

13 A. Campanile, B. Liguori, C. Ferone, D. Caputo and P. Aprea, *Sci Rep*, 2022, **12**, 3686.

14 X. Wang, Z. Dong, Q. Wang, C. Meng, W. Zhuang, J. Liu, Y. Song, Y. Jin and S. Yang, *Minerals*, 2020, **10**, 391.

15 Z. Hongna, Z. Yue, B. Huhe, Q. Haili and Z. Ruifen, *Journal of Porous Materials*, 2024, **31**, 989–1004.

16 J.-R. Li, J. Sculley and H.-C. Zhou, *Chem Rev*, 2012, **112**, 869–932.

17 C. Jiang, X. Wang, Y. Ouyang, K. Lu, W. Jiang, H. Xu, X. Wei, Z. Wang, F. Dai and D. Sun, *Nanoscale Adv*, 2022, **4**, 2077–2089.

18 G. Awasthi, S. Shivgotra, S. Nikhar, S. Sundarrajan, S. Ramakrishna and P. Kumar, *Polymers (Basel)*, 2022, **14**, 4710.

19 D. Li, A. Yadav, H. Zhou, K. Roy, P. Thanasekaran and C. Lee, *Global Challenges*, 2023, **8** 202300244.

20 V. F. Yusuf, N. I. Malek and S. K. Kailasa, *ACS Omega*, 2022, **7**, 44507–44531.

21 C. Pettinari and A. Tombesi, *Inorganics (Basel)*, 2023, **11**, 65.

22 S. Singh, N. Sivaram, B. Nath, N. A. Khan, J. Singh and P. C. Ramamurthy, *NPJ Clean Water*, 2024, **7**, 124.

23 U. Baig, A. Waheed and S. M. S. Jillani, *Chem Asian J*, 2023, **19**, 202300619.

24 G. Avci, S. Velioglu and S. Keskin, *ACS Appl Mater Interfaces*, 2018, **10**, 33693–33706.

25 C. Jiang, X. Wang, Y. Ouyang, K. Lu, W. Jiang, H. Xu, X. Wei, Z. Wang, F. Dai and D. Sun, *Nanoscale Adv*, 2022, **4**, 2077–2089.

26 C. Oh, A. Nandy, S. Yue and H. J. Kulik, *ACS Appl Mater Interfaces*, 2024, **16**, 55541–55554.

27 L. Zhang, G.-D. Wang, B. Zhang, G.-P. Yang, W.-Y. Zhang, L. Hou, Y.-Y. Wang and Z. Zhu, *J Mater Chem A Mater*, 2024, **12**, 25820–25828.

28 D. Li, A. Yadav, H. Zhou, K. Roy, P. Thanasekaran and C. Lee, *Global Challenges*, 2024, **8,** 202300244.

29 M.-A. Rezaie, A. Khojastehnezhad and A. Shiri, *Sci Rep*, 2024, **14**, 24644.

30 S. O. Hunter, A. Nikolich, M. R. Bryant, D. Skelton and C. Richardson, *Chemical Communications*, 2024, **60**, 14822–14825.

31 T. Gadzikwa and P. Matseketsa, *Dalton Transactions*, 2024, **53**, 7659–7668.

32 E. A. Abdelrahman and G. S. El-Sayyad, *Opt Quantum Electron*, 2024, **56**, 884.

33 E. A. Tomic, *J Appl Polym Sci*, 1965, **9**, 3745–3752.

34 U. Mueller, M. Schubert, F. Teich, H. Puetter, K. Schierle-Arndt and J. Pastré, *J. Mater. Chem.*, 2006, **16**, 626–636.

35 B. F. Hoskins and R. Robson, *J Am Chem Soc*, 1989, **111**, 5962–5964.

36 T. R. Cook, Y.-R. Zheng and P. J. Stang, *Chem Rev*, 2013, **113**, 734–777.

37 Y.-S. Ho and H.-Z. Fu, *Inorg Chem Commun*, 2016, **73**, 174–182.

38 N. R. Champness, *Dalton Transactions*, 2011, **40**, 10311.

39 C.-C. Wang and Y.-S. Ho, *Scientometrics*, 2016, **109**, 481–513.

40 S. Soni, P. K. Bajpai and C. Arora, *Characterization and Application of Nanomaterials*, 2020, **3**, 87–106.

41 M. J. Kalmutzki, N. Hanikel and O. M. Yaghi, *Sci Adv*.

42 O. M. Yaghi, M. O'Keeffe, N. W. Ockwig, H. K. Chae, M. Eddaoudi and J. Kim, *Nature*, 2003, **423**, 705–714.

43 R. J. Marshall, C. T. Lennon, A. Tao, H. M. Senn, C. Wilson, D. Fairen-Jimenez and R. S. Forgan, *J Mater Chem A Mater*, 2018, **6**, 1181–1187.

44 A. Ferguson, L. Liu, S. J. Tapperwijn, D. Perl, F.-X. Coudert, S. Van Cleuvenbergen, T. Verbiest, M. A. van der Veen and S. G. Telfer, *Nat Chem*, 2016, **8**, 250–257.

45 D. Jędrzejowski, M. Pander, W. Nitek, W. Bury and D. Matoga, *Chemistry of Materials*, 2021, **33**, 7509–7517.

46 Y. Zhang, X. Zhang, Z. Chen, K. Otake, G. W. Peterson, Y. Chen, X. Wang, L. R. Redfern, S. Goswami, P. Li, T. Islamoglu, B. Wang and O. K. Farha, *ChemSusChem*, 2020, **13**, 1710–1714.

47 M. Gupta and J. J. Vittal, *Coord Chem Rev*, 2021, **435**, 213789.

48 F. Zhang, Y. Zhang, X. Wang, J. Li and J. Yang, *Inorg Chem Front*, 2022, **9**, 5434–5443.

49 F. Guo, C. Su, Y. Fan, W. Shi and X. Zhang, *Inorg Chem*, 2020, **59**, 7135–7142.

50 G. Verma, S. Butikofer, S. Kumar and S. Ma, *Top Curr Chem*, 2020, **378**, 4.

51 S. A. Boer and D. R. Turner, *Cryst Growth Des*, 2016, **16**, 6294–6303.

52 H.-L. Jiang, T. A. Makal and H.-C. Zhou, *Coord Chem Rev*, 2013, **257**, 2232–2249.

53 S. Gautam, H. Agrawal, M. Thakur, A. Akbari, H. Sharda, R. Kaur and M. Amini, *J Environ Chem Eng*, 2020, **8**, 103726.

54 M. Eddaoudi, J. Kim, N. Rosi, D. Vodak, J. Wachter, M. O'Keeffe and O. M. Yaghi, *Science (1979)*, 2002, **295**, 469–472.

55 J. L. C. Rowsell and O. M. Yaghi, *Microporous and Mesoporous Materials*, 2004, **73**, 3–14.

56 H. Furukawa, Y. B. Go, N. Ko, Y. K. Park, F. J. Uribe-Romo, J. Kim, M. O'Keeffe and O. M. Yaghi, *Inorg Chem*, 2011, **50**, 9147–9152.

57 M. Ding, X. Cai and H.-L. Jiang, *Chem Sci*, 2019, **10**, 10209–10230.

58 X. Liu, H. Wang, C. Liu, J. Chen, Z. Zhou, S. Deng and J. Wang, *Chem & Bio Engineering*, 2024, **1**, 469–487.

59 D. Wang, H. Yao, J. Ye, Y. Gao, H. Cong and B. Yu, *Small*, 2024, **20**, 202404350.

60 H. Yang, F. Guo, P. Lama, W.-Y. Gao, H. Wu, L. J. Barbour, W. Zhou, J. Zhang, B. Aguila and S. Ma, *ACS Cent Sci*, 2018, **4**, 1194–1200.

61 X. Li, D. Sensharma, V. I. Nikolayenko, S. Darwish, A. A. Bezrukov, N. Kumar, W. Liu, X.-J. Kong, Z. Zhang and M. J. Zaworotko, *Chemistry of Materials*, 2023, **35**, 783–791.

62 S. Essalmi, S. Lotfi, A. BaQais, M. Saadi, M. Arab and H. Ait Ahsaine, *RSC Adv*, 2024, **14**, 9365–9390.

63 U. Ryu, S. Jee, P. C. Rao, J. Shin, C. Ko, M. Yoon, K. S. Park and K. M. Choi, *Coord Chem Rev*, 2021, **426**, 213544.

64 T. Zelenka, M. Baláž, M. Férová, P. Diko, J. Bednarčík, A. Királyová, Ľ. Zauška, R. Bureš, P. Sharda, N. Király, A. Badač, J. Vyhlídalová, M. Želinská and M. Almáši, *Sci Rep*, 2024, **14**, 15386.

65 B.-E. Channab, M. El Ouardi, O. Ait Layachi, S. E. Marrane, A. El Idrissi, A. BaQais and H. Ait Ahsaine, *Environ Sci Nano*, 2023, **10**, 2957–2988.

66 D. Chakraborty, A. Yurdusen, G. Mouchaham, F. Nouar and C. Serre, *Adv Funct Mater*, 2023**, 34**, 202309089.

67 F. Yuan, Y. Li, X.-Y. Ling, C.-M. Yuan, C.-S. Zhou, J. Wang, A. Singh, A. Kumar and F.-Y. Chen, *Inorg Chem Commun*, 2019, **109**, 107576.

68 M.-Y. Xu, G.-Y. Liang, J.-S. Feng, G.-M. Liang and X.-J. Wang, *Cryst Growth Des*, 2022, **22**, 1583–1593.

69 M. Sinchow, T. Konno and A. Rujiwatra, *Inorg Chem*, 2022, **61**, 10383–10392.

70 D. Blasi, S. Quici, S. Orlandi, P. Mercandelli, A. V. Sokolov, E. V. Alexandrov and L. Carlucci, *CrystEngComm*, 2022, **24**, 5474–5486.

71 A. Schneemann, V. Bon, I. Schwedler, I. Senkovska, S. Kaskel and R. A. Fischer, *Chem. Soc. Rev.*, 2014, **43**, 6062–6096.

72 X. Gao, M. Zheng, L. Qin, K. Shen and H. Zheng, *Cryst Growth Des*, 2016, **16**, 4711–4719.

73 J.-P. Zhang, H.-L. Zhou, D.-D. Zhou, P.-Q. Liao and X.-M. Chen, *Natl Sci Rev*, 2018, **5**, 907–919.

74 X. Zhang, Q. Yang, M. Yun, C. Si, N. An, M. Jia, J. Liu and X. Dong, *Acta Crystallogr B Struct Sci Cryst Eng Mater*, 2020, **76**, 1001–1017.

75 C. P. Raptopoulou, *Materials*, 2021, **14**, 310.

76 X. Cheng, L. Guo, H. Wang, J. Gu, Y. Yang, M. V. Kirillova and A. M. Kirillov, *Inorg Chem*, 2022, **61**, 12577–12590.

77 H. Arceo-Ruiz, E. Xochitiotzi-Flores, H. García-Ortega, N. Farfán, R. Santillan, S. Rincón and A. Zepeda, *Molecules*, 2023, **28**, 1816.

78 M. Beiranvand, D. Habibi and H. Khodakarami, *Sci Rep*, 2024, **14**, 27727.

79 Y. Wang, L. Zhao, S. Liu, G. Ji, C. He, Y. Tang and C. Duan, *ACS Appl Mater Interfaces*, 2023, **15**, 16744–16754.

80 K. T. Smith and K. C. Stylianou, *Dalton Transactions*, 2023, **52**, 16578–16585.

81 C.-K. Chang, T.-R. Ko, T.-Y. Lin, Y.-C. Lin, H. J. Yu, J. S. Lee, Y.-P. Li, H.-L. Wu and D.-Y. Kang, *Commun Chem*, 2023, **6**, 118.

82 F. ZareKarizi, M. Joharian and A. Morsali, *J Mater Chem A Mater*, 2018, **6**, 19288–19329.

83 C. Xiao, J. Tian, Q. Chen and M. Hong, *Chem Sci*, 2024, **15**, 1570–1610.

84 X. Duan, F. Ge, Q. Yan, Y. Liu and H. Zheng, *Chemistry – A Eur. J*, 2023, **30**, 202302784.

85 N. Hanikel, D. Kurandina, S. Chheda, Z. Zheng, Z. Rong, S. E. Neumann, J. Sauer, J. I. Siepmann, L. Gagliardi and O. M. Yaghi, *ACS Cent Sci*, 2023, **9**, 551–557.

86 X. Xu, L. Gao and S. Yuan, *Dalton Transactions*, 2023, **52**, 15233–15252.

87 J. Y. Choi, J. Flood, M. Stodolka, H. T. B. Pham and J. Park, *ACS Nano*, 2022, **16**, 3145–3151.

88 S. R. Jambovane, S. K. Nune, R. T. Kelly, B. P. McGrail, Z. Wang, M. I. Nandasiri, S. Katipamula, C. Trader and H. T. Schaef, *Sci Rep*, 2016, **6**, 36657.

89 T. H. Habtemariam, V. J. T. Raju and Y. Chebude, *RSC Adv*, 2022, **12**, 32652–32658.

90 Y. Gao, M.-J. Suh, J.-H. Kim and G. Yu, *ACS Appl Mater Interfaces*, 2022, **14**, 24351–24362.

91 Z.-S. Ma, H. Yang, K. Xing, K. Zhou, G. Lu and X.-Y. Liu, *Dalton Transactions*, 2024, **53**, 13320–13325.

92 L. Zhao, P. Liu, C. Deng, T. Wang, S. Wang, Y.-J. Tian, J.-S. Zou, X.-C. Wu, Y. Zhang, Y.-L. Peng, Z. Zhang and M. J. Zaworotko, *Nano Res*, 2023, **16**, 12338–12344.

93 C. Liu, J. Wang, J. Wan and C. Yu, *Coord Chem Rev*, 2021, **432**, 213743.

94 J. Letwaba, U. O. Uyor, M. L. Mavhungu, N. O. Achuka and P. A. Popoola, *RSC Adv*, 2024, **14**, 14233–14253.

95 Y. Wang, J. Ma, F. Jin, T. Li, N. Javanmardi, Y. He, G. Zhu, S. Zhang, J. Xu, T. Wang and Z. Feng, *Small Science*, 2024. **4**, 202400132.

96 D. Senthil Raja and D.-H. Tsai, *Chemical Communications*, 2024, **60**, 8497–8515.

97 M. Bilal, M. Adeel, T. Rasheed and H. M. N. Iqbal, *J. of Mater. Res. and Technol.*, 2019, **8**, 2359–2371.

98 S.-H. Feng and G.-H. Li, in *Modern Inorganic Synthetic Chemistry*, Elsevier, 2017, 73–104.

99 D. Sud and G. Kaur, *Polyhedron*, 2021, **193**, 114897.

100 Y. Li, D.-G. Cai, Z.-H. Zhu, H. Xu, T.-F. Zheng, J.-L. Chen, S.-J. Liu and H.-R. Wen, *Dalton Transactions*, 2023, **52**, 4167–4175.

101 Y. Bian, N. Xiong and G. Zhu, *Processes*, 2018, **6**, 122.

102 I. Thomas-Hillman, A. Laybourn, C. Dodds and S. W. Kingman, *J Mater Chem A Mater*, 2018, **6**, 11564–11581.

103 P. T. Phan, J. Hong, N. Tran and T. H. Le, *Nanomaterials*, 2023, **13**, 352.

104 A. Ramos Corona, J. Rodríguez López, R. Rangel Segura, M. M. Martínez Garcia, E. Flores, G. Rodríguez Gattorno and J. J. Alvarado Gil, *Inorg Chem*, 2024, **63**, 19536–19552.

105 J. Klinowski, F. A. Almeida Paz, P. Silva and J. Rocha, *Dalton Trans.*, 2011, **40**, 321–330.

106 P. T. Phan, J. Hong, N. Tran and T. H. Le, *Nanomaterials*, 2023, **13**, 352.

107 S. Tanaka, in *Metal-Organic Frameworks for Biomedical Applications*, Elsevier, 2020, pp. 197–222.

108 Y. Chen, H. Wu, Z. Liu, X. Sun, Q. Xia and Z. Li, *Ind Eng Chem Res*, 2018, **57**, 703–709.

109 L. Sondermann, Q. Smith, T. Strothmann, A. Vollrath, T. H. Yen Beglau and C. Janiak, *RSC Mechanochemistry*, 2024, **1**, 296–307.

110 S. Głowniak, B. Szczęśniak, J. Choma and M. Jaroniec, *Molecules*, 2024, **29**, 2698.

111 W. Wu, G. E. Decker, A. E. Weaver, A. I. Arnoff, E. D. Bloch and J. Rosenthal, *ACS Cent Sci*, 2021, **7**, 1427–1433.

112 H. Ren and T. Wei, *ChemElectroChem*, 2022, **9**, 202200196.

113 D. Ayu Setyowati, W. Wahyu Lestari, R. Adi Nugroho, T. Endah Saraswati, S. Budi Rahardjo, Y. Krisyuningsih Krisnandi, A. Zulfikar Pamungkas and D. Dendy, *ChemistrySelect*, 2024, **9**, 202402046.

114 R. Lalawmpuia, M. Lalhruaitluangi, Lalhmunsiama and D. Tiwari, *Environmental Engineering Research*, 2024, **29**, 230636–0.

115 A. Asghar, N. Iqbal, T. Noor, B. M. Kariuki, L. Kidwell and T. L. Easun, *Green Chemistry*, 2021, **23**, 1220–1227.

116 W.-J. Li, J. Lü, S.-Y. Gao, Q.-H. Li and R. Cao, *J. Mater. Chem. A*, 2014, **2**, 19473–19478.

117 Z.-Q. Li, L.-G. Qiu, T. Xu, Y. Wu, W. Wang, Z.-Y. Wu and X. Jiang, *Mater Lett*, 2009, **63**, 78–80.

118 J. Bedia, V. Muelas-Ramos, M. Peñas-Garzón, A. Gómez-Avilés, J. Rodríguez and C. Belver, *Catalysts*, 2019, **9**, 52.

119 W. M. Bloch, N. R. Champness and C. J. Doonan, *Angew. Chem. Int. Ed.*, 2015, **54**, 12860–12867.

120 J. Martí-Rujas, *Dalton Transactions*, 2020, **49**, 13897–13916.

121 H. L. B. Boström, S. Bette, S. T. Emmerling, M. W. Terban and B. V. Lotsch, *APL Mater*, 2022, **10**, 071106

122 T. Steenhaut, S. Lacour, G. Barozzino-Consiglio, K. Robeyns, R. Crits, S. Hermans and Y. Filinchuk, *Inorg Chem*, 2022, **61**, 11084–11094.

123 J. Berger, A.-S. Dönmez, A. Ullrich, H. Bunzen, R. A. Fischer and G. Kieslich, *Commun Chem*, 2022, **5**, 177.

124 H. M. Ng, N. M. Saidi, F. S. Omar, K. Ramesh, S. Ramesh and S. Bashir, in *Encyclopedia of Polymer Science and Technology*, Wiley, 2018, 1–29.

125 C. Healy, K. M. Patil, B. H. Wilson, L. Hermanspahn, N. C. Harvey-Reid, B. I. Howard, C. Kleinjan, J. Kolien, F. Payet, S. G. Telfer, P. E. Kruger and T. D. Bennett, *Coord Chem Rev*, 2020, **419**, 213388.

126 M. Safinejad, A. Rigi, M. Zeraati, Z. Heidary, S. Jahani, N. P. S. Chauhan and G. Sargazi, *BMC Chem*, 2022, **16**, 93.

127 B. Li, H. Wang and B. Chen, *Chem Asian J*, 2014, **9**, 1474–1498.

128 D. Dubbeldam, K. S. Walton, T. J. H. Vlugt and S. Calero, *Adv Theory Simul*.

129 W. Fan, X. Zhang, Z. Kang, X. Liu and D. Sun, *Coord Chem Rev*, 2021, **443**, 213968.

130 A. Felix Sahayaraj, H. Joy Prabu, J. Maniraj, M. Kannan, M. Bharathi, P. Diwahar and J. Salamon, *J Inorg Organomet Polym Mater*, 2023, **33**, 1757–1781.

131 K. Nath, K. R. Wright, A. Ahmed, D. J. Siegel and A. J. Matzger, *J Am Chem Soc*, 2024, **146**, 10517–10523.

132 R. Li, X. Han, Q. Liu, A. Qian, F. Zhu, J. Hu, J. Fan, H. Shen, J. Liu, X. Pu, H. Xu and B. Mu, *ACS Omega*, 2022, **7**, 20081–20091.

133 M. Kubo, T. Matsumoto and M. Shimada, *Materials*, 2023, **16**, 5416.

134 A. Ahmed, S. Seth, J. Purewal, A. G. Wong-Foy, M. Veenstra, A. J. Matzger and D. J. Siegel, *Nat Commun*, 2019, **10**, 1568.

135 A. G. Wong-Foy, A. J. Matzger and O. M. Yaghi, *J Am Chem Soc*, 2006, **128**, 3494–3495.

136 Z. Chen, K. O. Kirlikovali, K. B. Idrees, M. C. Wasson and O. K. Farha, *Chem*, 2022, **8**, 693–716.

137 X. Lin, I. Telepeni, A. J. Blake, A. Dailly, C. M. Brown, J. M. Simmons, M. Zoppi, G. S. Walker, K. M. Thomas, T. J. Mays, P. Hubberstey, N. R. Champness and M. Schröder, *J Am Chem Soc*, 2009, **131**, 2159–2171.

138 O. K. Farha, A. Özgür Yazaydın, I. Eryazici, C. D. Malliakas, B. G. Hauser, M. G. Kanatzidis, S. T. Nguyen, R. Q. Snurr and J. T. Hupp, *Nat Chem*, 2010, **2**, 944–948.

139 H. Furukawa, N. Ko, Y. B. Go, N. Aratani, S. B. Choi, E. Choi, A. Ö. Yazaydin, R. Q. Snurr, M. O'Keeffe, J. Kim and O. M. Yaghi, *Science (1979)*, 2010, **329**, 424–428.

140 C. Dey, T. Kundu, B. P. Biswal, A. Mallick and R. Banerjee, *Acta Crystallogr B Struct Sci Cryst Eng Mater*, 2014, **70**, 3–10.

141 J. F. Olorunyomi, S. T. Geh, R. A. Caruso and C. M. Doherty, *Mater Horiz*, 2021, **8**, 2387–2419.

142 W. P. Lustig, S. Mukherjee, N. D. Rudd, A. V. Desai, J. Li and S. K. Ghosh, *Chem Soc Rev*, 2017, **46**, 3242–3285.

143 N. Kajal, V. Singh, R. Gupta and S. Gautam, *Environ Res*, 2022, **204**, 112320.

144 D. Zhao, Y. Cui, Y. Yang and G. Qian, *CrystEngComm*, 2016, **18**, 3746–3759.

145 T. Rasheed and F. Nabeel, *Coord Chem Rev*, 2019, **401**, 213065.

146 M.-L. Hu, S. A. A. Razavi, M. Piroozzadeh and A. Morsali, *Inorg Chem Front*, 2020, **7**, 1598–1632.

147 S. Mukherjee and S. K. Ghosh, *Nat Rev Chem*, 2021, **5**, 600–601.

148 M. L. P. Reddy and S. Sivakumar, *Dalton Trans.*, 2013, **42**, 2663–2678.

149 N. K. Shee and H.-J. Kim, *Int J Mol Sci*, 2024, **25**, 4183.

150 Y. Zhao, Q. Wang, H. Wang, H. Zhangsun, X. Sun, T. Bu, Y. Liu, W. Wang, Z. Xu and L. Wang, *Sens Actuators B Chem*, 2021, **334**, 129610.

151 S.-S. Chen, L.-L. Li, S. Liu, S.-Y. Liu, W.-Z. Wang and X.-H. Xu, *J Mol Struct*, 2024, **1302**, 137504.

152 D. E. P. Vanpoucke, *The J. of Phys. Chem. C*, 2017, **121**, 8014–8022.

153 L. S. Xie, G. Skorupskii and M. Dincă, *Chem Rev*, 2020, **120**, 8536–8580.

154 Z. Han, T. Sun, R.-R. Liang, Y. Guo, Y. Yang, M. Wang, Y. Mao, P. R. Taylor, W. Shi, K.-Y. Wang and H.-C. Zhou, *J Am Chem Soc*, 2024, **146**, 15446–15452.

155 J.-J. Liu, Z.-J. Wang, S.-B. Xia, J. Liu and X. Shen, *Dyes and Pigments*, 2020, **172**, 107856.

156 J. Dong, D. Zhao, Y. Lu and W.-Y. Sun, *J Mater Chem A Mater*, 2019, **7**, 22744–22767.

157 S. Khatua, C. Krishnaraj, D. C. Baruah, P. Van Der Voort and H. S. Jena, *Dalton Transactions*, 2021, **50**, 14513–14531.

158 R. H. Alzard, L. A. Siddig, N. Saleh, H. L. Nguyen, Q. A. T. Nguyen, T. H. Ho, V. Q. Bui, K. Sethupathi, P. K. Sreejith and A. Alzamly, *Sci Rep*, 2022, **12**, 18812.

159 B. E. Meteku, J. Huang, J. Zeng, F. Subhan, F. Feng, Y. Zhang, Z. Qiu, S. Aslam, G. Li and Z. Yan, *Coord Chem Rev*, 2020, **413**, 213261.

160 W. Feng, Y. Liu, Y. Bi, X. Su, C. Lu, X. Han, Y. Ma, C. Feng and M. Ma, *Synth Met*, 2023, **294**, 117307.

161 C. Wang, X. Liu, T. Yang, D. Sridhar, H. Algadi, B. Bin Xu, Z. M. El-Bahy, H. Li, Y. Ma, T. Li and Z. Guo, *Sep Purif Technol*, 2023, **320**, 124144.

162 R. Wang, H. Qi, H. Zheng and Q. Jia, *Chinese Chemical Letters*, 2024, **35**, 109215.

163 A. E. Thorarinsdottir and T. D. Harris, *Chem Rev*, 2020, **120**, 8716–8789.

164 M. Arczyński and D. Pinkowicz, *Inorg Chem*, 2020, **59**, 13489–13501.

Chapter two

2.0 NDI Linkers Used in MOF Synthesis

2.1 Introduction

Naphthalene diimide (NDI) linkers are a class of organic ligands or building blocks used in the construction of Metal-Organic Frameworks (MOFs) and other coordination polymers.[1] MOFs are crystalline materials composed of metal ions or clusters connected by organic linkers.[2] NDI linkers have gained attention in recent years due to their unique structural and electronic properties, which make them valuable components in the design of MOFs and other porous materials.[3] NDI linkers consist of naphthalene diimide units, which are planar, aromatic molecules with a distinctive shape.[4] This planar structure allows for strong π-π stacking interactions when functionalised with a ligand binding group (pyridyl or carboxylate etc) which are key features in MOF design.[3] NDI linkers typically coordinate with metal ions through the group that is attached to the NDI, for example, pyridyl, commonly through the imide. This coordination forms strong and stable metal-ligand bonds, serving as the basis for the construction of MOF structures.[5] The coordination between NDI linkers and metal nodes can be highly tuneable, allowing for precise control over MOF properties.[6]

NDI linkers are known for their electron-deficient nature – a characteristic that makes them suitable for applications involving electron transport, charge transfer, and optoelectronic devices.[7] In MOFs, the electronic properties of NDI linkers can influence the overall electronic behaviour of the material.[8] Moreover, NDI linkers are modifiable via the introduction of different functional groups. These unique tunability properties allow for the customization of MOF properties, such as pore size, surface area, and chemical reactivity.[9] NDI-based MOFs

are often chemically stable, which is crucial for many applications, including catalysis, gas storage, and drug delivery.[10] The stability of these MOFs can be attributed to the strong metal-ligand bonds and the inherent chemical robustness of NDI linkers. Tailoring NDI linkers for specific applications is a common strategy in MOF synthesis.[11] NDI-based MOFs have been explored in a range of applications, including gas storage (hydrogen, methane, CO_2), gas separation, catalysis (heterogeneous catalysis), sensing (chemical sensors for gases and analytes), and drug delivery (encapsulation and controlled release of therapeutic agents).[12] Overall, NDI linkers offer versatility and unique electronic properties in MOF design which has expanded the range of MOF structures and functionalities, and ongoing research continues to explore new NDI-based MOFs for various applications in materials science and beyond.[13] It's important to note that the exact properties and uses of NDI compounds can vary depending on the specific derivative and the application in question.

There are several variations of NDI compounds but the most used for the synthesis of MOFs are either the carboxylate or the pyridyl NDI based in which the functional groups are attached via the imide region of the core NDI. The carboxylate and pyridyl NDIs are symmetrically designed with the same functional group at both ends. Usually, the carboxylate-based NDIs are toxic while the pyridyl-based NDIs are ditopic compounds. [14] Different types of NDI linkers are presented in scheme 2.1

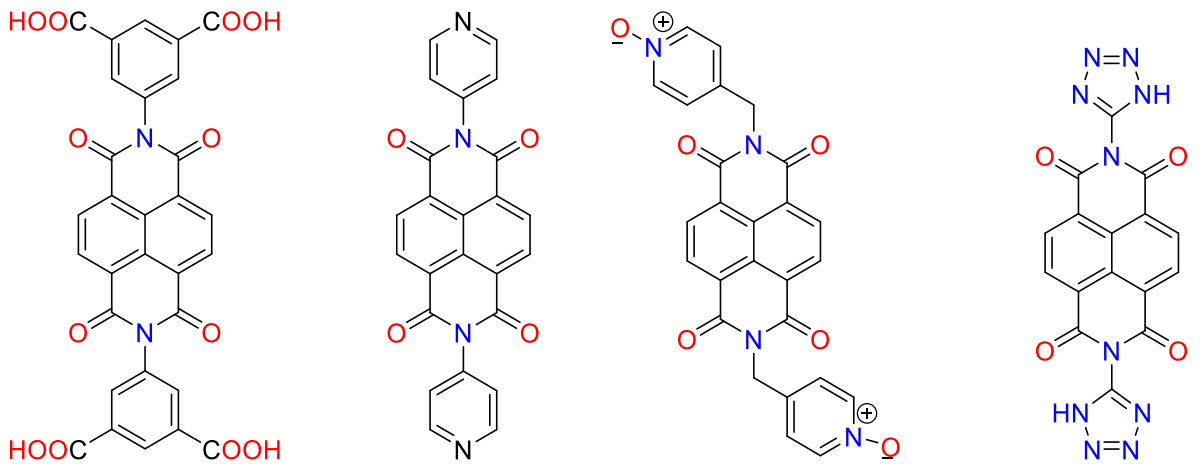

Scheme 2.1 Shows some NDI linkers used in the synthesis of MOFs: (a) carboxylic-based NDI;[15] [16](b)pyridyl-based NDI;[17,18] (c) N-oxydic pyridyl-based NDI;[19] and (d) azolate-based NDI;[20]

2.2 Aim

The research described in this chapter was aimed to synthesize a dinicotinic naphthalene diimide (DNNDI) ligand with the purpose of making lanthanide MOFs. The ligand and the lanthanide MOF were characterized by single crystal X-ray diffraction techniques and other spectroscopic techniques such as FTIR, TGA, and UV-visible and nuclear magnetic resonance.

2.3 Result and Discussion

2.3.1 Linker synthesis

NDI linker based on nicotinic acid was synthesized for use in the construction of lanthanide metal-organic frameworks. The synthesis followed a modified literature procedure.[21] A solution of 1,4,5,8-naphthalenete tracarboxylic bisanhydride (NTCA)and 5-amino nicotinic acid was dissolved in 20 mL of DMF in a 50 mL two-neck flask. The solution was heated under stirring at 100 ºC for 15 minutes forming a white cloudy suspension. 800 mg of 1,4,5,8-

naphthalenetetracarboxylic dianhydride (NTCDA) was added giving rise to a brown solution. After 20 h, the reaction was cooled to room temperature. The solid component was filtered under vacuum and washed with DMF, acetone, and diethyl ether to obtain an off-white powder with a yield of 94.5%. ^{1}H NMR (400 MHz; $CDCl_3$) δ=13.71 (s, 2H), 9.19 (d, *J*=1.8, 2H), 8.92 (d, *J*=2.3, 2H)8.78 (s, 4H)8.52(m, 2H),7.96(s, 2H) scheme 2.2 presents the synthesis pathway for the reaction.

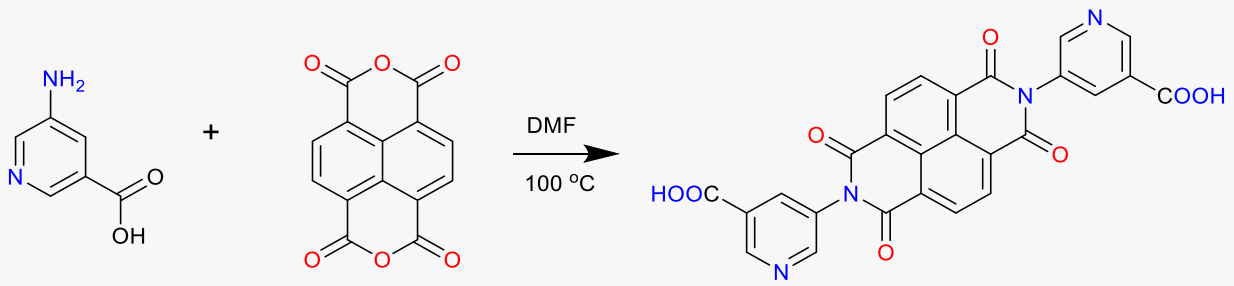

Scheme 2.2: Shows the synthesis of Dinicotinic naphthalene diimide (DNNDI) Ligand;[21]

2.3.2: Single Crystal X-Ray Crystallographic Studies of DNNDI

Crystals of the DNNDI linker were obtained from its toluene solution in slow evaporation. A single crystal was selected and mounted on a single crystal X-ray diffractometer. During data collection, the crystal was kept at 100k and solved with SHELXT using the Olex2[22] structure solution program. Structural refinement gave rise to the structure depicted in Figure 2.1.

Figure 2.1: View of the single crystal structure of DNNDI. Carbon - grey; Oxygen – red; nitrogen – blue

2.3.3 Fourier-Transform Infrared Spectroscopy (FTIR)

Fourier-transform infrared spectroscopy (FTIR) is a powerful analytical technique used to identify functional groups, characterize chemical bonds, and analyze the molecular structure of a wide range of materials. It provides information about the vibrational modes of molecules, which arise from the interactions between atoms within the molecule. Figure 2.2 shows the FTIR spectrum of the DNNDI ligand. The spectrum shows absorption bands between 3600-3650 cm^{-1} that is for O-H starching vibration, 300-3100 cm^{-1} which is assigned to C-H stretching (sp^2 hybridized C-H) bonds from the carboxylic acid groups, 1717 cm^{-1} for imide C=O asymmetric stretch, and 1682 cm^{-1} for carboxyl C=O stretching and imide C=O symmetrical stretching which confirmed the presence of carboxylic acid groups and imide ring.

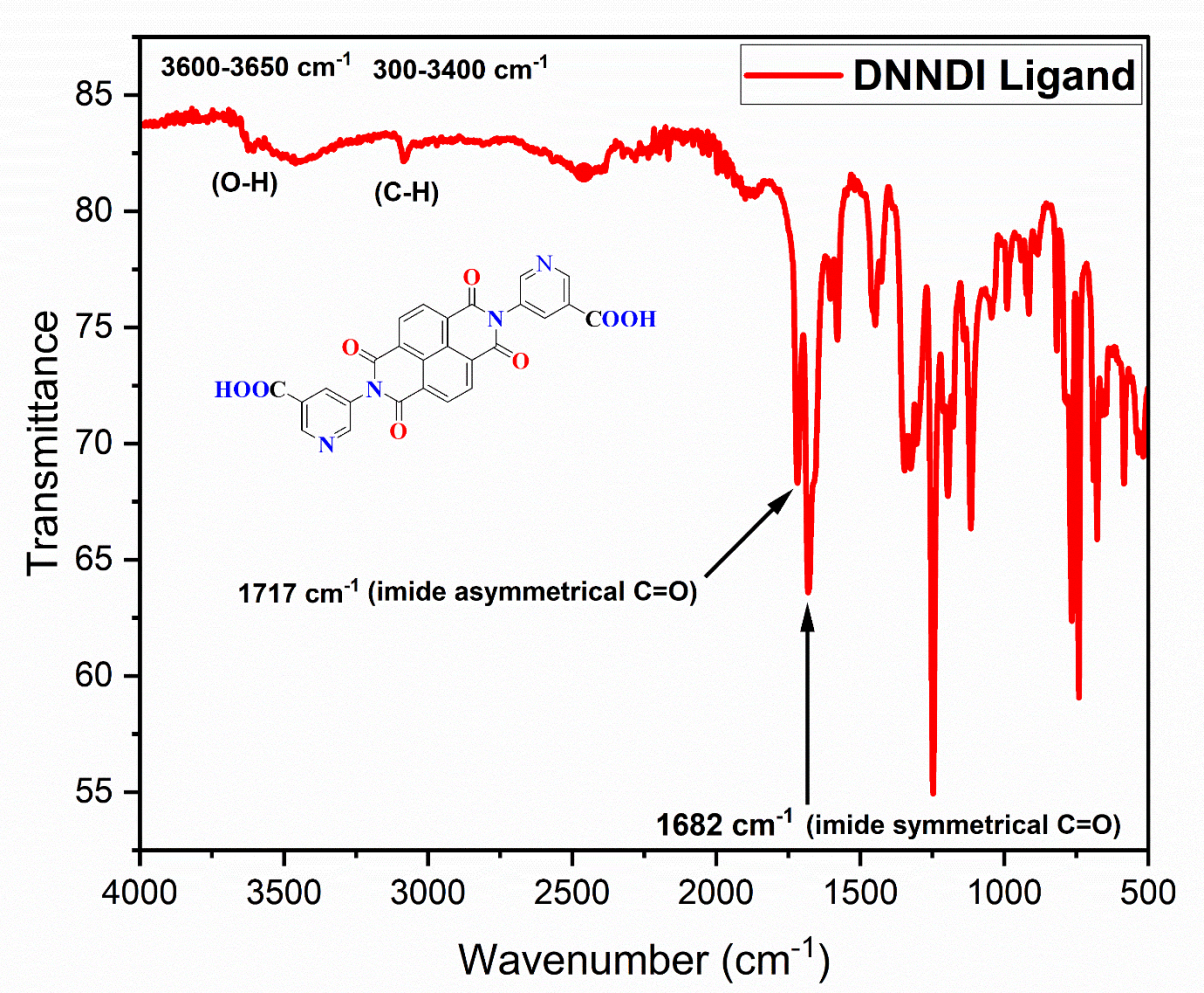

Figure 2.2 FTIR Spectrum of solid Dinicotic Naphthalene Diimide (DNNDI)

2.3.4 Thermogravimetric (TGA) and Differential Thermogravimetric (DTG) Analysis

The TGA/DTG of the DNNDI ligand was studied. 10 mg of the sample was used for thermogravimetric analysis to gain insight into the stability of the material. It was observed that there was no loss of any solvent molecules at 85 ºC and 245 ºC, and decomposition of the material at 400 ºC as shown in Figure 2.3.:

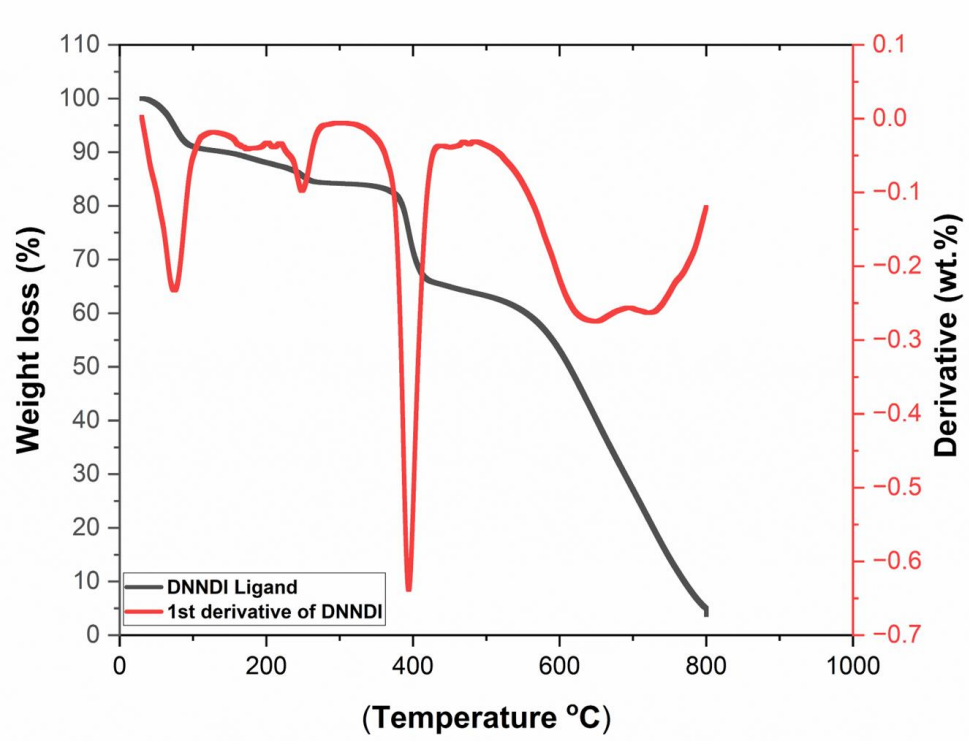

Figure 2.3: TGA/DTG of Dinicotinic Naphthalene Diimide Ligand (black line is the weight loss in % while the Red line is the derivative of the weight lost in %)

2.3.5 UV- Vis Spectroscopic measurement

The absorption spectrum of a molecule provides information about the electronic transitions occurring within the material. In solids, the absorption spectrum can be influenced by various factors such as band structure, electronic states, crystal structure, and the presence of defects or impurities. These factors can result in characteristic absorption bands or peaks in the spectrum, which can be analyzed to determine the properties of the molecule, or material. Figure 2.4 presents the solid-state UV-vis absorption spectrum of DNNDI ligand, recorded using 10 mg of sample. The spectrum of DNNDI shows a strong absorbance in the UV wavelength range of 200 – 450 nm, corresponding to π-π* transitions within the aromatic core of the NDI. This type of absorbance shift and the charge-transfer bands are consistent with the NDI molecules.[23,24]

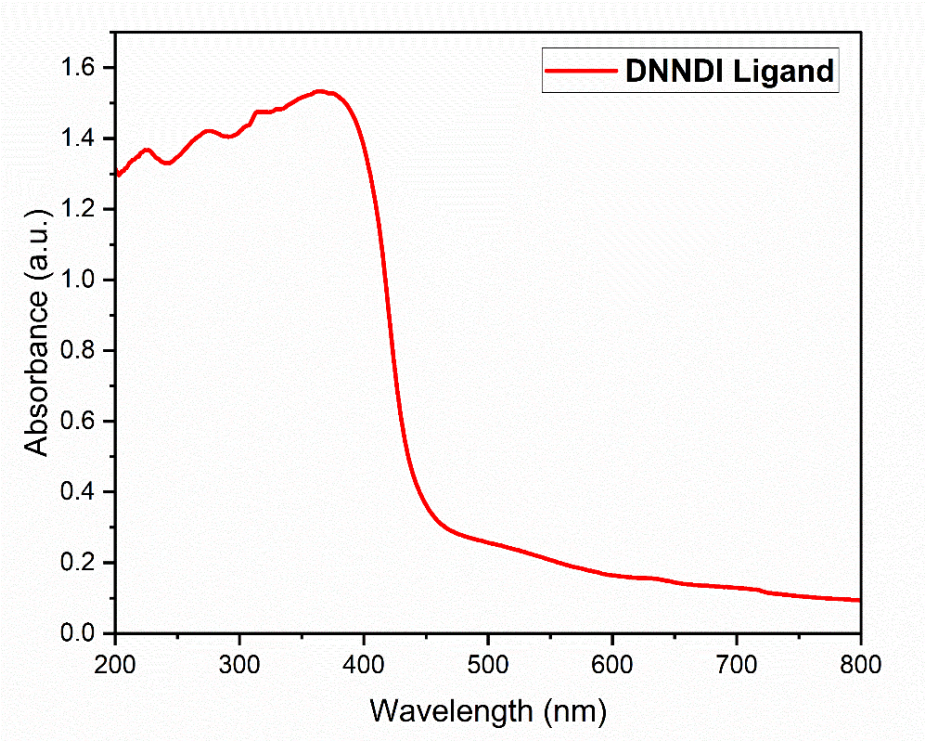

Figure 2.4: Solid state UV-Vis absorption spectrum for Dinicotinic Naphthalene diimide ligand.

2.4 Conclusion

The synthesis of dinicotinic naphthalene diimide ligand (DNNDI) was successful following a reported procedure using NDA and 5-amino nicotinic acid. Various characterization techniques including NMR, FTIR, UV, and TGA were employed to ascertain the viability of the material that was intended to be used for the construction of the metal-organic framework with lanthanide clusters reported in Chapter Three.

2.5 Synthesis of Nicotinic Acid NDI Metal-Organic Frameworks

2.5.1 Introduction

Herein, the hydrothermal synthesis of the seven-novel isostructural DNNDI-MOFs based on lanthanide metals (Y(III) Sm(III), Er(III) Yb(III) and Lu(III)) are reported. Lanthanide MOFs are a subclass of MOFs that incorporate lanthanide elements into their structures.[25–27] Lanthanides are known for their unique electronic configuration which makes them interesting candidates for a variety of applications.[28] When incorporated into MOFs, lanthanides can introduce specific properties and functionalities, such as fluorescence and magnetism, to these porous materials. Nicotinic acid and its derivatives have been used to make a variety of different coordination networks, with distinct connectivity caused by the presence of pyridyl nitrogen and the carboxylic attachment.[29,30] Similarly, nicotinic acids are functionalized to act as coordinative sites by incorporating the substituent groups.[31,32] Nicotinic acid-containing MOFs have gained interest in various applications due to their unique properties and the potential applications for nicotinic acid (also known as niacin or vitamin B3) as a ligand. These applications span from healthcare to environmental and industrial uses.[33–35] MOFs constructed with either NDI based ligands or nicotinic acid in combination with different metal clusters have been extensively reported.[36–39] But there is little or no information about the use of nicotinic acid functionalised NDI ligands for the purpose of synthesizing MOFs. Scheme 2.3 shows some nicotinic acids used as ligands in the synthesis of MOFs.

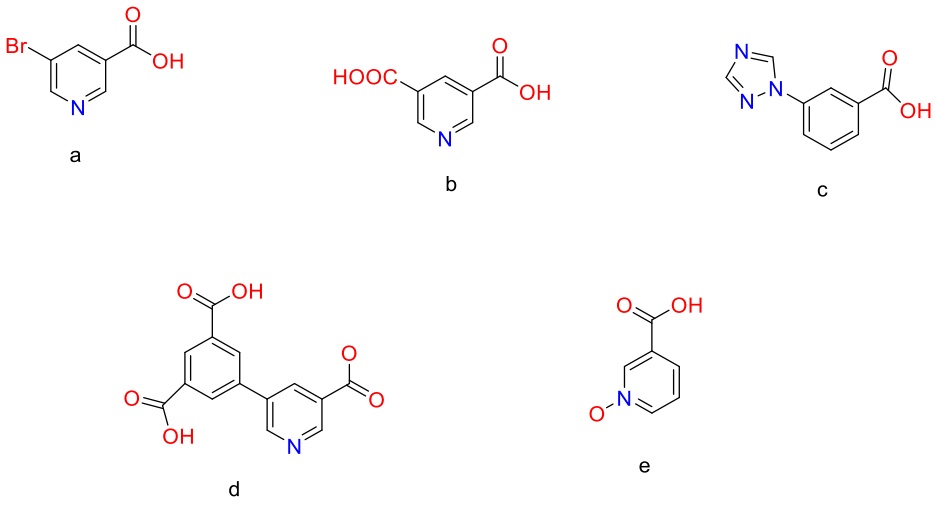

Scheme 2.3 is the representation of some nicotinic acid used in MOF synthesis.

2.6 Result and Discussion

The solvothermal method of synthesis was employed in carrying out the crystallization of the lanthanide metal-organic frameworks with the DNNDI ligand reported in this chapter. In this thesis this traditional method of synthesis was performed in scintillation vials which have been pre-treated with Sigmacote, reaction mixtures were sonicated for 5-10 minutes prior to heating facilitating MOFs synthesis. Several attempts were made using different metal-to-ligand ratios, solvent concentrations, and reaction times. Successful syntheses resulted in the crystallization of needle-like materials suitable for X-ray diffraction experiments. Two different crystal systems, monoclinic or tetragonal, were seen in the resulting MOFs. The frameworks observed were isotopological, with each MOF adopting the same framework structure. Two examples, one for each crystal system, will be discussed in this chapter, as representative examples of the MOF structures, with the aim of identifying differences in the structures. The general synthetic method for these frameworks is seen as summarized in Scheme 2.4.

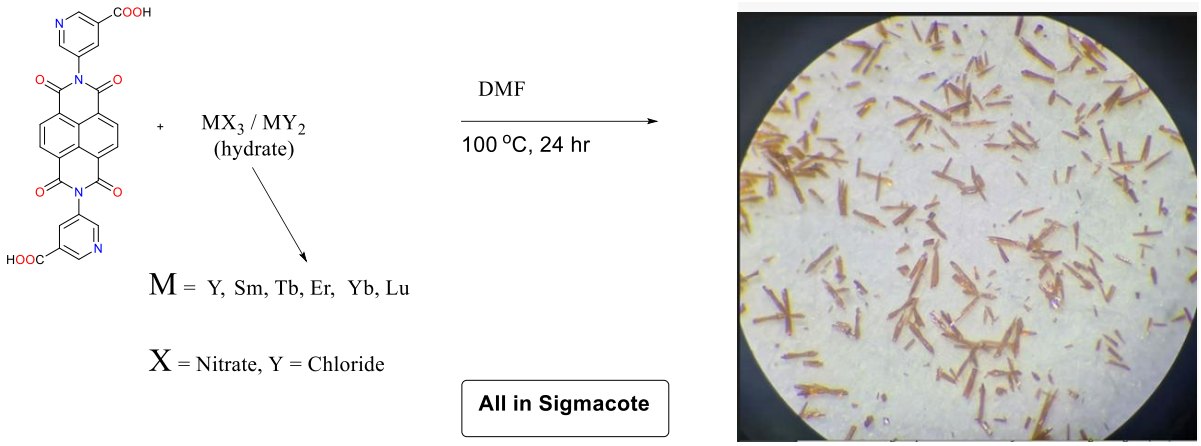

Scheme 2.4 Pictures the General Synthetic Method for the LN-DNNDI Framework

2.6.1: Powder–ray diffraction experiment

As displayed in Figure 2.5, the structure of the crystalline material for all the compounds was also assessed by powder X-ray diffraction (PXRD). The diffraction patterns were recorded at diffraction angles which range from 2Θ values of 5 to 70º. The pattern of the PXRD for five Ln-MOFs confirmed the presence of porous material having some sharp and distinct peaks. Although based on the PXRD data also, the MOFs can be regarded as disordered since the peaks are few in each. Different methods for the PXRD measurement and orientation such as 'spin' and 'no-spin', different sample holders (PMMA and low background holders), and different solvents (acetone and methanol) that do not affect the crystallinity of the material were used, the best peaks intensities were observed in the 'no-spin' orientation measurement. When compared to the simulated patterns, however, little did we say about the similarities which could be due to lanthanide contraction, prepared orientation, or the presence of unreacted starting material.

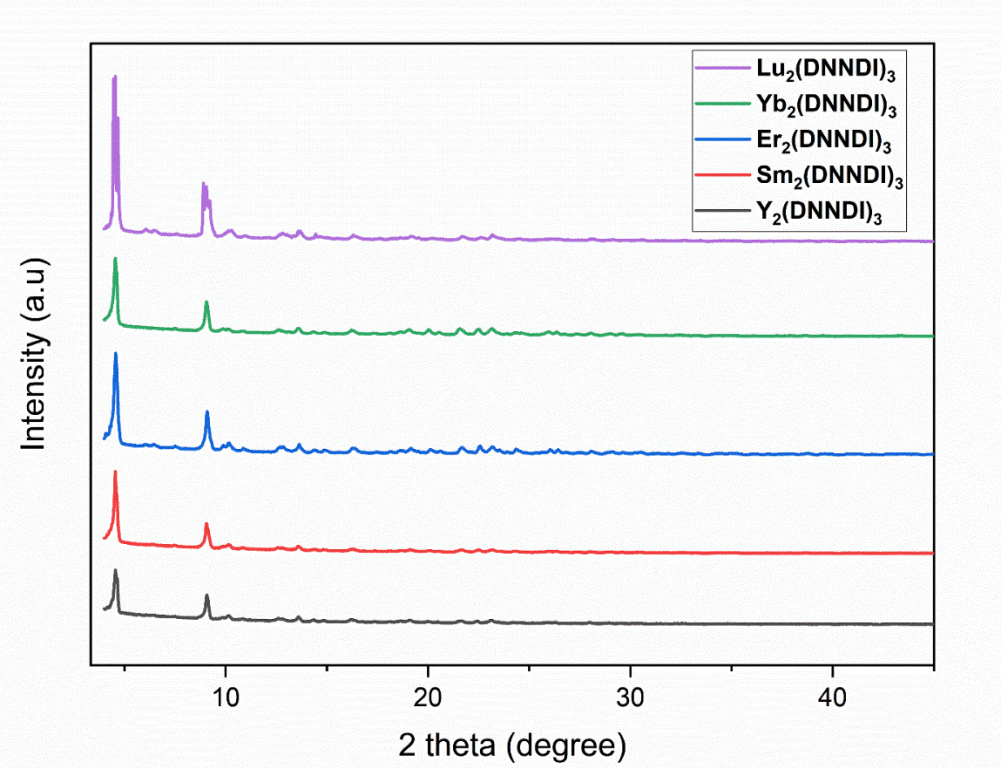

Figure 2.5 PXRD patterns of Five Lanthanoid MOFs with DNNDI Linker measured with No-spin Orientation.

Since the frameworks are istopological and in similar crystal systems, with four being tetragonal and one monoclinic crystal system, one system for each will be discussed in this chapter to compare their differences and study their similarities.

2.6.2 Synthesis and Crystal Structure of $Yb_2(DNNDI)_3$

Crystals of $Yb_2(DNNDI)_3$ suitable for study by single crystal X-ray diffraction experiments were solvothermally prepared through the reaction of $Yb(NO_3)_3.5H_2O$ with DNNDI in a 20 mL Sigmacoted scintillation vial, using DMF as solvent and tightly capped. The reaction was carried out for 24 h at a temperature of 100 °C. During single crystal diffraction analysis, the

crystal was kept at 120 K during data collection on a single crystal X-ray diffractometer. Using Olex2[40], the structure was solved with the SHELXT[41] structure solution program using intrinsic phasing and refined with the SHELX[41] refinement package using least square minimization. The crystal data refinement parameters for 1 are given in Table 2.1 below:

Table 2.1: Crystallographic Data and Refinement Parameters for 1 (NB: The empirical formula for this was deduced after the solvent had been removed

Empirical formula	**$C_{45}H_{29}N_8O_{14}Yb$**
Formula weight	1078.80
Temperature/K	120(2)
Crystal system	Tetragonal
Space group	$I4_1/a$
a/Å	38.6305(2)
b/Å	38.6305(2)
c/Å	16.02120(10)
α/°	90
β/°	90
γ/°	90
Volume/Å^3	23908.7(3)
Z	16
ρ_{calc}g/cm^3	1.199
μ/mm^{-1}	3.393
F(000)	8592.0
Crystal size/mm^3	0.450 × 0.080 × 0.080

Radiation	CuKα (λ = 1.54184)
2Θ range for data collection/°	5.972 to 157.97
Index ranges	-49 ≤ h ≤ 49, -48 ≤ k ≤ 46, -19 ≤ l ≤ 13
Reflections collected	89838
Independent reflections	12658 [R_{int} = 0.0489, R_{sigma} = 0.0251]
Data/restraints/parameters	12658/0/617
Goodness-of-fit on F^2	1.050
Final R indexes [I>=2σ (I)]	R_1 = 0.0381, wR_2 = 0.0986
Final R indexes [all data]	R_1 = 0.0414, wR_2 = 0.1011
Largest diff. peak/hole / e $Å^{-3}$	0.62/-0.79

Single crystal data analysis of the $Yb_2(DNNDI)_3$ compound reveals that it crystallizes in the tetragonal centrosymmetric space group $I4_1/a$. The asymmetric unit Figure 2.6 comprises a ytterbium atom, a full, and a half DNNDI ligand both of which are coordinated to Yb (III) in a monodentate fashion, one metal-coordinated DMF and a half-occupied solvate DMF, as shown in Figure 2.6.

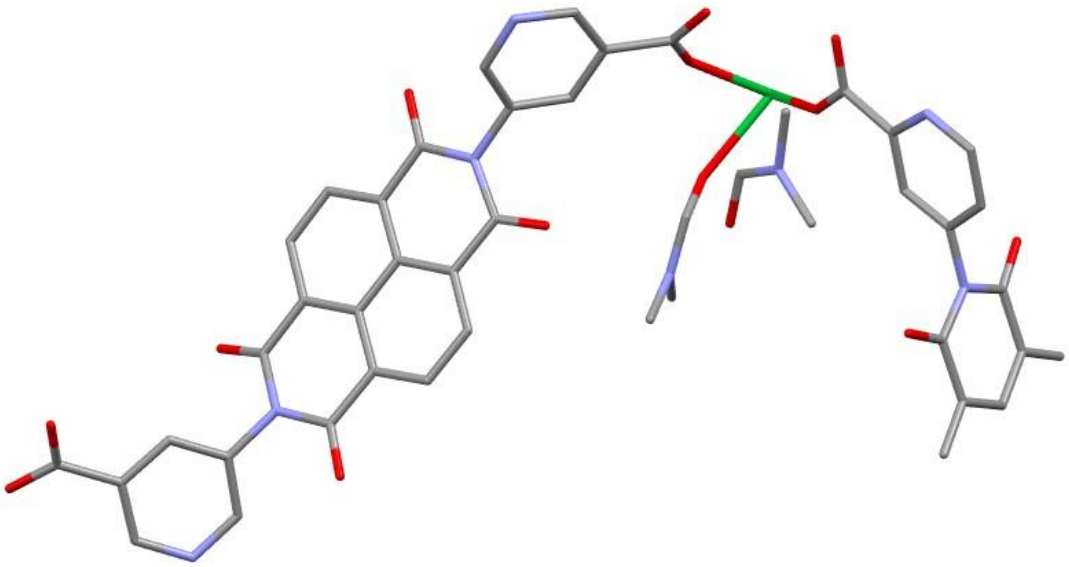

Figure 2.6 Asymmetric Unit of $Yb_2(DNNDI)_3$ Metal Organic Framework (grey = C, green = Yb, blue = N and red = oxygen; hydrogen atoms have been omitted for clarity).

The extended structure of $Yb_2(DNNDI)_3$ is a three-dimensional framework based on a Yb-O-C rod secondary building unit (SBU)[42] that is composed of 8 coordinated Yb(III) cations with a distorted bicapped trigonal prism geometry[43] around the central metal atom shown, see Figure 2.7 and 2.8. Six carboxylate groups are bonded to each ytterbium atom from a different DNNDI ligand and terminal DMF molecule. The carboxyl groups are bonded to the metal atom in different fashions, with four coordinated to the metal in a bridging bis-bidentate fashion and two carboxylates bonded to the metal centre respectively in a chelating/bridging bidentate fashion mode A at one end and bridging bidentate mode at the other end as in mode B and B' shown in Scheme 2.5. Each rod is joined at the edge and corner to form the YbO_8 polyhedra. The ligand, DNNDI unit connects each rod to four neighboring rods and also exhibits an anti-conformation.[44]

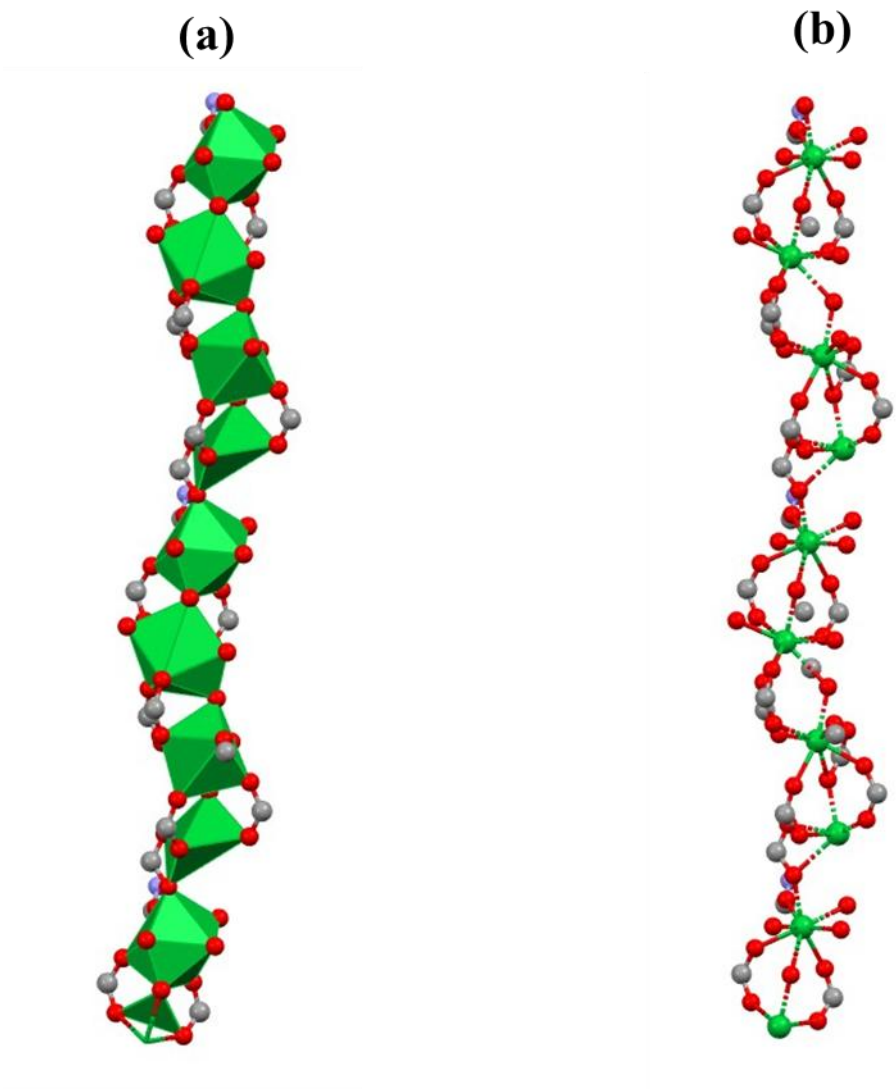

Figure 2.7 Secondary building unit of $Yb_2(DNNDI)_3$ MOF showing (a) Polyhedral representation and (b) ball and stick, both viewed along the crystallographic a-axis.

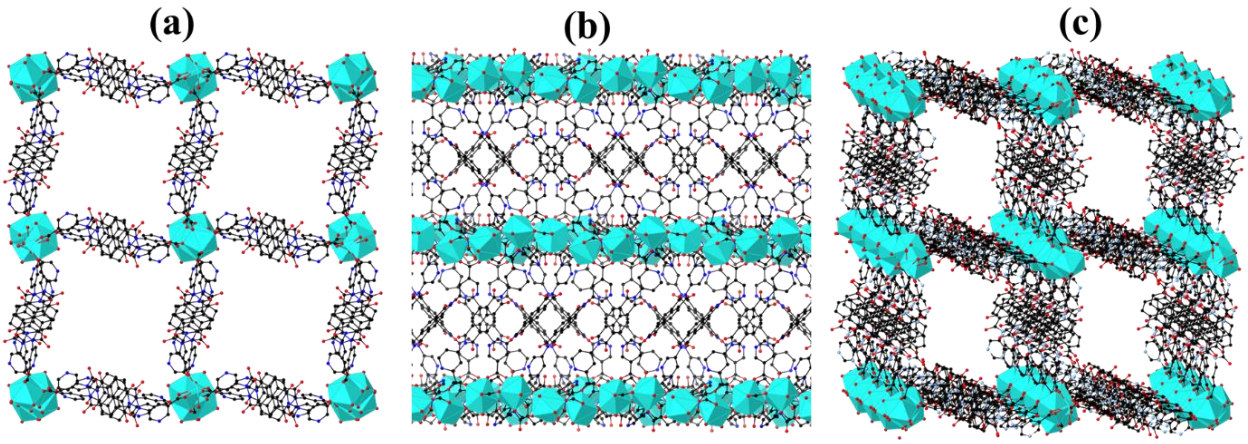

Figure 2.8 Secondary building unit of $Yb_2(DNNDI)_3$ MOF showing (a) Framework structure of the same MOF showing the pores (b) showing how the SBUs are linked to form the framework viewed along the c-crystallographic axis. (c) a twisted view showing how metal are pointing to the pores

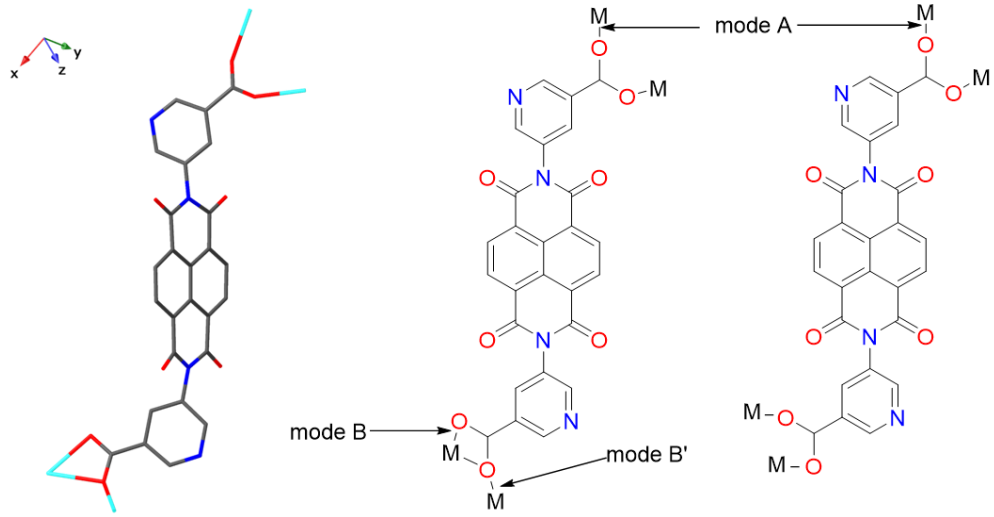

Scheme 2.5: Anti-conformation in coordination nodes shown by DNNDI ligand in $Yb_2(DNNDI)_3$ MOF.

2.6.3: Synthesis and Crystal Structure of $Sm_2(DNNDI)_3$ MOF

A crystal of $Sm_2(DNNDI)_3$ compound suitable for single X-ray diffraction was prepared by the reaction of a mixture of $SmCl_2$ and DNNDI with 2mL DMF and 1mL water in a tightly capped 20mL scintillation vial. The mixture was stirred for 5-20 minutes and allowed to crystallize for 48 hours in 80 ºC oven. The structure of the MOF was confirmed by SCXRD. During data collection on a single crystal diffractometer, the crystals were kept at 120 K. The structural data obtained were solved with the SHELXT[41] structure solution program using intrinsic phasing and refined with the SHELX[41] refinement package using Least Square minimization. on Olex2[40]. The crystal data refinement parameter for $Sm_2(DNNDI)_3$ is given in Table 3.2.

Figure 2.9 shows the asymmetric unit which consists of two independent samarium atoms with three molecules of DNNDI. In addition, two molecules of DMF are coordinated to the metal with three and half ordered free DMF molecules and another six disordered DMF molecules in the pores. The distorted DMFs were removed by solvent-masked[40] function in Olex-2. Each Sm(III) is coordinated to two DMF molecule. Also, in a bridging isomonodentate fashion, all the metal clusters are surrounded by two carboxylic groups with one from DNNDI molecule and the other from a different DNNDI molecule.

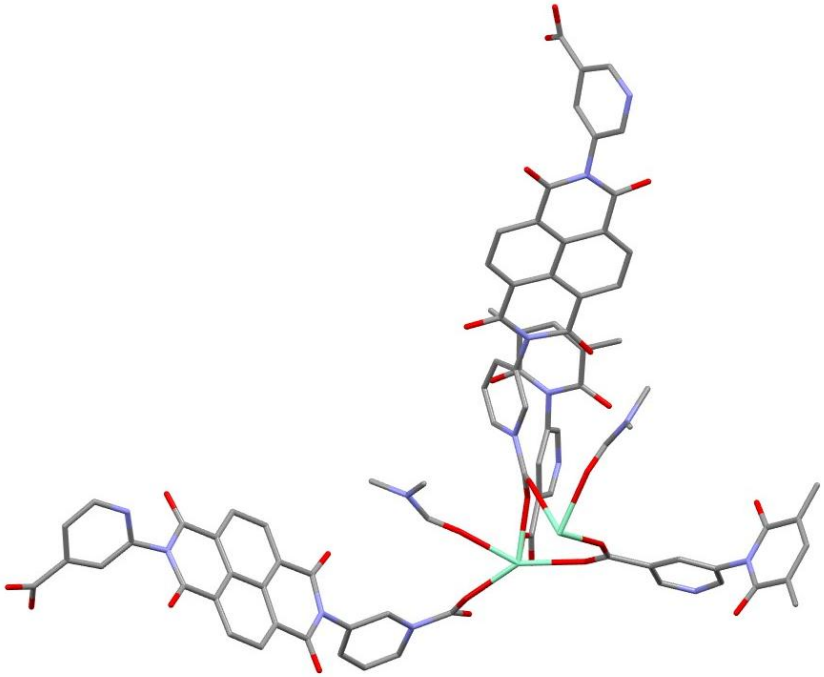

Figure 2.9: Asymmetric unit of $Sm_2(DNNDNI)_3$ view along the crystallographic b-axis. (Cyan = samarium, blue=nitrogen, red=oxygen and grey=scarbon, hydrogen and DMF molecules were omitted for clarity)

Figure 2.10 displays the extended structure of $Sm_2(DNNDI)_3$. It was observed that the MOF based on Sm(III) is analogous, isotopological to the Yb(III) compound discussed above, with similar secondary building blocks and bonds around the central metal atom and DMF molecules pointing into the pore from each angle. By using Mercury crystal software[45], the solvent-accessible void for $Sm_2(DNNDI)_3$ was calculated to be 11079.33 Å/unit cell (i.e., 44.8%) is accessible to solvent as seen also in Figure 2.10.

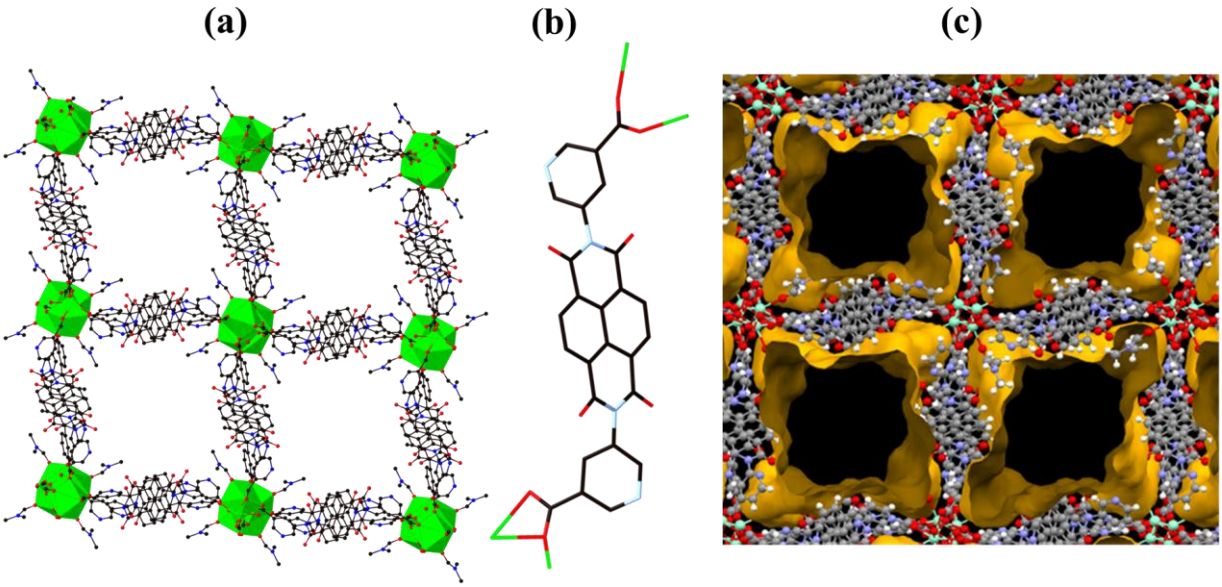

Figure 2.10: Extended structure of $Sm_2(DNNDI)_3$ picturing (a) the pores and (b) metal to ligand bond and (c)`solvent accessible void (Cyan= Samarium, blue=nitrogen, red=oxygen and grey=carbon, hydrogen and guest DMF molecules were omitted for clarity)

Table 2.2: Crystallographic Data and Refinement Parameters for $Sm_2(DNNDI)_3$

Empirical formula	$C_{42}H_{23}N_7O_{13}Sm$
Formula weight	984.02
Temperature/K	100.15
Crystal system	monoclinic
Space group	I2/a
a/Å	39.1295(6)
b/Å	16.30700(10)
c/Å	38.8870(5)

α/°	90
β/°	95.2930(10)
γ/°	90
Volume/Å^3	24707.4(5)
Z	16
ρ_{calc}g/cm^3	1.058
μ/mm^{-1}	7.574
F(000)	7840.0
Crystal size/mm^3	0.178 × 0.033 × 0.022
Radiation	Cu Kα (λ = 1.54178)
2Θ range for data collection/°	4.536 to 140.14
Index ranges	-46 ≤ h ≤ 47, -15 ≤ k ≤ 19, -43 ≤ l ≤ 47
Reflections collected	195403
Independent reflections	23345 [R_{int} = 0.0919, R_{sigma} = 0.0404]
Data/restraints/parameters	23345/0/1139
Goodness-of-fit on F^2	1.081
Final R indexes [I>=2σ (I)]	R_1 = 0.0938, wR_2 = 0.2593
Final R indexes [all data]	R_1 = 0.1059, wR_2 = 0.2701
Largest diff. peak/hole / e Å^{-3}	4.62/-2.24

2.6.4 Thermogravimetric analysis (TGA) and Differential thermogravimetric

This is a technique used to study the thermal stability and decomposition of MOF materials. It involves measuring the weight change of a sample as a function of temperature or time while it is subjected to a controlled temperature program. In the context of MOFs, TGA is often used to investigate their thermal stability. The analysis involves the gradual heating of a sample of

the MOF and recording the weight loss as a function of temperature. In principle, a thermally stable material will experience little or no change in mass as a result of heating the sample. TGA determines the maximum temperature of a MOF material, and it collapses at a slight increase above that temperature. [46–48] Figure 2.11 depicts thermogravimetric analysis carried out on as-synthesised MOF materials which allows assessment of the thermal stability recorded between 100 ^{o}C – 900 ^{o}C and at a heating rate of 10 ^{o}C min^{-1}. Materials employed for this study were recorded using samples where the original reaction solvent (DMF) had been washed with acetone. It was observed that pore and coordinated solvent molecules were lost between 50-300 ^{0}C. It was also observed that all the framework structures are stable up to about 465 ^{0}C after which there were sharp slopes of the materials which signifies the collapse of the materials.

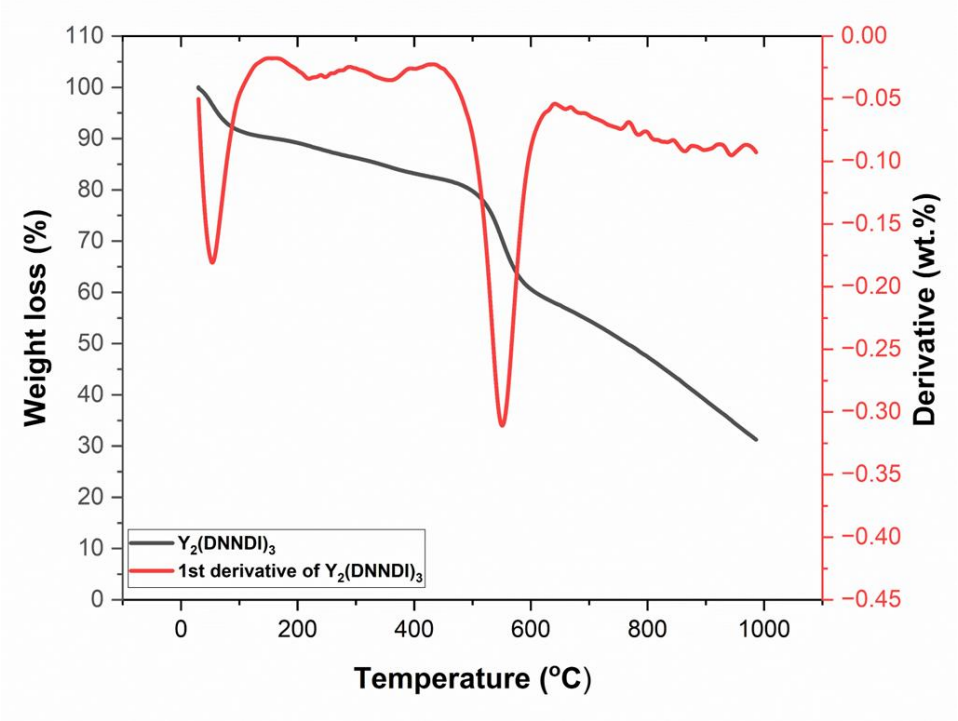

Figure 2.11: Shows the TGA-DTG thermogram and 1st derivative for $Y_2(DNNDI)_3$ MOF (black line is the weight loss in % while the Red line is the derivative of the weight lost in %

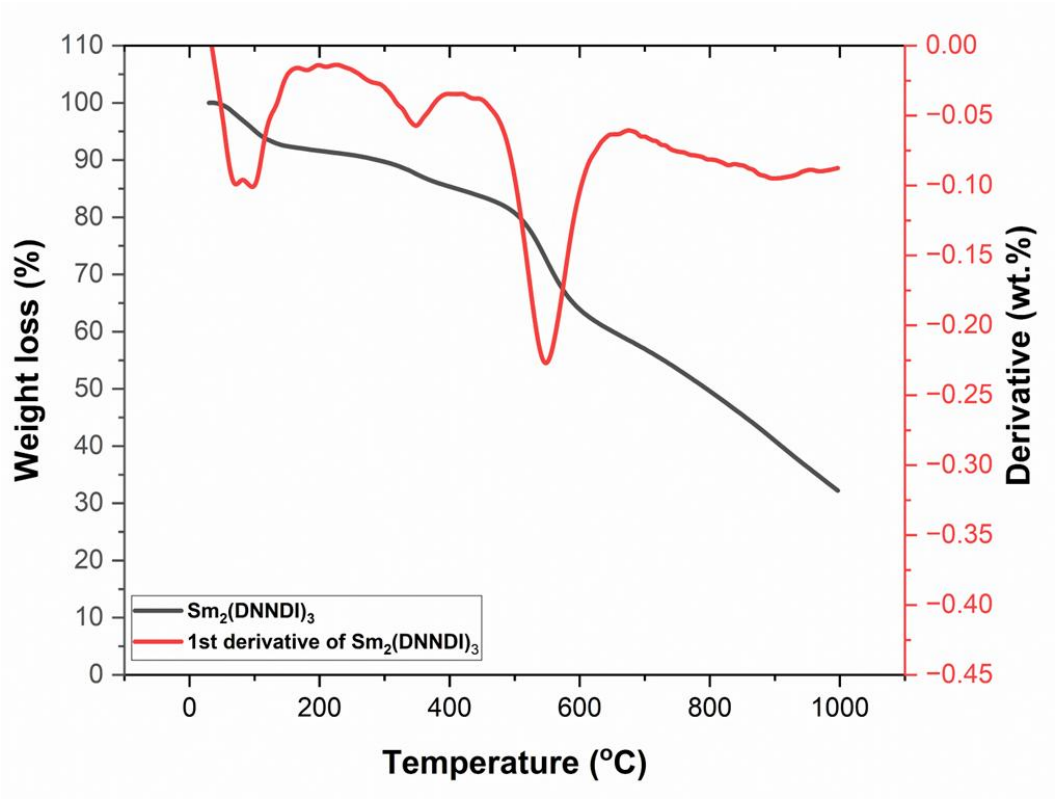

Figure 2.12: Shows the TGA-DTG thermogram and 1st derivative for $Sm_2(DNNDI)_3$ MOF (black line is the weight loss in % while the red line is the derivative of the weight lost in %)

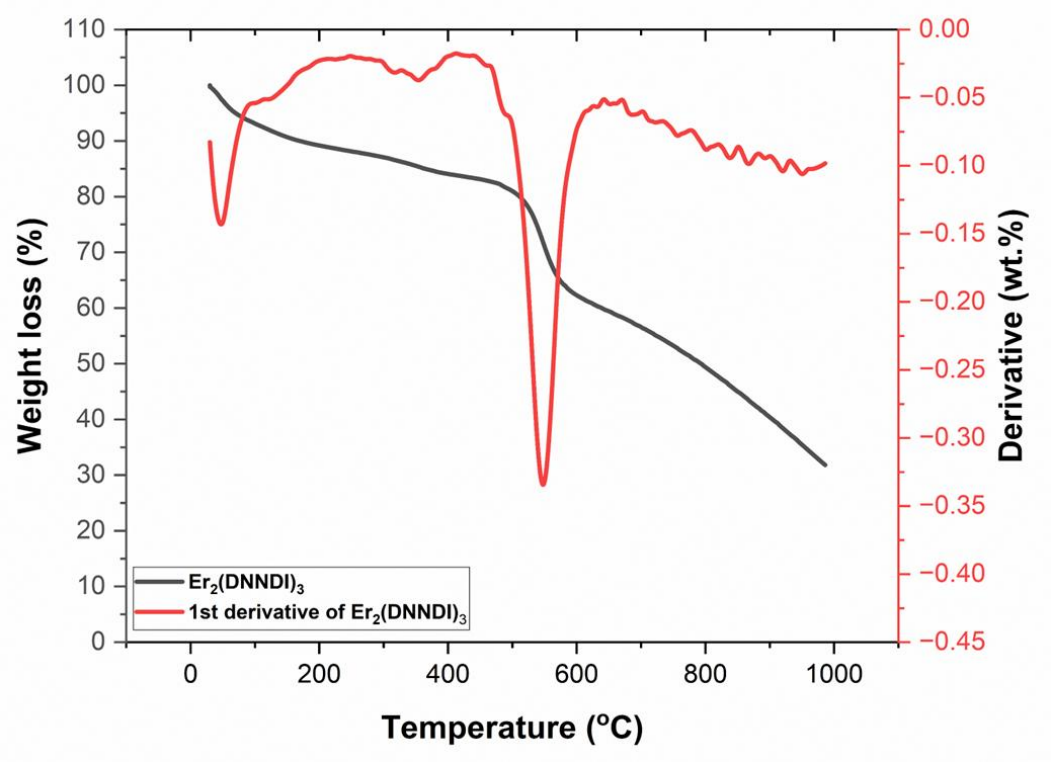

Figure 2.13: Shows the TGA-DTG thermogram and 1st derivative for $Er_2(DNNDI)_3$ MOF (black line is the weight loss in % while the red line is the derivative of the weight lost in %)

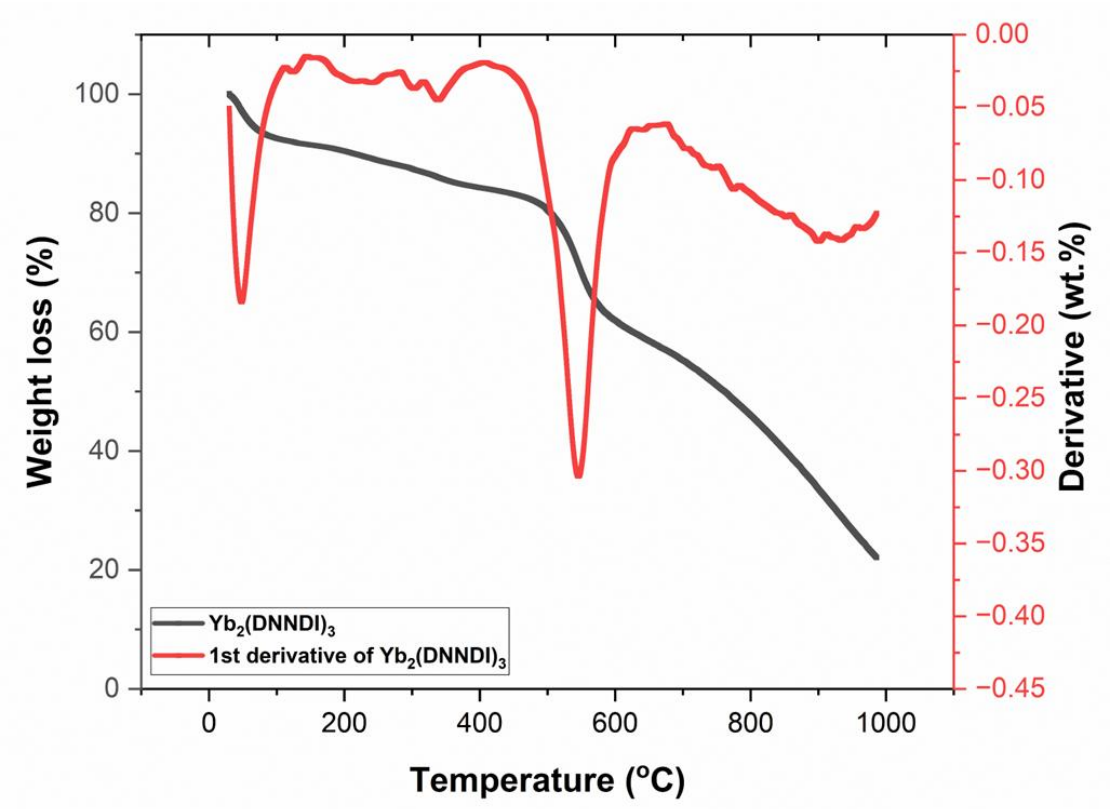

Figure 2.14: Shows the TGA-DTG thermogram and 1st derivative $Yb_2(DNNDI)_3$ MOF (black line is the weight loss in % while the red line is the derivative of the weight lost in %)

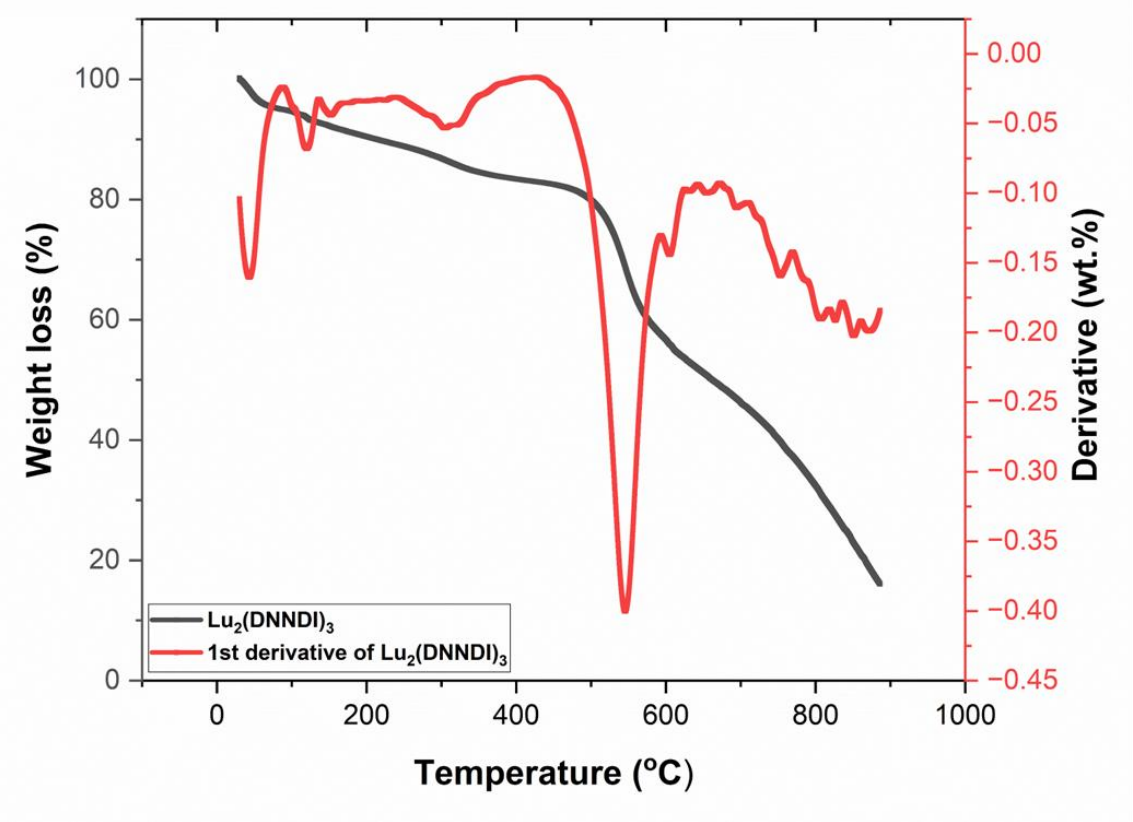

Figure 2.15 Shows the TGA-DTG thermogram and 1st derivative for $Lu_2(DNNDI)_3$. MOF (black line is the weight loss in % while the red line is the derivative of the weight lost in %)

2.6.5 UV-Vis Spectroscopy

MOFs typically exhibit electronic transitions in the UV-visible range due to the presence of metal centres and organic ligands.[49,50] These transitions involve the promotion of electrons from filled to empty orbitals, such as π-π* or metal-to-ligand charge transfer (MLCT) transitions.[51,52] Uv/vis spectroscopy can identify these transitions and provide information about the electronic structure of the MOF.[53,54] Figure 2.16 Presents the UV-Vis spectroscopic analysis of all the as-synthesised MOFs alongside the ligand. Solid-state UV-visible spectroscopy was employed to analyse all the systems to gain insight into the electronic structure and properties of the MOFs. It was observed that there was a significant difference

between the framework systems and the ligand as a result of irradiation and radical formation with an increase in absorption gradually across the spectrum. The structures of the irradiated samples were also observed to be similar to the original sample as shown in the PXRD plots and TGA curves above.

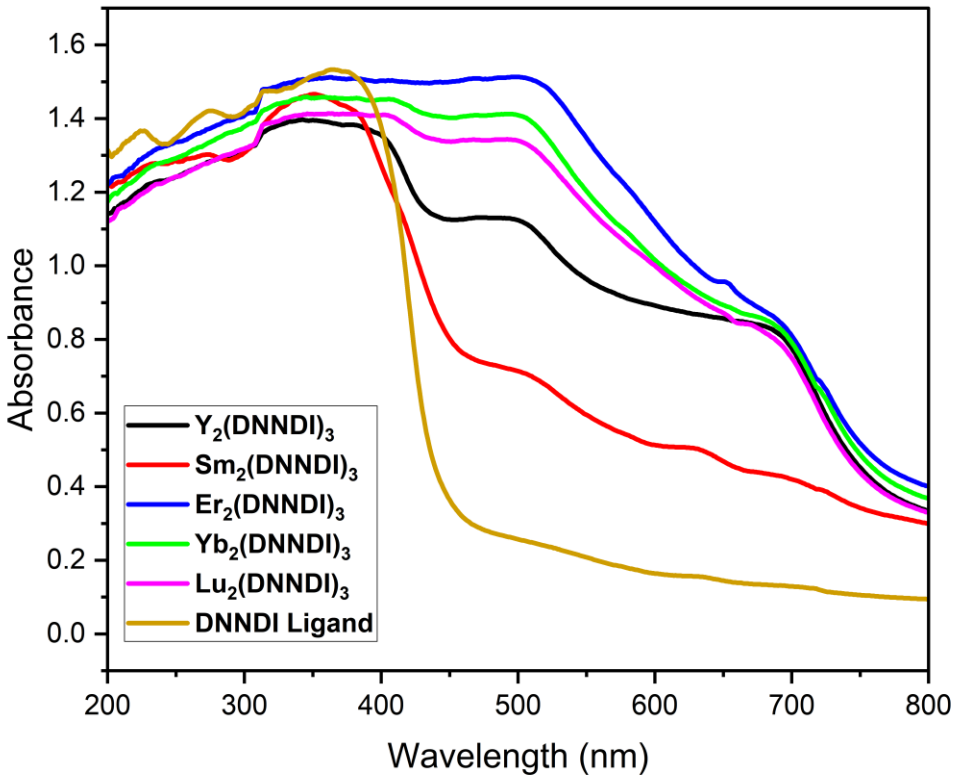

Figure 2.16: Shows the solid-state UV-vis spectroscopic Data of the As-synthesized Ln-MOFs.

2.6.6 Fourier Transform Infrared Spectroscopy (FTIR)

FTIR spectroscopy was employed to characterize the as-synthesized Ln-MOFs and the identification of new functional groups in the systems. Figure 2.17 presents the infra-red spectra for the five MOFs. The spectra of all the MOFs and the 'free' DNNDI ligand showed nearly the same peaks except for $Y_2(DNNDI)_3$ and $Yb_2(DNNDI)_3$ where two broad bands at

2980 cm^{-1} and 2935 cm^{-1} were observed. These bands are attributed to the CH stretching vibration of DNNDI ligand and guest organic molecules.[55] By comparing the FTIR spectra of MOFs with that of the free DNNDI linker, there were only minor peak differences with small shifts in the carbonyl region (ca. 1600 cm^{-1}). The two strong bands at 1629 cm^{-1} and 1662 cm^{-1} for Y/Yb-MOFs were assigned to the asymmetric and symmetric modes of coordinated groups respectively.[56] A shift to a lower wavenumber of carboxylate functionality confirms the coordination between the lanthanide ion and the carbonyl groups.

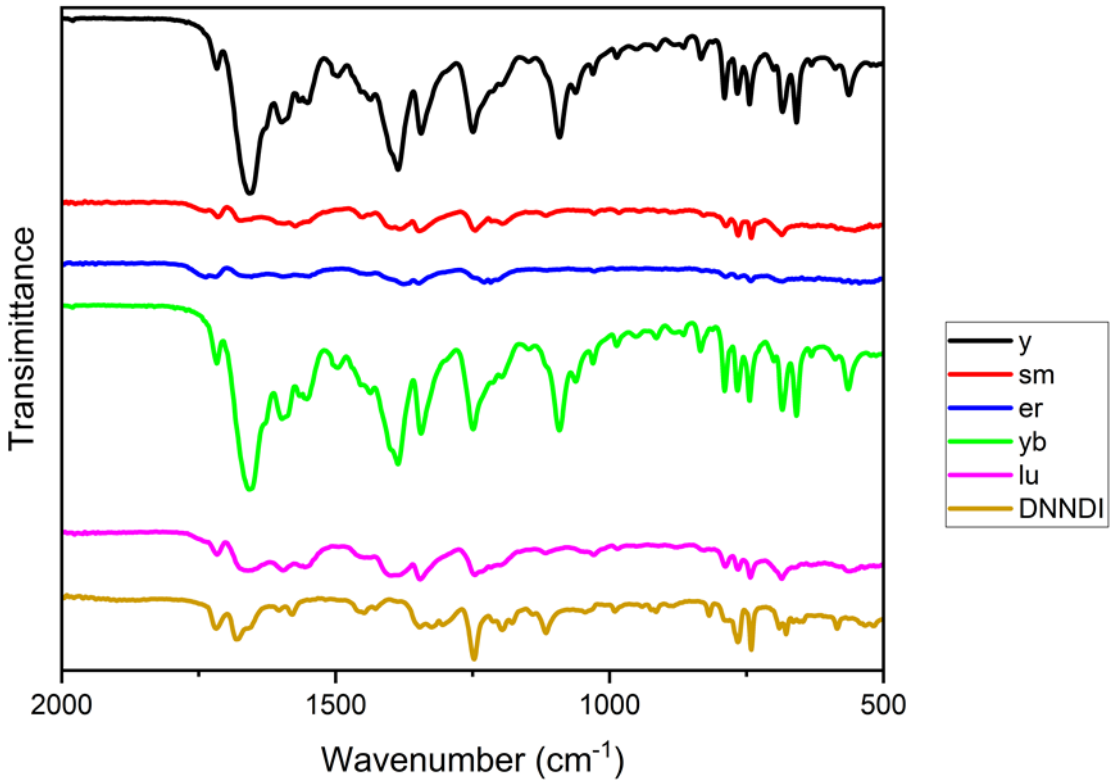

Figure 2.17: Solid state FTIR spectra for all the as-synthesized Ln-MOFs and Naphthalene diimide Ligand (DNNDI) Ligand.

2.6.7 Brunauer-Emmett-Teller (BET) Surface Area Analysis

Brunauer -Emmet-Teller and Barrett-Joyner – Halenda (BJH) methods were explored to study the surface properties including surface area, pore size, pore distribution, and pore diameter of all the framework materials. Figure 2.18 shows the nitrogen adsorption-desorption isotherms of the as-synthesized lanthanide MOFs, with measurements made using the BET method. A steady increase in N_2 adsorption was observed between p/p_0 0.4 and 0.9 for both $Sm_2(DNNDI)_3$ and $Yb_2(DNNDI)_3$ MOFs which signifies the presence of mesoporeous materials. Following this, the framework materials could also be classified as type I isotherms, for having high fractions of fine micropores and low fractions of mesopores.

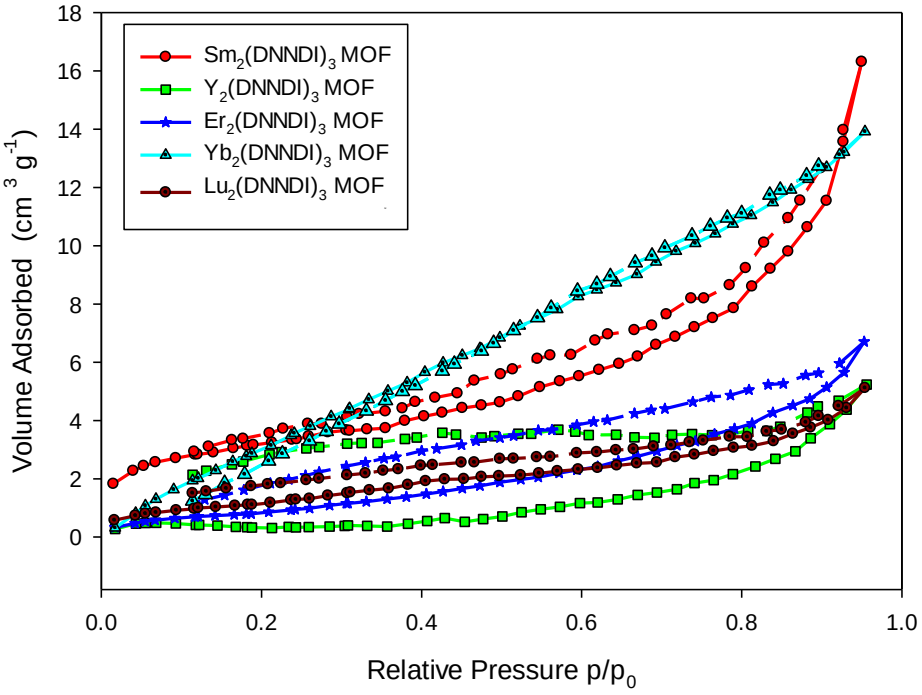

Figure 2.18: Showing the N_2 Adsorption Isotherms of As-synthesized Ln-MOFs.

2.6.8 Scanning Electron Microscopy (SEM)/ Energy Dispersive X-Ray Analysis (EDX)

The SEM images of all the as-synthesized MOFs were studied, see Figure 2.19, and these clearly show that all of the MOFs adopt needle-like single crystalline materials. Dimensions of the crystals are in the range of 700 nm -1.2 µm. When coupled with EDX, information about elemental composition and distribution in all the systems was obtained which shows the presence and percentage of all the elements in the MOFs.

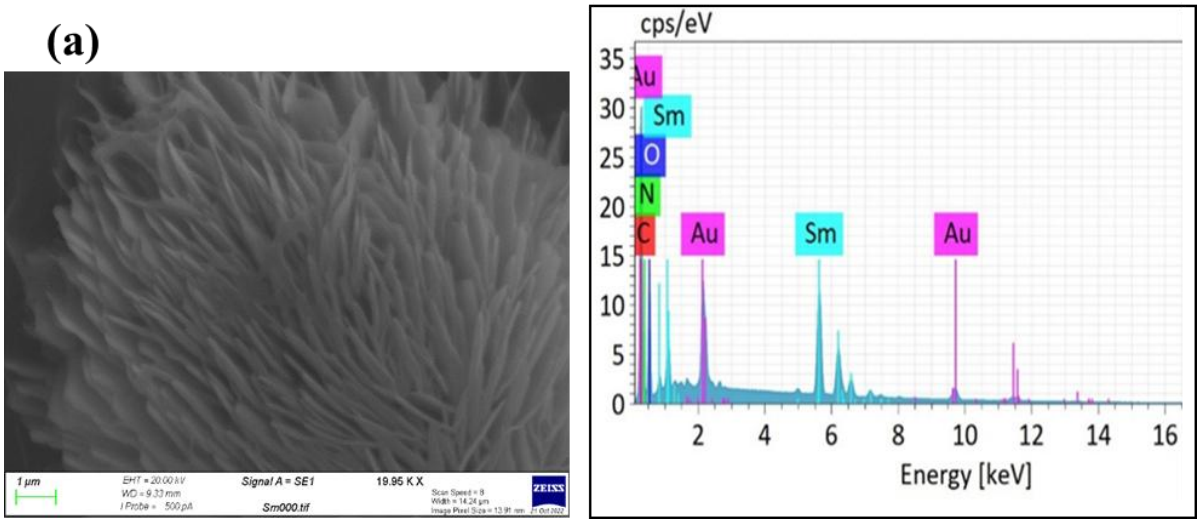

(b)

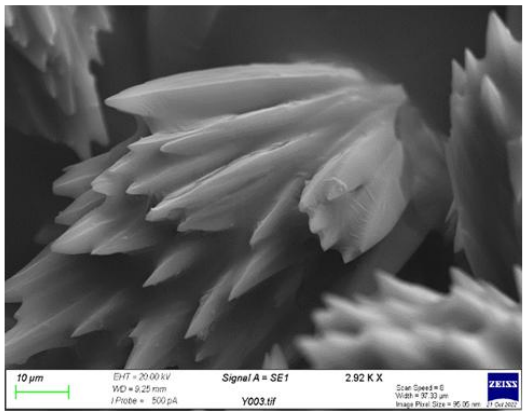
10 µm
Signal A = SE1
2.92 K X
Y003.tif

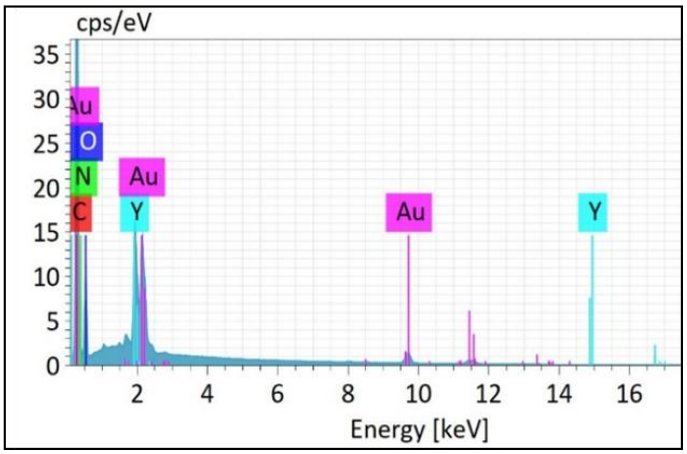
cps/eV
35
30
25
20
15
10
5
0
Au
O
N
C
Au
Y
Au
Y
2
4
6
8
10
12
14
16
Energy [keV]

(c)

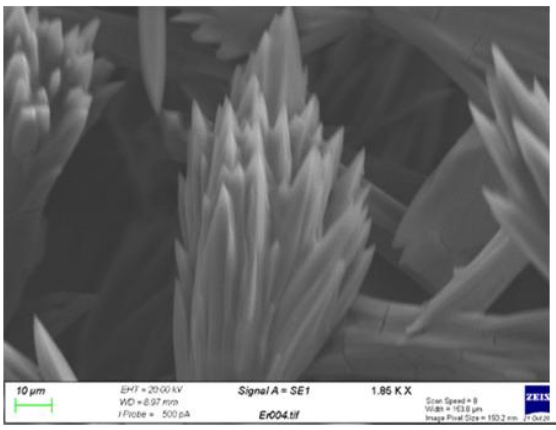
10 µm
Signal A = SE1
1.95 K X
Er004.tif

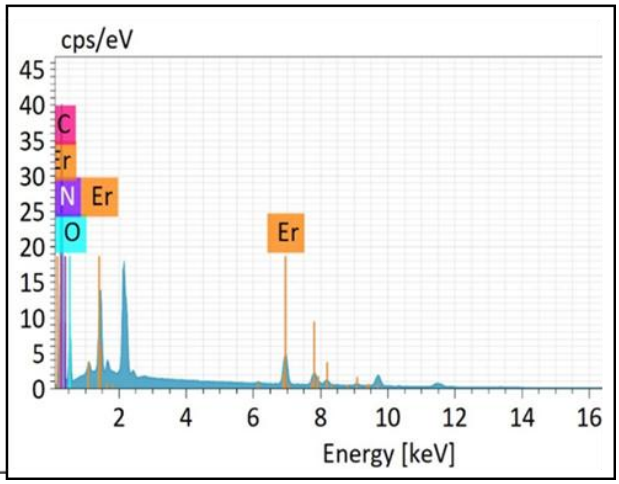
cps/eV
45
40
35
30
25
20
15
10
5
0
C
N
Er
O
Er
2
4
6
8
10
12
14
16
Energy [keV]

(d)

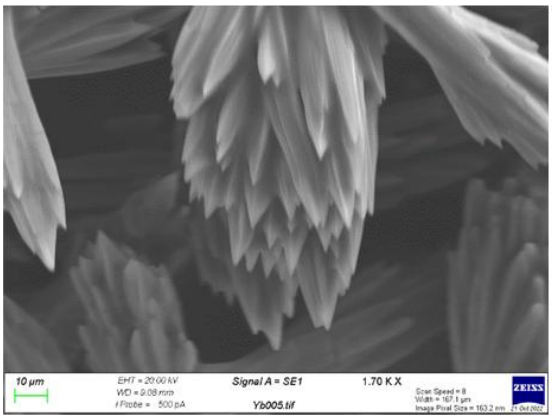
10 µm
Signal A = SE1
1.70 K X
Yb005.tif

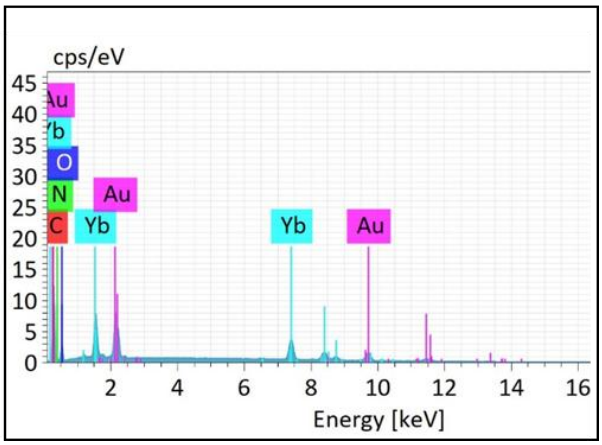
cps/eV
45
40
35
30
25
20
15
10
5
0
Au
O
N
Au
C
Yb
Yb
Au
2
4
6
8
10
12
14
16
Energy [keV]

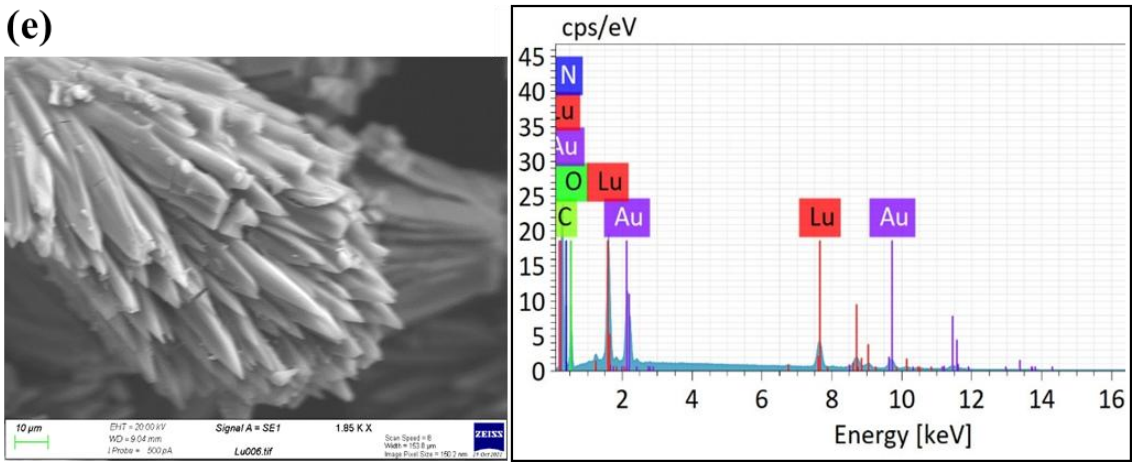

Figure 2.19: SEM images left and EDX right for (a)$Sm_2(DNNDI)_3$, (b) $Y_2(DNNDI)_3$, (c) $Er_3(DNNDI)_3$, (d) $Yb_2(DNNDI)_3$ and (e) $Lu_2(DNNDI)_3$ MOF.

2.7 Conclusion

Novel lanthanide metal-organic frameworks based on a naphthalene diimide ligand (DNNDI) were synthesized and the framework was characterized by different techniques including single crystal X-ray crystallography, powder X-ray diffraction, IR and UV-visible spectroscopic analysis, and electron microscopy. Five different lanthanide ions, yttrium, samarium, erbium, ytterbium, and lutetium, were used for the construction of the framework systems. Whilst the framework based on Er(III), Yb(III), Y(III), and Lu(III) crystallized in the tetragonal space group *I*41/a, Yb(III) crystallizes in the monoclinic space group *C*2/c. The MOFs are isostructural and isotopological having been built from the same SBUs. Thermal stability and N_2 adsorption were studied for all the MOFs. PXRD patterns of all the systems were found to be similar. The UV-vis spectra were studied for all MOFs and found to be as anticipated for NDI-based MOF systems. The thermal stability and differential gravimetric of the systems were used to determine the exact weight loss of the systems. It was also observed that in all the systems reported in this chapter, the pyridyl nitrogens of the nicotinic acid groups do not

coordinate to the lanthanides, as expected, which suggests that they may potentially be used for post-synthetic modifications with guests.

2.8 Material Method

2.8.1 Synthesis of [$Sm_2(DNNDI)_3.DMF.H_20$]

To a 25 mL sigma coted scintillation vial containing 17.4 mg (0.068mmol) of $SmCl_2$ and 17mg (0.034mmol) of DNNDI, 2mL of DMF and 1 mL H_2O were added and sonicated for five minutes until all reagents completely dissolved. The vial was tightly capped and transferred into an oven at 120 ° C for 24hrs. The resulting solids were needle-like colourless crystals which were separated and washed with fresh DMF. Samples suitable for X-ray diffraction studies were collected and analysed.

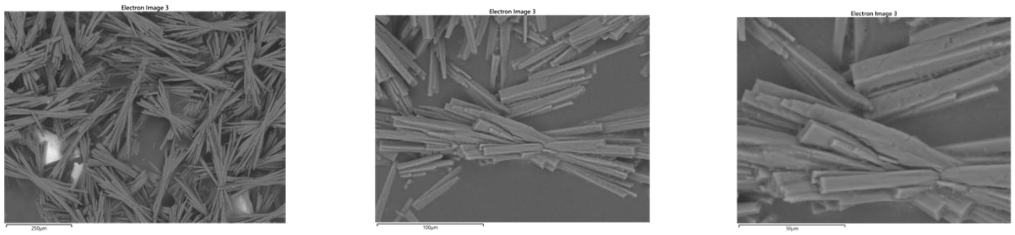

Figure 2.20: SEM images of $Sm_2(DNNDI)_3$ MOF crystals at Different Magnification (250 µm, 100 µm and 50 µm)

2.8.2 Synthesis of [$Y_2(DNNDI)_3DMF$]

To a 25 mL sigmacoted scintillation vial containing 9 mg (0.034mmol) of $Y(NO_3)_3$ and 17mg (0.034 mmol) of DNNDI, 2.5mL DMF was added and sonicated for five minutes until the solutes completely dissolved to form a solution. (Tightly capped the vial and transferred it into) an oven at 100 ° C for 24 hours. The resulting solids were needle-like colorless crystalline

material suitable for X-ray diffraction and were washed with fresh DMF pending XRD analysis.

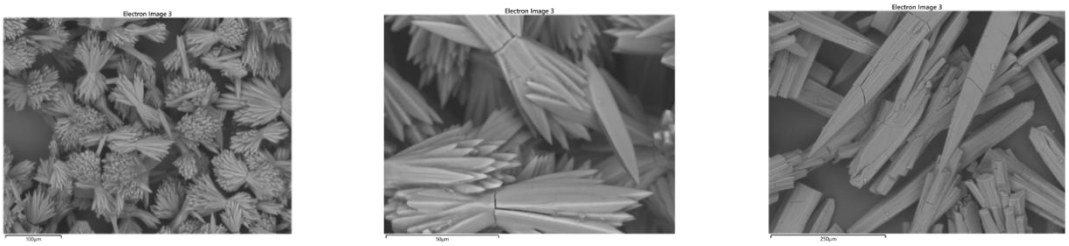

Figure 2.21 SEM images of $Y_2(DNNDI)_3$ MOF crystals at Different Magnification (100 µm, 50 µm, 250 µm)

2.8.3 Synthesis of [$Er_2(DNNDI)_3$ 2.5 DMF]

To a 25 mL sigmacoted scintillation vial containing 15 mg (0.034 mmol) of $Er_2(NO_3)_3$ and 17mg (0.034 mmol) of DNNDI, 2.5mL DMF was added and sonicated for five minutes until the solutes completely dissolved to form a solution. (Tightly capped the vial and transferred it into) an oven at 100 ºC for 24 hours. The resulting solids were needle-like colourless crystalline material suitable for X-ray diffractions and were washed with fresh DMF pending XRD analysis.

2.8.4 Synthesis of [$Yb_2(DNNDI)_3$ 2.5 DMF]

To a 25 mL sigma coted scintillation vial containing 12mg (0.034 mmol) of $Yb_2(NO_3)_3$ and 17mg (0.034 mmol) of DNNDI, 2.5mL DMF was added and sonicated for five minutes until the solutes completely dissolved to form a solution. (Tightly capped the vial and transferred it into) an oven at 100 ºC for 24 hours. The resulting solids were needle-like colorless crystals suitable for X-ray diffractions and were washed with fresh DMF pending XRD analysis.

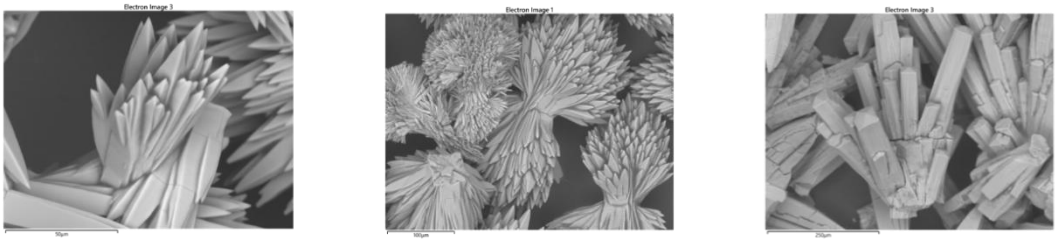

Figure 2.22: SEM images of $Yb_2(DNNDI)_3$ MOF crystals at different magnifications (50 µm, 100 µm, 250 µm)

2.8.5 Synthesis of [$Lu_2(DNNDI)_3$ 2.5 DMF]

To a 25 mL sigmacoted scintillation vial containing 12 mg (0.034 mmol) of $Lu_2(NO_3)_3$ and 17mg (0.034 mmol) of DNNDI, 2.5 mL DMF was added and sonicated for five minutes until the solutes completely dissolved to form a solution. Tightly capped the vial and transferred it into an oven at 100 º C for 24 hours. The resulting solids were needle-like colorless crystalline material suitable for X-ray diffractions and were washed with fresh DMF pending XRD analysis.

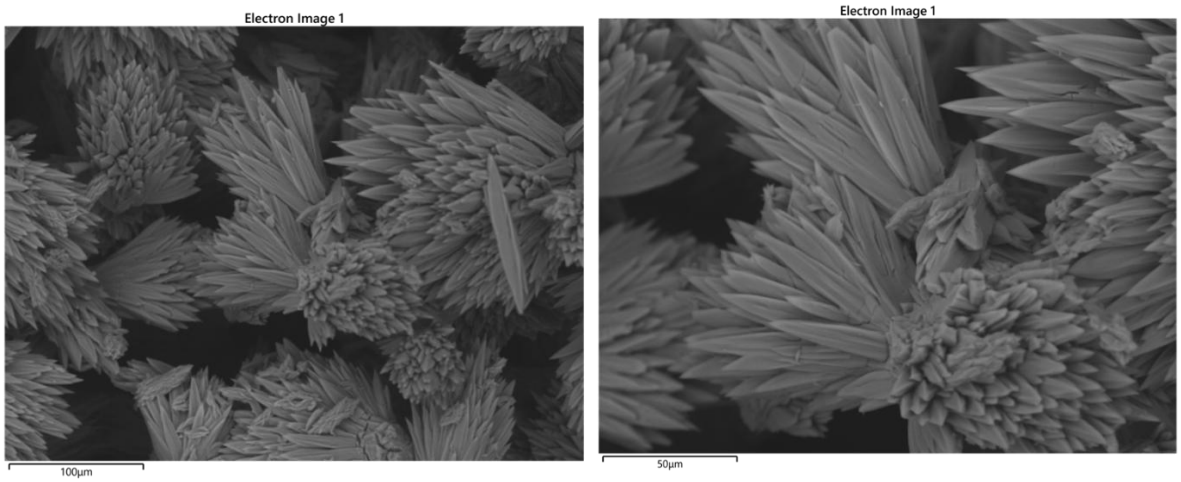

Figure 2.23: SEM images of $Lu_2(DNNDI)_3$ MOF crystals at different magnifications (100 µm, 50 µm)

2.9 References

1 L. Yang, P. Langer, E. S. Davies, M. Baldoni, K. Wickham, N. A. Besley, E. Besley and N. R. Champness, *Chem Sci*, 2019, **10**, 3723–3732.

2 S. L. Griffin and N. R. Champness, *Coord Chem Rev*, 2020, **414**, 213295.

3 Y. Zhou and L. Han, *Coord Chem Rev*, 2021, **430**, 213665.

4 A. Diac, M. Matache, I. Grosu and N. D. Hădade, *Adv Synth Catal*, 2018, **360**, 817–845.

5 J. Li, A. Kumar, B. A. Johnson and S. Ott, *Nat Commun*, 2023, **14**, 4388.

6 J. Li and S. Ott, *Acc Chem Res*, 2024, **57**, 2836–2846.

7 M. A. Jameel, T. C.-J. Yang, G. J. Wilson, R. A. Evans, A. Gupta and S. J. Langford, *J Mater Chem A Mater*, 2021, **9**, 27170–27192.

8 Z. Xu, A. Chandresh, A. Mauri, M. Esmaeilpour, V. Monnier, F. Odobel, L. Heinke, W. Wenzel, M. Kozlowska, S. Diring, R. Haldar and C. Wöll, *Angew. Chem. Int. Edit.* ***63****, 1433-7851*

9 B. A. Johnson, A. Bhunia, H. Fei, S. M. Cohen and S. Ott, *J Am Chem Soc*, 2018, **140**, 2985–2994.

10 W. Dai, W. Wei, Z. Yao, S. Xiang and Z. Zhang, *Inorg Chem Commun*, 2022, **141**, 109497.

11 D. Bůžek, J. Hynek, M. Kloda, V. Zlámalová, P. Bezdička, S. Adamec, K. Lang and J. Demel, *Inorg Chem Front*, 2024, **11**, 5319–5335.

12 Y. Liu, Z. Li, Y. Han, Z. Ji, H. Li, Y. Liu, Y. Wei, C. Chen, X. He and M. Wu, *ChemSusChem*, 2023, **16**, 202202305.

13 X. Wu, K. Wang, J. Lin, D. Yan, Z. Guo and H. Zhan, *J Colloid Interface Sci*, 2021, **594**, 73–79.

14 L. Sun, M. G. Campbell and M. Dincă, *Angewandte Chemie International Edition*, 2016, **55**, 3566–3579.

15 M.-H. You, M.-H. Li, H.-H. Li, Y. Chen and M.-J. Lin, *Dalton Transactions*, 2019, **48**, 17381–17387.

16 B. Garai, A. Mallick and R. Banerjee, *Chem Sci*, 2016, **7**, 2195–2200.

17 E. Castaldelli, K. D. G. Imalka Jayawardena, D. C. Cox, G. J. Clarkson, R. I. Walton, L. Le-Quang, J. Chauvin, S. R. P. Silva and G. J.-F. Demets, *Nat Commun*, 2017, **8**, 2139.

18 C. R. Pfeiffer, N. Biggins, W. Lewis and N. R. Champness, *CrystEngComm*, 2017, **19**, 5558–5564.

19 Z. Xiang, Y.-B. Shan, T. Li, C.-C. Huang, X.-H. Huang and M.-J. Lin, *Acta Crystallogr C Struct Chem*, 2019, **75**, 38–45.

20 Y. Fu, W. Zhang and H. Ma, *Chempluschem*, 2024, **89**, 202400236.

21 S. Jensen, K. Tan, W. P. Lustig, D. S. Kilin, J. Li, Y. J. Chabal and T. Thonhauser, *Chemistry of Materials*, 2019, **31**, 7933–7940.

22 O. V. Dolomanov, L. J. Bourhis, R. J. Gildea, J. A. K. Howard and H. Puschmann, *J Appl Crystallogr*, 2009, **42**, 339–341.

23 J. Shukla and P. Mukhopadhyay, *Eur. J. Org Chem*, 2019, **2019**, 7770–7786.

24 T. A. Welsh, O. Matsarskaia, R. Schweins and E. R. Draper, *New Journal of Chemistry*, 2021, **45**, 14005–14013.

25 E. Echenique-Errandonea, R. F. Mendes, F. Figueira, D. Choquesillo-Lazarte, G. Beobide, J. Cepeda, D. Ananias, A. Rodríguez-Diéguez, F. A. Almeida Paz and J. M. Seco, *Inorg Chem*, 2022, **61**, 12977–12990.

26 Y. Zhang, S. Liu, Z.-S. Zhao, Z. Wang, R. Zhang, L. Liu and Z.-B. Han, *Inorg Chem Front*, 2021, **8**, 590–619.

27 S. Sun, Y. Zhao, J. Wang and R. Pei, *J Mater Chem B*, 2022, **10**, 9535–9564.

28 Q. Zhang, S. O'Brien and J. Grimm, *Nanotheranostics*, 2022, **6**, 184–194.

29 D. McHugh, W. Tong, A. Bezrukov, P. Farras, M. J. Zaworotko, J. Mayans, J. M. Skelton, S. Barnett, A. R. Pallipurath and C. Papatriantafyllopoulou, *Eur. J. Inorg. Chem*, 2024, **28**, 202400541.

30 R. H. Alzard, L. A. Siddig, N. Saleh, H. L. Nguyen, Q. A. T. Nguyen, T. H. Ho, V. Q. Bui, K. Sethupathi, P. K. Sreejith and A. Alzamly, *Sci Rep*, 2022, **12**, 18812.

31 Y. Cao, Y. Zhang, L. Gu, X. Qin, H.-Y. Li, H.-D. Bian and F.-P. Huang, *New Journal of Chemistry*, 2020, **44**, 10681–10688.

32 Z.-P. Dong, F. Zhao, L. Zhang, Z.-L. Liu and Y.-Q. Wang, *New J. of Chem.*, 2020, **44**, 10239–10249.

33 M. Al Sharabati, R. Sabouni and G. A. Husseini, *Nanomaterials*, 2022, **12**, 277.

34 G.-Y. Zhu, Z. Liu, J. Wang, X. Niu, T. Wang, G.-X. Jin and J.-P. Ma, *RSC Adv*, 2020, **10**, 30650–30655.

35 S. Yan, L. Xu and X. Li, *World J. of Mechanics*, 2018, **08**, 1–10.

36 G. Radha, T. Leelasree, D. Muthukumar, R. S. Pillai and H. Aggarwal, *New Journal of Chemistry*, 2021, **45**, 12931–12937.

37 Z. Guo, D. K. Panda, M. A. Gordillo, A. Khatun, H. Wu, W. Zhou and S. Saha, *ACS Appl Mater Interfaces*, 2017, **9**, 32413–32417.

38 A. J. Mohan Reddy, M. S. Surendra Babu and P. Nagaraju, *Solid State Sci*, 2022, **125**, 106819.

39 Y.-T. Yan, F. Cao, W.-Y. Zhang, S.-S. Zhang, F. Zhang and Y.-Y. Wang, *New Journal of Chemistry*, 2018, **42**, 9865–9875.

40 O. V. Dolomanov, L. J. Bourhis, R. J. Gildea, J. A. K. Howard and H. Puschmann, *J Appl Crystallogr*, 2009, **42**, 339–341.

41 G. M. Sheldrick, *Acta Crystallogr C Struct Chem*, 2015, **71**, 3–8.

42 A. Schoedel, M. Li, D. Li, M. O'Keeffe and O. M. Yaghi, *Chem Rev*, 2016, **116**, 12466–12535.

43 F. González Chávez and H. I. Beltrán, *New J. of Chem.,* 2021, **45**, 6600–6610.

44 A. L. Spek, *Acta Crystallogr C Struct Chem*, 2015, **71**, 9–18.

45 C. F. Macrae, I. Sovago, S. J. Cottrell, P. T. A. Galek, P. McCabe, E. Pidcock, M. Platings, G. P. Shields, J. S. Stevens, M. Towler and P. A. Wood, *J Appl Crystallogr*, 2020, **53**, 226–235.

46 S. M. McClure, M. Lundwall, F. Yang, Z. Zhou and D. W. Goodman, *J. of Physics Condensed Matter*, 2019, **21**, 474223.

47 A. Wang, D. Austin, A. Karmakar, G. M. Bernard, V. K. Michaelis, M. M. Yung, H. Zeng and H. Song, *ACS Catal*, 2017, **7**, 3681–3692.

48 W. Yang, Z. Wang, S. Song, H. Chen, X. Wang, J. Cheng, R. Sun and J. Han, *Biomass Bioenergy*, 2019, **130**, 105356.

49 M. A. Nasalevich, C. H. Hendon, J. G. Santaclara, K. Svane, B. van der Linden, S. L. Veber, M. V. Fedin, A. J. Houtepen, M. A. van der Veen, F. Kapteijn, A. Walsh and J. Gascon, *Sci Rep*, 2016, **6**, 23676.

50 J. Espín, L. Garzón-Tovar, A. Carné-Sánchez, I. Imaz and D. Maspoch, *ACS Appl Mater Interfaces*, 2018, **10**, 9555–9562.

51 K. Roztocki, W. Gromelska, F. Formalik, A. Giordana, L. Andreo, G. Mahmoudi, V. Bon, S. Kaskel, L. J. Barbour, A. Janiak and E. Priola, *ACS Mater Lett*, 2023, **5**, 1256–1260.

52 Q. Ye, D. R. Cairnie, D. Troya, N. Kumar, X. Yang and A. J. Morris, *J Am Chem Soc*, 2024, **146**, 101–105.

53 P. H. M. Andrade, C. Volkringer, T. Loiseau, A. Tejeda, M. Hureau and A. Moissette, *Appl Mater Today*, 2024, **37**, 102094.

54 M. Treger, A. Hannebauer, A. Schaate, J. L. Budde, P. Behrens and A. M. Schneider, *Physi. Chem. Chemical Physics*, 2023, **25**, 6333–6341.

55 S. Gao, Y. Sui, F. Wei, J. Qi, Q. Meng, Y. Ren and Y. He, *J Colloid Interface Sci*, 2018, **531**, 83–90.

56 C. Ye, Q. Qin, J. Liu, W. Mao, J. Yan, Y. Wang, J. Cui, Q. Zhang, L. Yang and Y. Wu, *J Mater Chem A Mater*, 2019, **7**, 4998–5008.

Chapter three

3.0 Host-guest interactions in Metal-organic Framework

3.1 Introduction

The hybrid nature of MOFs serves as a unique opportunity for functionalizing their framework for structural diversity as opposed to conventional, purely inorganic, solid-state materials.[1] Without compromising the purity and crystallinity of the MOFs, post-synthetic modification of MOFs (PSM) offers a promising pathway for achieving structural diversity and potentially new properties.[2,3] The host-guest experiment typically involves studying the interactions between a host material, such as a metal-organic framework (MOF), and guest molecules.[4] In the context of MOFs, which are porous materials with well-defined structures, host-guest behaviour typically suggests the encapsulation of guest molecules within the pores of the MOF,[5] without altering the crystallinity of the material. In this chapter, the host-guest chemistry involving MOFs and molecular ferrocene (Fc) or phenothiazine (PTZ) will be reported. This can be achieved through various methods depending on the MOFs and the specific properties of the guest.

Ferrocene, with its distinctive iron-containing sandwich structure, can impart unique electronic and redox properties to MOFs.[6,7] It is often considered a unique organometallic compound, a representative of the wider family of sandwich complexes.[8–11] Ferrocene can be added to a framework structure as a guest species, Fc@MOF,[7,12–14] which can modify the properties of the MOF. Ferrocene-based MOFs represent a hybrid class of materials with potential application in redox activity, gas sensing and storage, electrocatalysis, and magnetic and photocatalysis.[7] There are some common aspects in both scenarios, primarily related to its structural and electronic properties. Fc@MOFs can be prepared by a number of methods including

electrodeposition,[15] one-pot, low diffusion, vapour-assisted[7] and facile synthetic methods.[16] MOFs are usually first synthesized prior to encapsulation of ferrocene into the framework material, post-synthetically.[17]

The study of NDIs' redox behaviour is crucial for understanding their electronic and electrochemical properties, which, in turn, influences their performance in various applications.[18] The redox activity of NDIs is of interest due to their ability to accept and donate electrons.[19] In the context of NDIs, the representation of the distribution of the electrons shows regions of positive and negative electrostatic potential. This map is often color-coded, with red indicating electron-rich (negative potential) regions and blue indicating electron-poor (positive potential) regions. A typical example of this is the map of the electrostatic potential of DPNDI[20] (where DPNDI = di-(4-pyridyl)-NDI)) which is shown in Figure 3.1.

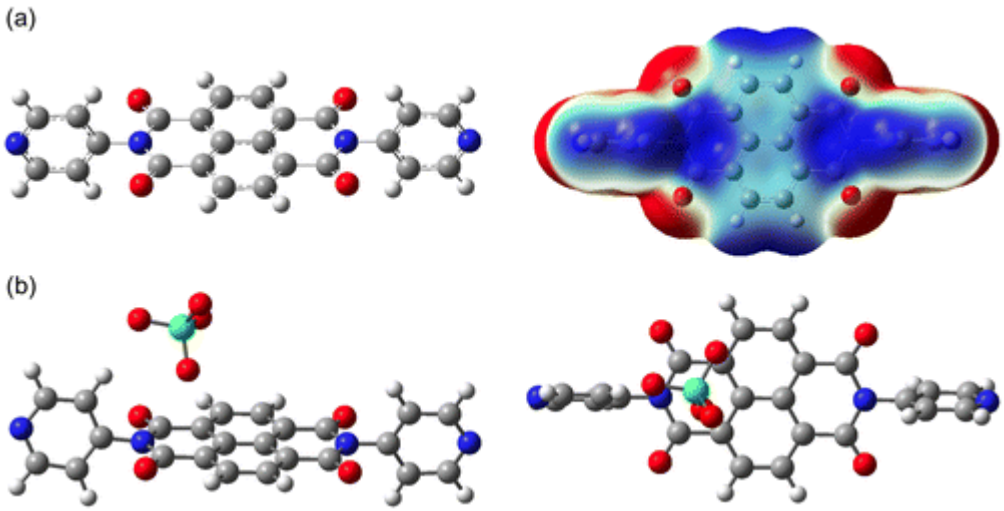

Figure 3.1: DPNDI structure (top left) depicting the electrostatic potential map, with blue and red regions indicating the electron-deficient and electron-rich areas respectively.[20]

Phenothiazine or its derivatives have been extensively studied as a photoactive molecule with properties in radical generation, biological activity, and light-controllable isomerization.[21–24]

Upon photoexcitation in solution, phenothiazine can undergo radical formation and isomerization.[25] While phenothiazine itself is not a typical ligand for MOF synthesis, its derivatives have been extensively explored for incorporation into MOFs.[26,27] Phenothiazine and its derivatives may act as redox-active centres within a MOF contributing to catalytic processes.[28,29] By incorporating phenothiazine into MOFs, it may be possible to create electrode materials for batteries or supercapacitors with improved redox properties.[30] Depending on the specific modifications of phenothiazine, the resulting MOF may exhibit interesting photophysical properties which could be relevant for applications in optoelectronics and sensing, gas sensing and separation, magnetism, and catalysis.[31–36] A typical example of phenothiazine-based MOFs is Zn-L5 which has excellent third-order nonlinear properties, (Figure 3.2).[29]

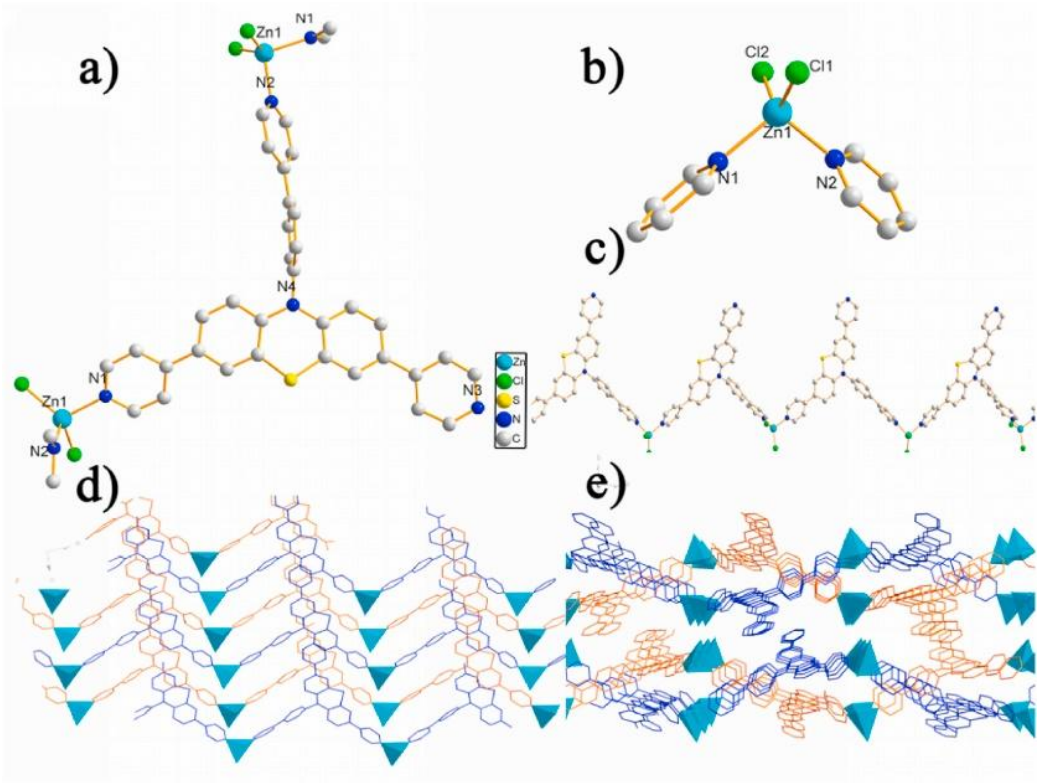

Figure 3.2: Phenothiazine based MOF (Zn-L5) with (a) schematic representation of a ligand as a unit (b) schematic representation of a Zn metal cluster; (c) schematic representation of 1D chain; (d) view of Zn-L5 along the crystallographic b-axis; view along the crystallographic c-

axis; in Figure d and e blue polyhedron represent the Zn metal cluster; H atoms are omitted for clarity.[29]

3.2 Aim

In this chapter we aim to post-synthetically modify the as-synthesized Ln-NDI-based MOFs, see previous chapter, by taking advantage of the electron deficiency of the NDI group to incorporate electron-rich ferrocene or phenothiazine, and determining the host-guest environment, and studying the fluorescent nature of the materials. Phenothiazine-based MOFs (PZ-MOFs) could exhibit unique properties stemming from the redox-active properties of phenothiazines and the porous nature of MOFs. Lanthanum (La), Gadolinium (Gd) and Lututium (Lu) are the smallest, medium and biggest lanthanides that give clear picture of the general trends in ionic radii, chemical reactivity and specific applications and hence are good representatives and can provide valuable insights into the properties and behavior of the entire lanthanide series.

3.3 Result and Discussion

3.3.1 Preparation and Crystal Analysis of Fc@MOFs

The as-synthesised MOFs were subjected to solvent exchange to remove any unreacted material by decanting the mother liquor from the reaction vials, and washing the samples three times with 2 mL acetone at 1hr intervals. The materials were then soaked into 2 mL acetone for three days. Subsequently, the crystals were washed with 2 mL acetone and soaked again with 0.10m L acetone solution of ferrocene in a 20 mL scintillation vial at room temperature. After 10 days, all the crystals changed colour from colourless to orange indicating the incorporation of ferrocene into the framework materials. The same procedure was repeated for

three different MOFs, specifically $La_2(DNNDI)_3$MOF, $Gd_2(DNNDI)_3$MOF and $Lu_2(DNNDI)_3$MOF.

No apparent damage was observed on the crystals after the post-synthetic modification of the framework materials. Thereafter, crystals from each experiment were carefully selected and mounted for SEM/EDX analysis. Elemental mapping by scanning across a specific area of the crystal and generating spatial distribution maps for each element was conducted. The resulting EDX data shows that in each crystalline MOF material, ferrocene is observed in the materials, see Figure 3.3. These results do not allow identification of Fc inclusion within or on the surface of the MOF.

(a)

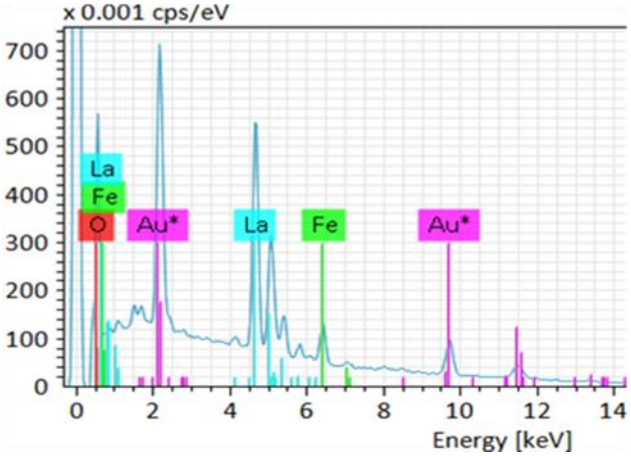

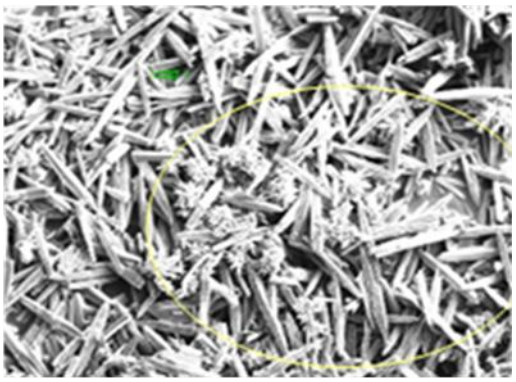

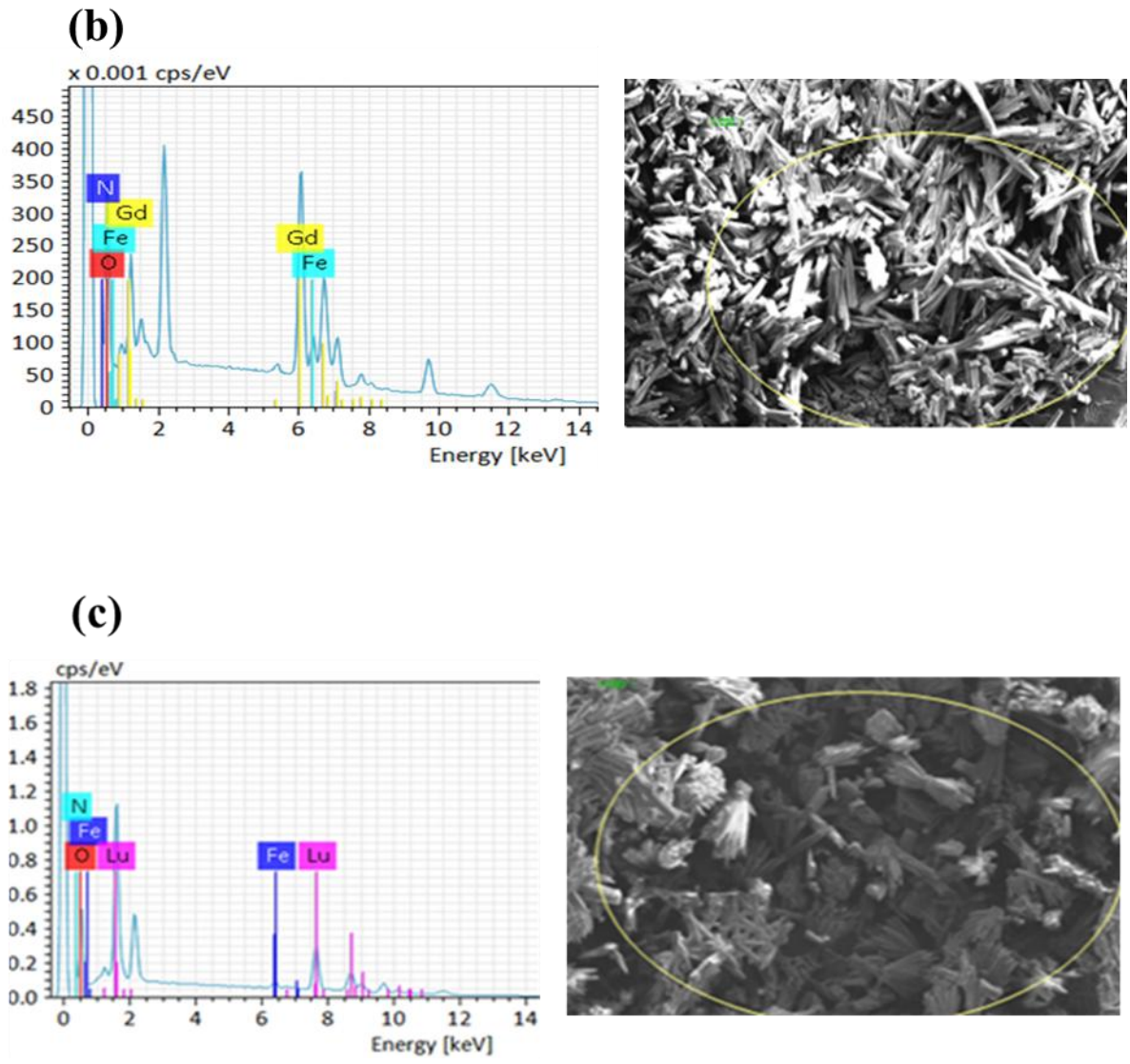

Figure 3.3: shows the SEM/EDX data for the Fc counts on the $Ln_2(DNNDI)_3$ a) $La_2(DNNDI)_3$, b) $Gd_2(DNNDI)_3$ and c) $Lu_2(DNNDI)_3$.

3.3.2 Preparation and Crystal Analysis of PTZ@MOFs

These experiments were performed similarly to those for the preparation of Fc@MOFs described above differing only in the guest molecule. After decanting the mother liquor, the crystals were washed with 2 mL acetone three times at an hour interval. Thereafter, the crystals were soaked in 2 mL acetone for 76 hours. Subsequently, the crystals were washed again with

2 mL acetone and soaked into 0.10 mL phenothiazine acetone solution for another 10 days. It was evident that the crystals did change very slightly from pale yellow to slightly red which indicates the successful inclusion of the guest into the MOFs, with no change in the quality and purity of all the crystals. Crystals in each experiment were selected for SEM/EDX analysis to determine the inclusion of phenothiazine in the MOF. Elemental mapping by scanning across a specific area of the crystal and generating spatial distribution maps for each element was conducted. The results showed that there is deposition of PTZ in each single crystal as shown in figure 3.4 below.

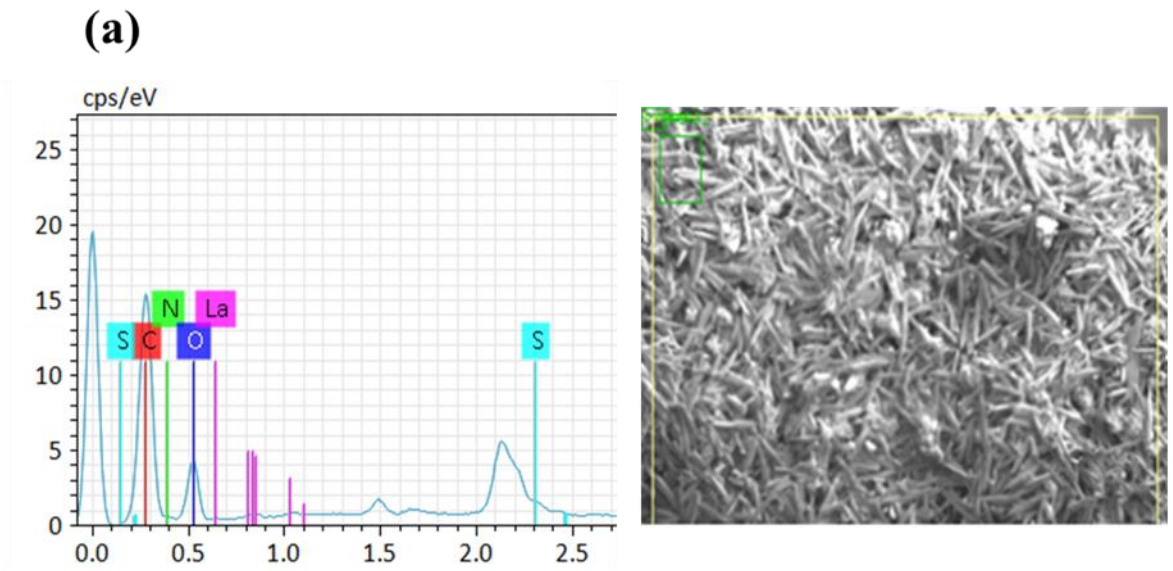

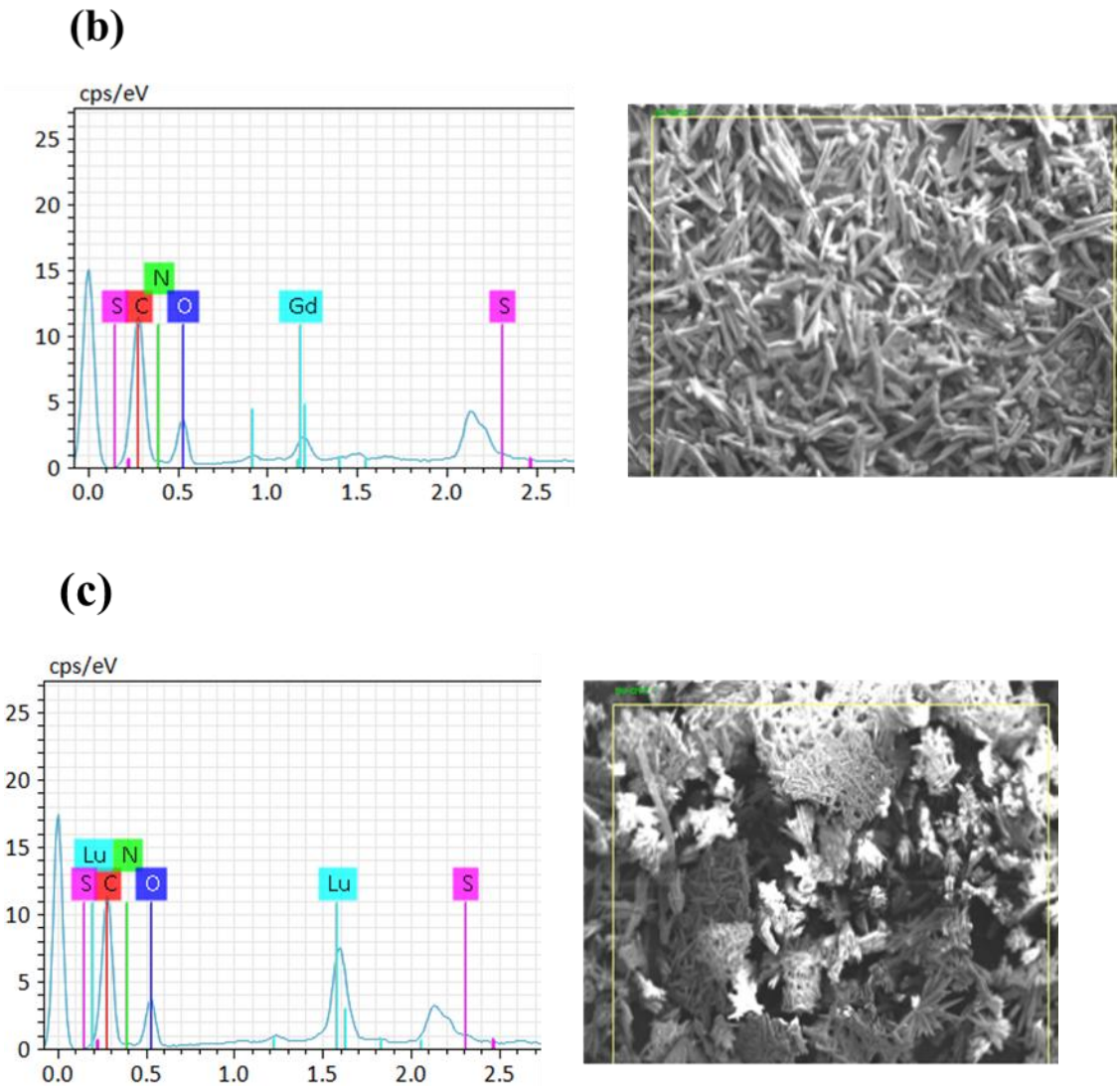

Figure 3.4: SEM/EDX of phenothiazine counts on the $Ln_2(DNNDI)_3$; a) $La_2(DNNDI)_3$, b) $Gd_2(DNNDI)_3$ and c) $Lu_2(DNNDI)_3$. MOFs

3.4 UV-visible Spectroscopic data Fc@MOFs and PTZ@MOFs

Figure 3.5: Shows UV-Vis data for post-synthetically modified MOFs (Fc@MOFs and PTZ@MOFs) revealed that both families of MOFs retain their optical properties, which further confirms the stability of the material even after guest encapsulation.

(a)

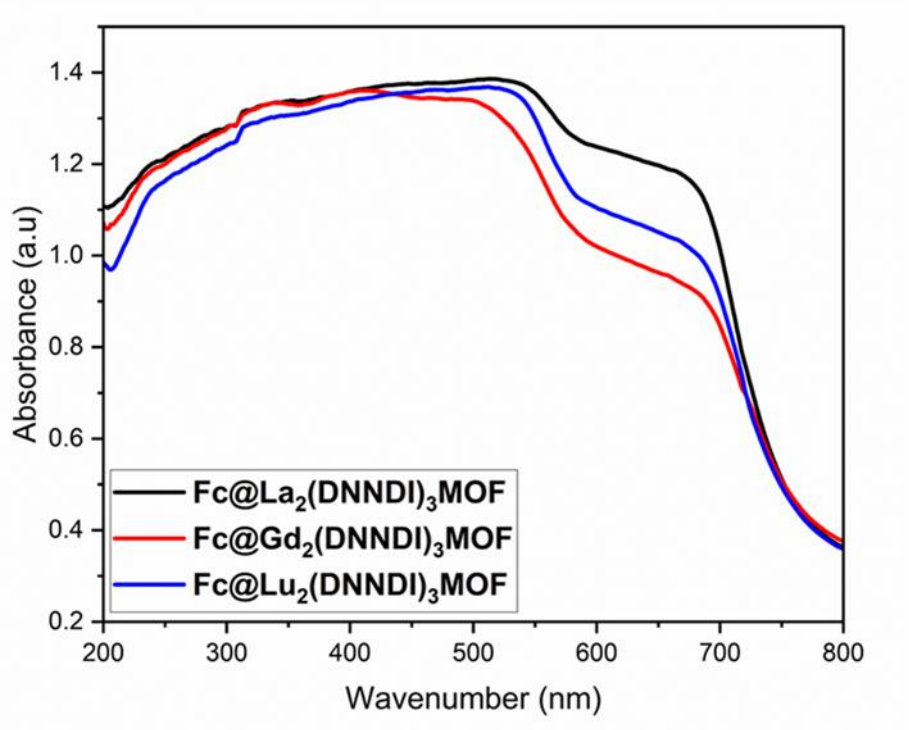
Absorbance (a.u)
Wavenumber (nm)
Fc@La2(DNNDI)3MOF
Fc@Gd2(DNNDI)3MOF
Fc@Lu2(DNNDI)3MOF

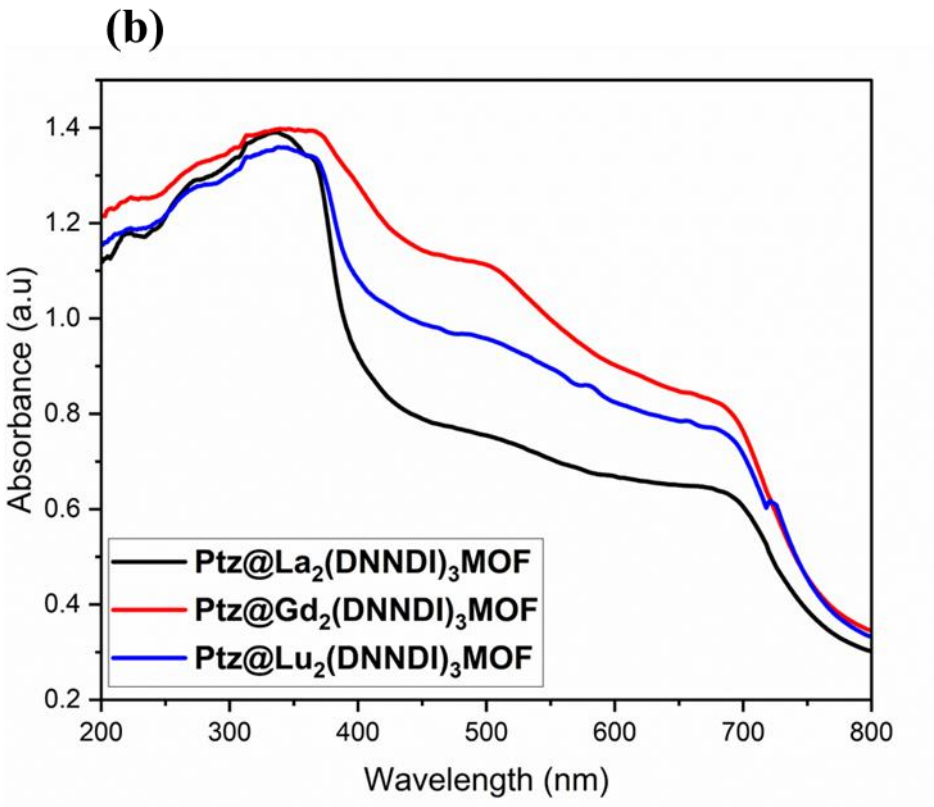

Figure 3.5: Shows the solid-state UV-visible data for a) Fc@MOFs and b) PTZ@MOFs. Each figure shows encapsulation of the guest in $La_2(DNNDI)_3$ (black line); $Gd_2(DNNDI)_3$ (red line) and $Lu_2(DNNDI)_3$ (blue line).

3.5 Conclusion

Understanding the interaction between a host molecule or structure and a guest molecule allows for the creation of tailored systems with specific properties and functions. Host molecules can form inclusion complexes with guests, where the guest molecule is partially or fully enclosed within the host cavity. Experiments involving encapsulation of ferrocene and phenothiazine into Ln-MOFs have been successfully performed and characterized. SEM/EDX mapping revealed that the inclusion of both guests into the framework structures was successful. Guest molecule's presence was confirmed to be on both the surface of the crystals and in single crystals. UV-visible spectroscopy was used to study the optical properties of the materials.

3.6 Material and Methods

3.6.1 Preparations of Fc@$La_2(DNNDI)_3$. MOFs

The as-synthesised framework $La_2(DNNDI)_3$MOF was subjected to acetone solvent exchange for three days after carefully decanting the mother liquor from the 20mL scintillation vial used for the original synthesis. MOF crystals were washed three times and soaked in 2mL acetone for three days before soaking in 2mL of 0.10M solution of ferrocene for 10 days. The crystals changed colour from pale yellow to orange, indicating that ferrocene was successfully hosted by the MOF.

3.6.2 Preparations of Fc@$Gd_2(DNNDI)_3$. MOFs

The as-synthesised framework $Gd_2(DNNDI)_3$MOF was subjected to acetone solvent exchange for three days after carefully decanting the mother liquor from the 20mL scintillation vial used for the original synthesis. MOF crystals were washed three times and soaked in 2mL acetone for three days before soaking in 2mL of 0.10M solution of ferrocene for 10 days. The crystals changed colour from pale yellow to orange, indicating that ferrocene was successfully hosted by the MOF.

3.6.3 Preparations of Fc@$Lu_2(DNNDI)_3$. MOFs

The as-synthesised framework $Lu_2(DNNDI)_3$MOF was subjected to acetone solvent exchange for three days after carefully decanting the mother liquor from the 20mL scintillation vial used for the original synthesis. MOF crystals were washed three times and soaked in 2mL acetone for three days before soaking in 2mL of 0.10M solution of ferrocene for 10 days. The crystals

changed colour from pale yellow to orange, indicating that ferrocene was successfully hosted by the MOF.

3.6.4 Preparations of PTZ@$La_2(DNNDI)_3$. MOFs

The as-synthesised framework $La_2(DNNDI)_3$MOF was subjected to acetone solvent exchange for three days after carefully decanting the mother liquor from the 20mL scintillation vial used for the original synthesis. MOF crystals were washed three times and soaked in 2mL acetone for three days before soaking in 2mL of 0.10M solution of phenothiazine for 10 days. The crystals changed colour from pale yellow to orange, indicating that ferrocene was successfully hosted by the MOF.

3.6.5 Preparations of PTZ@$Gd_2(DNNDI)_3$. MOFs

The as-synthesised framework $Gd_2(DNNDI)_3$MOF was subjected to acetone solvent exchange for three days after carefully decanting the mother liquor from the 20mL scintillation vial used for the original synthesis. MOF crystals were washed three times and soaked in 2mL acetone for three days before soaking in 2mL of 0.10M solution of phenothiazine for 10 days. The crystals changed colour from pale yellow to orange, indicating that ferrocene was successfully hosted by the MOF.

3.6.6 Preparations of PTZ@$Lu_2(DNNDI)_3$. MOFs

The as-synthesised framework $Lu_2(DNNDI)_3$MOF was subjected to acetone solvent exchange for three days after carefully decanting the mother liquor from the 20mL scintillation vial used for the original synthesis. MOF crystals were washed three times and soaked in 2mL acetone

for three days before soaking in 2mL of 0.10M solution of phenothiazine for 10 days. The crystals changed colour from pale yellow to orange, indicating that ferrocene was successfully hosted by the MOF.

3.7 References

1 O. M. Yaghi, M. J. Kalmutzki and C. S. Diercks, In *Introduction to Reticular Chemistry*, Wiley, 2019, 145–176.

2 L. Figueroa-Quintero, D. Villalgordo-Hernández, J. J. Delgado-Marín, J. Narciso, V. K. Velisoju, P. Castaño, J. Gascón and E. V. Ramos-Fernández, *Small Methods*, 2023, **7**, 202201413.

3 N. S. Portillo-Vélez, J. L. Obeso, J. A. de los Reyes, R. A. Peralta, I. A. Ibarra and M. T. Huxley, *Commun Mater*, 2024, **5**, 247.

4 X. Liu, B. Qian, D. Zhang, M. Yu, Z. Chang and X. Bu, *Coord Chem Rev*, 2023, **476**, 214921.

5 M. D. Allendorf, R. Medishetty and R. A. Fischer, *MRS Bull*, 2016, **41**, 865–869.

6 T. N. Nguyên Lê, K. Kondratenko, I. Arbouch, A. Moréac, J.-C. Le Breton, C. van Dyck, J. Cornil, D. Vuillaume and B. Fabre, *The J. of Physical Chemistry C*, 2024, **128**, 7706–7722.

7 Z. Huang, H. Yu, L. Wang, X. Liu, T. Lin, F. Haq, S. Z. Vatsadze and D. A. Lemenovskiy, *Coord Chem Rev*, 2021, **430**, 213737.

8 U. Rauf, G. Shabir, S. Bukhari, F. Albericio and A. Saeed, *Molecules*, 2023, **28**, 5765.

9 H. Kong, Q. Chu, C. Fang, G. Cao, G. Han and X. Li, *Advanced Science*, 2021, **8**, 202100241.

10 R. Rajak, M. Saraf, A. Mohammad and S. M. Mobin, *J Mater Chem A Mater*, 2017, **5**, 17998–18011.

11 A. Chakraborty, J. Acharya and V. Chandrasekhar, *ACS Omega*, 2020, **5**, 9046–9054.

12 W. Zhang, D. Banerjee, J. Liu, H. T. Schaef, J. V. Crum, C. A. Fernandez, R. K. Kukkadapu, Z. Nie, S. K. Nune, R. K. Motkuri, K. W. Chapman, M. H. Engelhard, J. C. Hayes, K. L. Silvers, R. Krishna, B. P. McGrail, J. Liu and P. K. Thallapally, *Advanced Materials*, 2016, **28**, 3572–3577.

13 G. Ye, Q. He, S. Liu, K. Zhao, Y. Su, W. Zhu, R. Huang and Z. He, *J Mater Chem A Mater*, 2019, **7**, 16508–16515.

14 J. Qin, M. Cho and Y. Lee, *ACS Appl Mater Interfaces*, 2019, **11**, 11743–11748.

15 Y. Sun, H. Jin, X. Jiang and R. Gui, *Anal Chem*, 2020, **92**, 2866–2875.

16 K. Ge, S. Sun, Y. Zhao, K. Yang, S. Wang, Z. Zhang, J. Cao, Y. Yang, Y. Zhang, M. Pan and L. Zhu, *Angew. Chem. Int. Ed*, 2021, **60**, 12097–12102.

17 W. Luo, L. Tang, X. Wang, S.-J. Lin and Z. Cai, *ACS Appl Nano Mater*, 2023, **6**, 22406–22415.

18 J. Jung, A. Selerowicz, P. Maczugowska, K. Halagan, R. Rybakiewicz-Sekita, M. Zagorska and A. Stefaniuk-Grams, *Materials*, 2021, **14**, 4026.

19 V. Medabalmi, M. Sundararajan, V. Singh, M.-H. Baik and H. R. Byon, *J Mater Chem A Mater*, 2020, **8**, 11218–11223.

20 A. Mitra, R. J. Clark, C. T. Hubley and S. Saha, *Supramol Chem*, 2014, **26**, 296–301.

21 J. A. Christensen, B. T. Phelan, S. Chaudhuri, A. Acharya, V. S. Batista and M. R. Wasielewski, *J Am Chem Soc*, 2018, **140**, 5290–5299.

22 Y. Fang, X. Lian, Y. Huang, G. Fu, Z. Xiao, Q. Wang, B. Nan, J. Pellois and H. Zhou, *Small*, 2018, 47, 201802709.

23 Z. Zhao, J. Ren, Y. Yuan, Z. Sun, W. Chen, X. Su, G. Zhang and L. Chen, *ACS Appl Polym Mater*, 2023, **5**, 1577–1584.

24 P. S. Gangadhar, G. Reddy, S. Prasanthkumar and L. Giribabu, *Physical Chemistry Chemical Physics*, 2021, **23**, 14969–14996.

25 V. Hahn, A. Mikolasch, J. Weitemeyer, S. Petters, T. Davids, M. Lalk, J.-W. Lackmann and F. Schauer, *ACS Omega*, 2020, **5**, 14324–14339.

26 M. Abdallah, T.-T. Bui, F. Goubard, D. Theodosopoulou, F. Dumur, A. Hijazi, J.-P. Fouassier and J. Lalevée, *Polym Chem*, 2019, **10**, 6145–6156.

27 C. Gu, N. Hosono, J.-J. Zheng, Y. Sato, S. Kusaka, S. Sakaki and S. Kitagawa, *Science (1979)*, 2019, **363**, 387–391.

28 J. Zhou, L. Mao, M.-X. Wu, Z. Peng, Y. Yang, M. Zhou, X.-L. Zhao, X. Shi and H.-B. Yang, *Chem Sci*, 2022, **13**, 5252–5260.

29 J. Jia, J. Wang, M. Li, C. Gong, G. Liang, Y. Song and Y. She, *Dyes and Pigments*, 2022, **205**, 110398.

30 T. S. Renani, S. M. Khoshfetrat, J. Arjomandi, H. Shi and S. Khazalpour, *J Mater Chem A Mater*, 2021, **9**, 12853–12869.

31 A. M. Rice, C. R. Martin, V. A. Galitskiy, A. A. Berseneva, G. A. Leith and N. B. Shustova, *Chem Rev*, 2020, **120**, 8790–8813.

32 B. Mondal, A. K. Ghosh and P. S. Mukherjee, *J Org Chem*, 2017, **82**, 7783–7790.

33 J. Park, D. Feng, S. Yuan and H. Zhou, *Angewandte Chemie International Edition*, 2015, **54**, 430–435.

34 W. Danowski, T. van Leeuwen, W. R. Browne and B. L. Feringa, *Nanoscale Adv*, 2021, **3**, 24–40.

35 H. F. Drake, G. S. Day, Z. Xiao, H.-C. Zhou and M. R. Ryder, *Trends Chem*, 2022, **4**, 32–47.

36 Z. Liu, L. Zhang and D. Sun, *Chemical Communications*, 2020, **56**, 9416–9432.

Chapter four

4.0 Mixed-Metal MOFs

4.1 Introduction

Mixed-metal MOFs, also known as bimetallic or multi-metallic MOFs, referring to metal-organic frameworks that incorporate more than one type of metal ion within their structure.[1] The presence of two metal ions situated anywhere within a MOF compound is referred to as mixed-metal MOF as defined by Chen and coworkers.[2] The incorporation of multiple metal species into a MOF can lead to unique and tuneable properties, making these materials versatile and suitable for various applications. This idea has in recent times gained particular attention as the need to further increase the robustness of MOF materials for multifunctionality evolves.[3] The combination of different metals in MOF can result in greatly enhanced properties that can provide better opportunities in terms of tuning the properties of a particular material for application in diverse fields.[4] For example, mixed-metal MOFs (MM-MOFs) may exhibit improved water stability and catalytic reactions.[5] When compared with single-metal MOFs, MM-MOFs are found to provide effective performance in various applications including catalysis, gas storage and separation, construction of photoactive materials, and sensing.[6,7]

The procedure for the fabrication of MM-MOF is similar to that of single-metal MOFs. It is generally classified as either one-pot synthesis or post-synthetic modification. Whilst the former involves mixing multiple metal ions and organic ligands in a single reaction vessel to form the desired MOF structure without the need for intermediate purification steps, the latter involves chemically modifying the framework structure of the MOF after its synthesis. One-pot synthesis offers several advantages, including simplicity, efficiency, and scalability but does not allow control over the distribution of metal during the synthesis. Post-synthetic

modification presents new functionalities, alters the properties, or fine-tunes the performance of the MOFs for specific applications.[4]

As a rule of thumb, the feasibility of making MM-MOFs depends on the choice of the metal clusters when the ligand is multitopic.[8,9] Metal ions that have the same or similar chemical properties such as ionic radius and Coulombic charge can readily provide the construction of homogenous co-incorporation of different metals into a single framework system.[10] Conversely, employing hetero-multitopic linkers in the synthesis allows for the construction of multi-metal MOFs with metal ions of different chemical and physical properties which is not possible with the common multitopic linkers. In this process, the ligands with different donor atoms can readily coordinate with metal ions that are of different Lewis acids and geometry to form a MM-MOF.[11–14]

A direct or one-pot method of MM-MOF synthesis has been explored in the literature.[15,16] For instance, a 2018 publication by *Li et al.*[14] demonstrated the one-pot synthesis of a quaternary MOF combining Cu-based triangular, Zn-based octahedral, and Zn-based square planar units. This method facilitated the formation of complex multi-metal frameworks with potential applications in various fields furthermore, In 2021, a study by Gao *et al.*[17] reported the successful one-pot synthesis of bimetallic Zn/Mg-MOF-74 with varying Zn/Mg ratios. This facile method resulted in materials exhibiting enhanced CO_2 adsorption and catalytic conversion properties compared to their monometallic counterparts. Additionally, a 2023 study by Xu *et al.*[18] introduced a stepwise construction approach for multi-component MOFs, contrasting it with traditional one-pot reactions. While the stepwise method offers precise control over component placement, the authors acknowledge that one-pot synthesis remains a widely used and efficient strategy for assembling multi-component frameworks. Figure 4.1 illustrates a sketch of MM-MOF using two metal ions where two different metal clusters are coordinated to an organic linker to form an MM-MOF system.

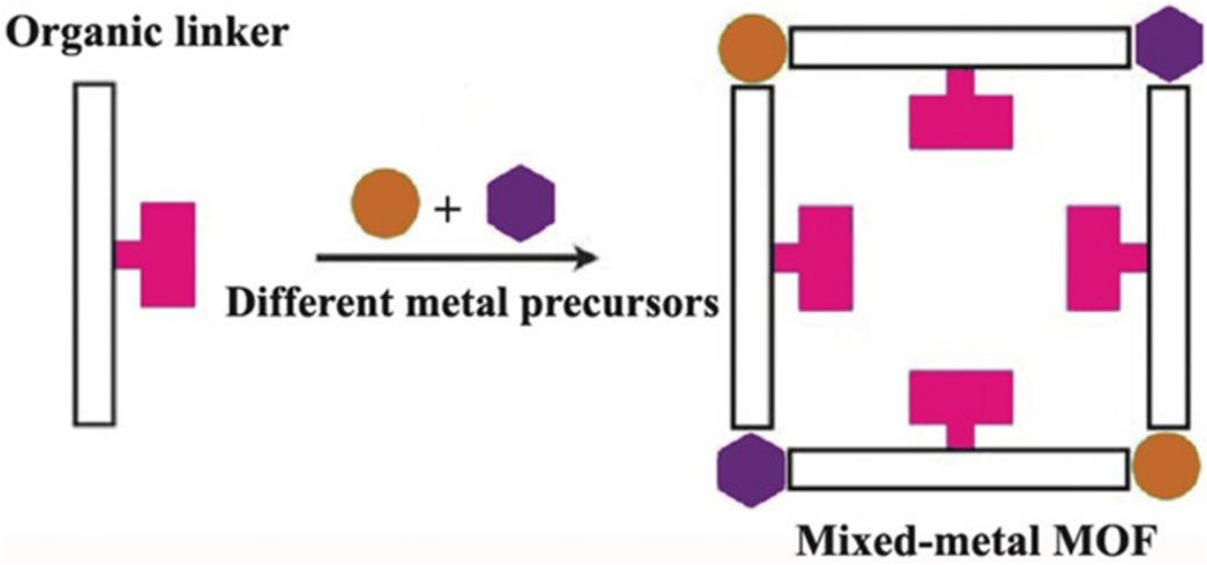

Figure 4.1: Direct methods of MM -MOFs synthesis using two metals.

A typical example of MM-MOF was MOF-74 which showcased the successful preparation and incorporation of ten different metal atoms into a single framework, MOF74-M (M= any metal) constructed by Yaghi and co-workers.[19] In this chapter we report a similar approach in Yaghi's study[14] it was observed that the solvent used for the reaction posed only a minor influence on the cations when compared to the temperature, which increases the nucleation process and crystal growth in MOF synthesis. Although the MM-MOF study mostly involved two metal ions mixing to form a bimetallic MOF, Yaghi demonstrated that up to 10 metals could be incorporated into MOF74-M (M= any metal). The application of such systems for sensing and drug delivery was extensively studied and shown to be better when compared to their single-metal systems counterpart. The scanning electron microscopy (SEM)/EDX mapping revealed an inhomogeneous metal distribution because of the difference in the crystal growth rate of the mixed MOF-74 materials.

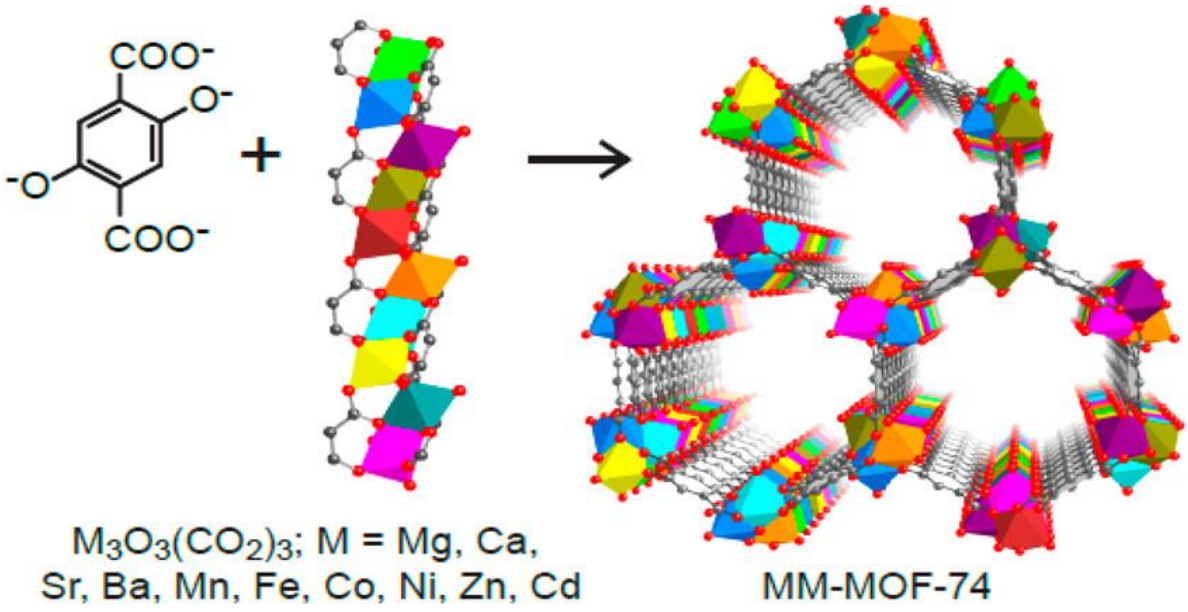

Figure 4.2: MOF 74-M (M= any metal) material consisting of ten different mix-metals within the same framework structure.

4.1.2. Aim

The work described in this chapter aimed to synthesize mix-metal naphthalene diimide MOFs based on lanthanide metal clusters and to characterize the systems using PXRD, EDX, and other spectroscopic techniques to understand the interaction of those clusters with the nicotinic acid NDI DNNDI.

4.2. Result and Discussion

The procedure employed for the synthesis of MM-MOF is very similar to the single metal MOF discussed in Chapter Three. Different lanthanide metal cations (La, Gd, and Lu) were employed for the crystallization of NDI-based MOF in a suitable solvent and heated for 24 h at 100 ° C in a sigmacoted vial. The resulting crystals were characterized by the PXRD, TGA, and SEM/EDX to determine the porosity, thermal stability, and the presence, size, and position of

metals in the system. Crystals obtained from MM-MOF are generally of poorer quality when compared to crystals of single metal synthesis reported in chapter three.

4.2.1. PXRD of Mix-Metal MOFs

The powder X-ray diffraction pattern of the MM-MOFs was studied to identify the crystalline phases present in the sample and determine their relative proportion. Figure 4.3 presents the PXRD of the MM-MOF system containing lanthanum, gadolinium, and lutetium. The fact that crystals of the mixed metal MOF look quite tiny when compared to the single metal MOFs, their peak patterns of MM-MOF are similar with distinct peaks at angle 4.1 as can be seen below.

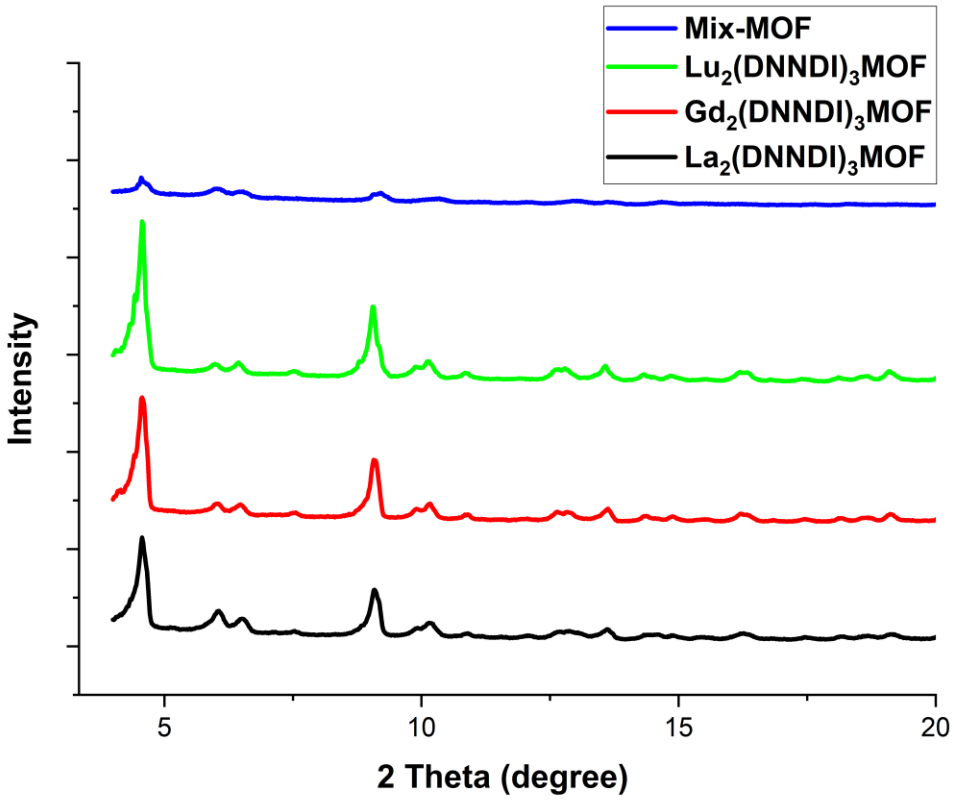

Figure 4.3: Power Diffraction Pattern of single lanthanide MOFs and Mixed Metal MOFs with lanthanum, gadolinium and lutetium – $M_2(DNNDI)_3$ (M = La, Gd, Lu).

4.2.2: SEM-EDX Mapping of Mix-Metal MOF

The formation of MOF systems can also be studied using SEM-EDX mapping which allows us to spatially resolve the distribution of different elements within the sample and provide information on the elemental composition and distribution within the mixed MOF. Figure 4.4 shows the SEM-EDX of mixed MOF systems containing lanthanum, gadolinium, and lutetium cations. At a specific peak relative to the counts for each element, a peak was observed for the lanthanum, gadolinium and lutetium metals which signifies the formation of MOF with the mentioned clusters.

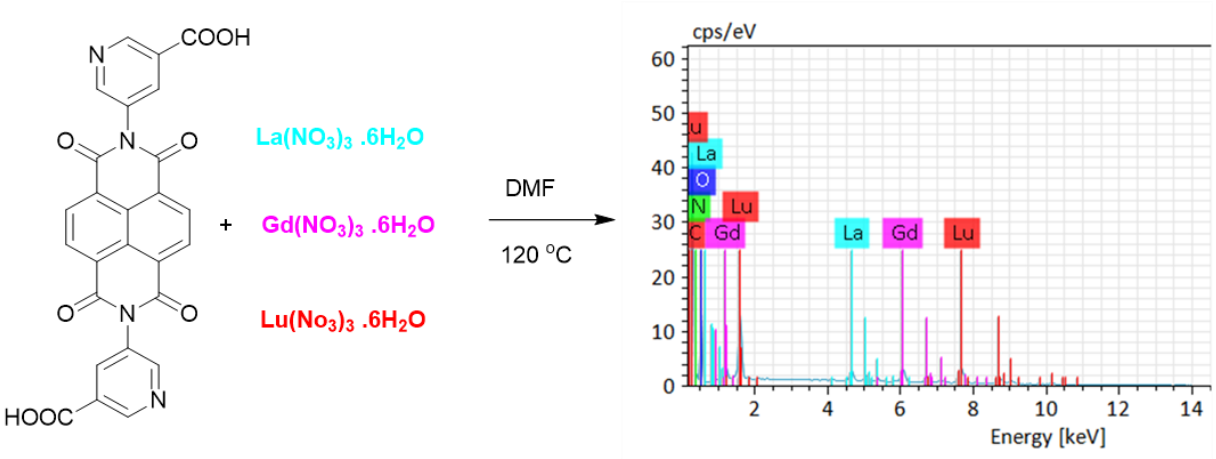

Figure 4.4: SEM-EDX mapping for mixed metal MOF containing lanthanum, gadolinium, and lutetium clusters, $M_2(DNNDI)_3$ (M = La, Gd, Lu).

It should come as no surprise that the ionic radius of the metal cation determines the metal ratio in the mixed MOFs. Therefore, the ratio of the above mixed MOF is in the order of Lu>Gd>La with specific ratio as 11.56 Lu, 5.52 Gd and 3.08 La, see appendix V table for EDX ratio for mixed MOF. Similarly, there is no correlation between the unit cell parameters of the single as-synthesized lanthanoid MOF discussed in chapter two and the metal content of the mixed MOFs.

4.2.3. Thermal Gravimetric Analysis of mix-metal MOF

For a MM-MOF, TGA/DTA provides valuable information about its thermal stability, decomposition temperatures, and the composition of the material. Figure 4.4 shows a similar stability with a single metal MOF described in chapter three. The material was stable up to 500°C.

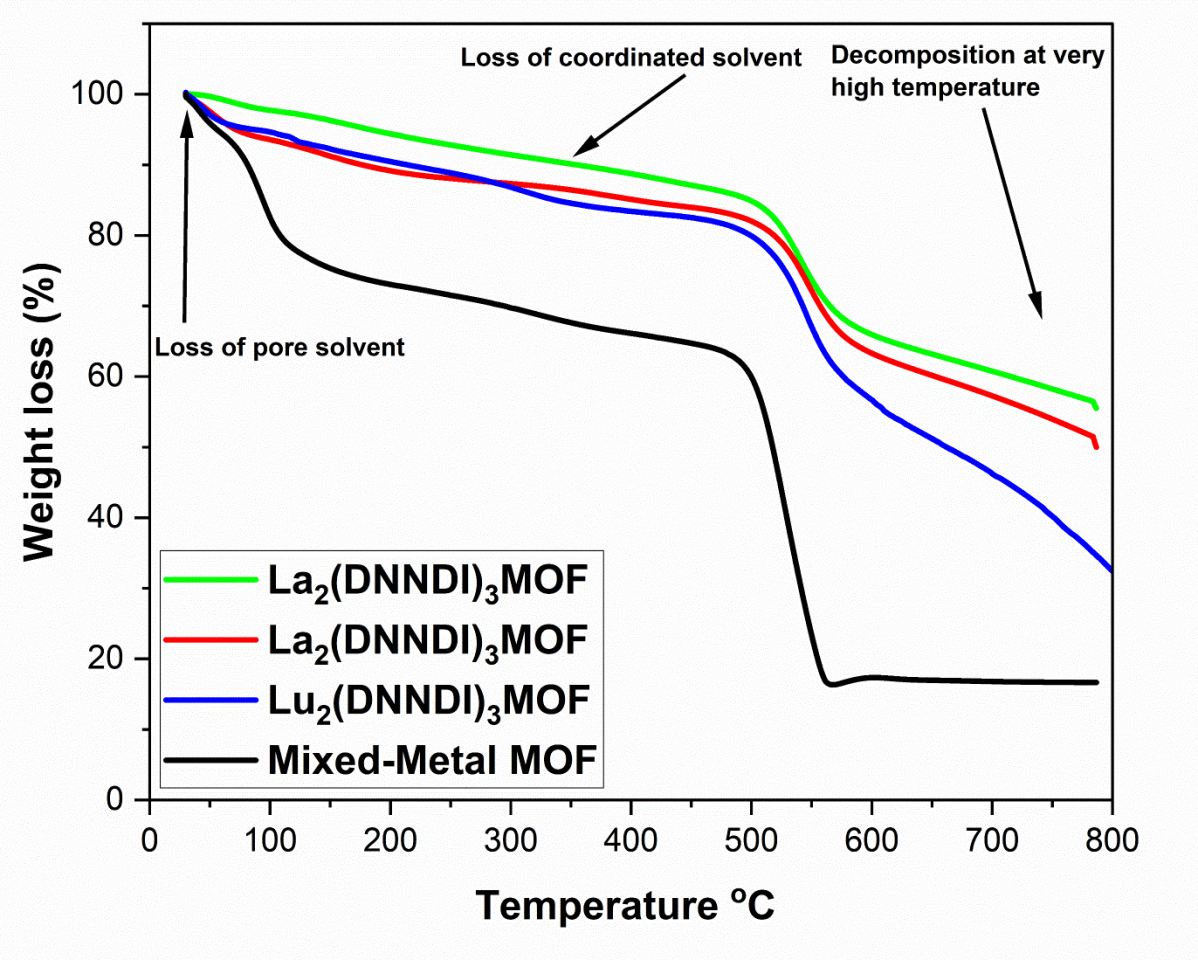

Figure 4.5: shows the thermal stability of single and mixed-metal lanthanide MOFs with lanthanum, gadolinium and lutetium metals, $M_2(DNNDI)_3$ (M = La, Gd, Lu).

4.2.4 UV-Vis of MM-MOF

The solid-state UV-visible spectroscopy of MM-MOFs can be used to ascertain the optical properties of the material. A sample of MM-MOF $M_2(DNNDI)_3$ (M = La, Gd, Lu) was studied by solid-state UV-visible spectroscopy and the spectrum is shown in Figure 4.5. As with the single metal MOF discussed in chapter three, the mixed metal MOF exhibits similar optical properties.

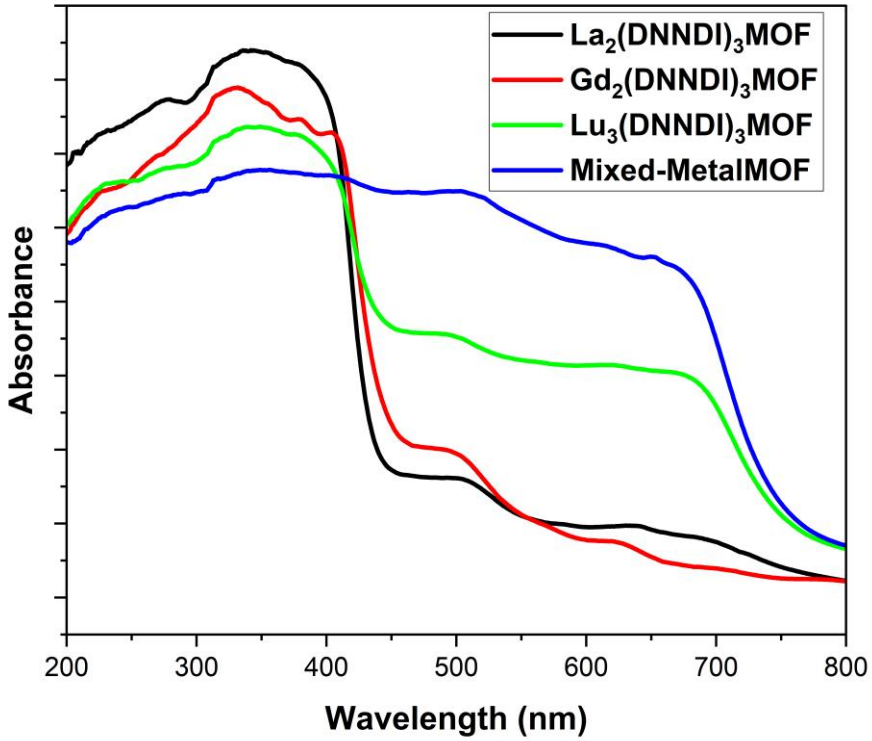

Figure 4.5: shows the UV-visible spectra for the single lanthanide MOFs and the mixed Metal MOF with lanthanum, gadolinium and lutetium metals, $M_2(DNNDI)_3$ (M = La, Gd, Lu).

4.3 Conclusion

Mixed metal MOF represents a rapidly evolving research area with tremendous potential for advancing materials science and technology. In this study, we demonstrated the potential for lanthanide to form mixed MOFs, with ratios following the ionic radius of the metal cations. The smaller metals tend to crystallise into the MOF faster than the bigger ones across the period. Scanning electron microscopy (SEM/EDX) mapping also revealed that there was an inhomogeneous metal distribution in the framework.

4.4 Material and Method

4.4.1 Synthesis of Mixed Metal MOF

To a 25 mL sigmacoted scintillation vial containing 7.5 mg (0.017 mmol) of $La(NO_3)_3.6H_2O$, 6 mg (0.016 mmol) of $Gd(NO_3)_3.6H_2O$, 6 mg (0.017 mmol) of $Lu_2(NO_3)_3$, and 17 mg (0.034 mmol) of DNNDI, 2.5 mL DMF was added and sonicated for five minutes until all reactants completely dissolved to form a solution. The vial was tightly capped and transferred into an oven at 100 ^oC for 24 hours. The resulting solid was a colourless crystalline material suitable for PXRD, SEM/EDX, and solid-state UV-visible. Samples were washed with fresh DMF prior to analysis**.**

4.5 General Conclusion

This work underscores the adaptability of DNNDI-based ligands in forming robust lanthanide MOFs with uncoordinated functional groups, enabling diverse post-synthetic modifications. The structural versatility and functional potential of DNNDI-based lanthanide MOFs, demonstrated through host-guest chemistry and mixed-metal frameworks, highlight their

promise in advancing MOF applications. The combination of robust structural motifs, uncoordinated functional groups, and mixed-metal adaptability invites future work into designing materials for sustainable energy applications, precision catalysis, molecular sensing technologies, gas adsorption, optoelectronic devices and the development of smart materials with responsive properties.

4.6 References

1 S. Abednatanzi, P. Gohari Derakhshandeh, H. Depauw, F.-X. Coudert, H. Vrielinck, P. Van Der Voort and K. Leus, *Chem Soc Rev*, 2019, **48**, 2535–2565.

2 D. Shi, C.-J. Cui, M. Hu, A.-H. Ren, L.-B. Song, C.-S. Liu and M. Du, *J Mater Chem C Mater*, 2019, **7**, 10211–10217.

3 H. Dong, X. Zhang, X.-C. Yan, Y.-X. Wang, X. Sun, G. Zhang, Y. Feng and F.-M. Zhang, *ACS Appl Mater Interfaces*, 2019, **11**, 45080–45086.

4 M. Y. Masoomi, A. Morsali, A. Dhakshinamoorthy and H. Garcia, *Angewandte Chemie International Edition*, 2019, **58**, 15188–15205.

5 S. A. Ahmed, D. Bagchi, H. A. Katouah, Md. N. Hasan, H. M. Altass and S. K. Pal, *Sci Rep*, 2019, **9**, 19372.

6 M. Li, G. Zhang, A. Boakye, H. Chai, L. Qu and X. Zhang, *Front Bioeng Biotechnol*. 2921, 2296-4185

7 W. Gao, H. T. Ngo, Z. Niu, W. Zhang, Y. Pan, Z. Yang, V. R. Bhethanabotla, B. Joseph, B. Aguila and S. Ma, *ChemSusChem*, 2020, **13**, 6273–6277.

8 A. Alkaş, J. Cornelio and S. G. Telfer, *Chem Asian J*, 2019, **14**, 1167–1174.

9 C. Castillo-Blas and F. Gándara, *Isr. J. Chem*, 2018, **58**, 1036–1043.

10 M. Zhu, H. Chen, H. Li, H. Zhang, L. Liu, Q. Hong, Z. Yao, L. Wang and Z. Zhang, *Inorg Chem Front*, 2024, **11**, 4432–4438.

11 R. Abazari, S. Sanati, N. Li and J. Qian, *Inorg Chem*, 2023, **62**, 18680–18688.

12 Y. Wang, G. Ning and D. Li, *Chemistry – A Eur. J.*, 2024, **30**, 202400360.

13 C. López-García, S. Canossa, J. Hadermann, G. Gorni, F. E. Oropeza, V. A. de la Peña O'Shea, M. Iglesias, M. Angeles Monge, E. Gutiérrez-Puebla and F. Gándara, *J Am Chem Soc*, 2022, **144**, 16262–16266.

14 S. Yuan, J.-S. Qin, J. Li, L. Huang, L. Feng, Y. Fang, C. Lollar, J. Pang, L. Zhang, D. Sun, A. Alsalme, T. Cagin and H.-C. Zhou, *Nat Commun*, 2018, **9**, 808.

15 A. Dhakshinamoorthy, A. M. Asiri and H. Garcia, *Catal Sci Technol*, 2016, **6**, 5238–5261.

16 R. Jaryal, R. Kumar and S. Khullar, *Coord Chem Rev*, 2022, **464**, 214542.

17 Z. Gao, L. Liang, X. Zhang, P. Xu and J. Sun, *ACS Appl Mater Interfaces*, 2021, **13**, 61334–61345.

18 X. Xu, L. Gao and S. Yuan, *Dalton Transactions*, 2023, **52**, 15233–15252.

19 L. J. Wang, H. Deng, H. Furukawa, F. Gándara, K. E. Cordova, D. Peri and O. M. Yaghi, *Inorg Chem*, 2014, **53**, 5881–5883.

Chapter five

5.0 Material and method

5.1 Reagent and purification

All reagents and chemicals were purchased from Alfa Aesar, Fisher Scientific, Sigma-Aldrich, or VWR international and used in their original, unaltered state without any additional modifications or preparation. Glassware was flame-dried under vacuum and backfilled with dinitrogen.

5.2 General Equipment

5.2.1 Nuclear Magnetic Resonance Spectroscopy (NMR)

Bruker AVANCE NEO 400 MHz spectrometer was used to obtain NMR spectra, which were normalized to residual solvent signals unless otherwise stated. Deuterated solvents were used as indicated.

5.2.2 Thermogravimetric Analysis (TGA)

The thermal gravimetric experiments were conducted on PerkinElmer TGA8000. The samples were heated from ambient temperature to 1000°C under the influence of N_2 at a rate of 10°C/min.

5.2.3 Infrared spectroscopy (IR)

Using an Agilent Fourier Transform Spectrometer, FTIR-8400S, equipped with a Diamond ATR unit, infrared spectra of solids were recorded.

5.2.4 Single crystal X-ray diffractometry (SCXD)

Single crystal data collection was carried out on an ROD, Synergy Custom system, HyPix diffractometer. The crystals were mounted in Fomblin oil and kept at 293(2) K or 100(2) K, and using monochromated (Cu Kα) irradiation (λ = 1.54178 Å).

5.2.5 Powder X-ray crystallography

All powder X-ray data were collected at room temperature using Bruker D8 diffractometer which was equipped with Cu K_α (1.5444 Å) radiation or the Panalytical Empyrean equipped with Cu Kα radiation (λ = 1.5444 Å) operating at 40 kV and 40 mA and on a diffracted-beam graphite monochromator and in the 2θ range from 3 to 50° with a step size of 0.02°.

5.2.6 UV-Vis spectroscopy

UV-vis reflection spectra were recorded on a Cary 50 UV/Vis spectrometer. For analysis, the solid samples were positioned between two quartz slides and the wavelength range for recording the absorption spectra was 200 to 1000 nm.

5.2.7 Scanning Electron Microscopy (SEM)

ZEIST EVO 15 scanning electron microscopy (SEM) coupled with Bruker EDX was used to conduct the morphology studies of all the gold-coated samples using a back-scattered electron detector (BSE) detector.

Chapter six

6.0 Appendix

Appendix I: PXRD data for ten lanthanide MOFs

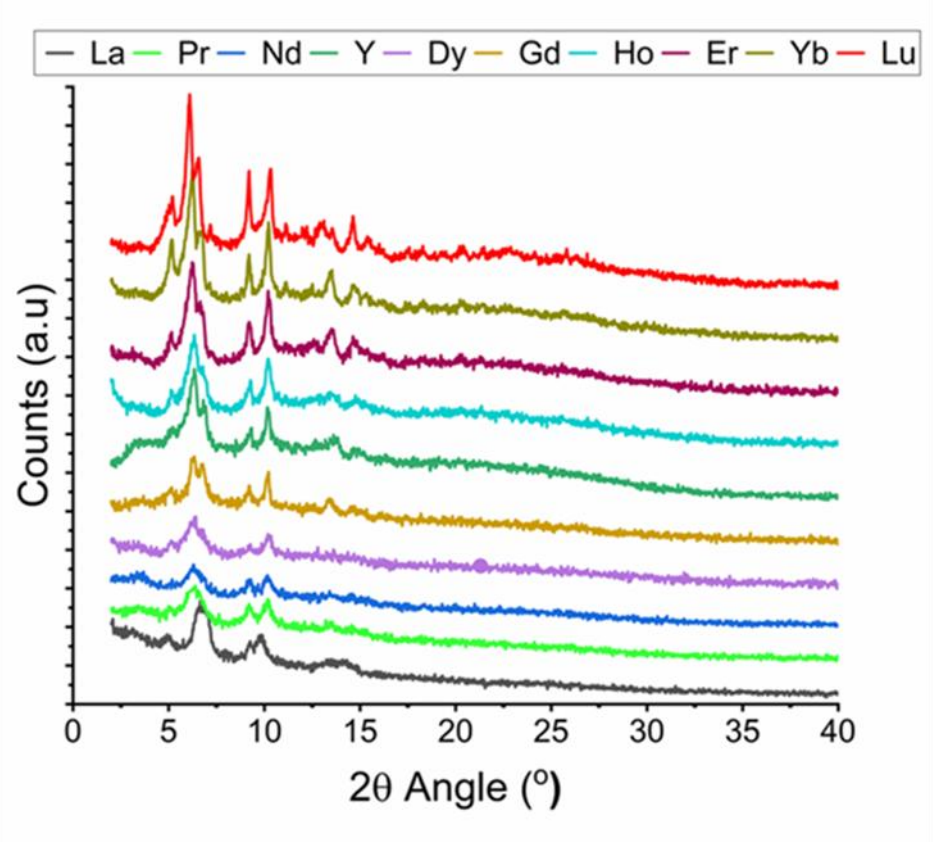

Appendix II: Crystal data for $Sm_2(DNNDNI)_3$ MOF

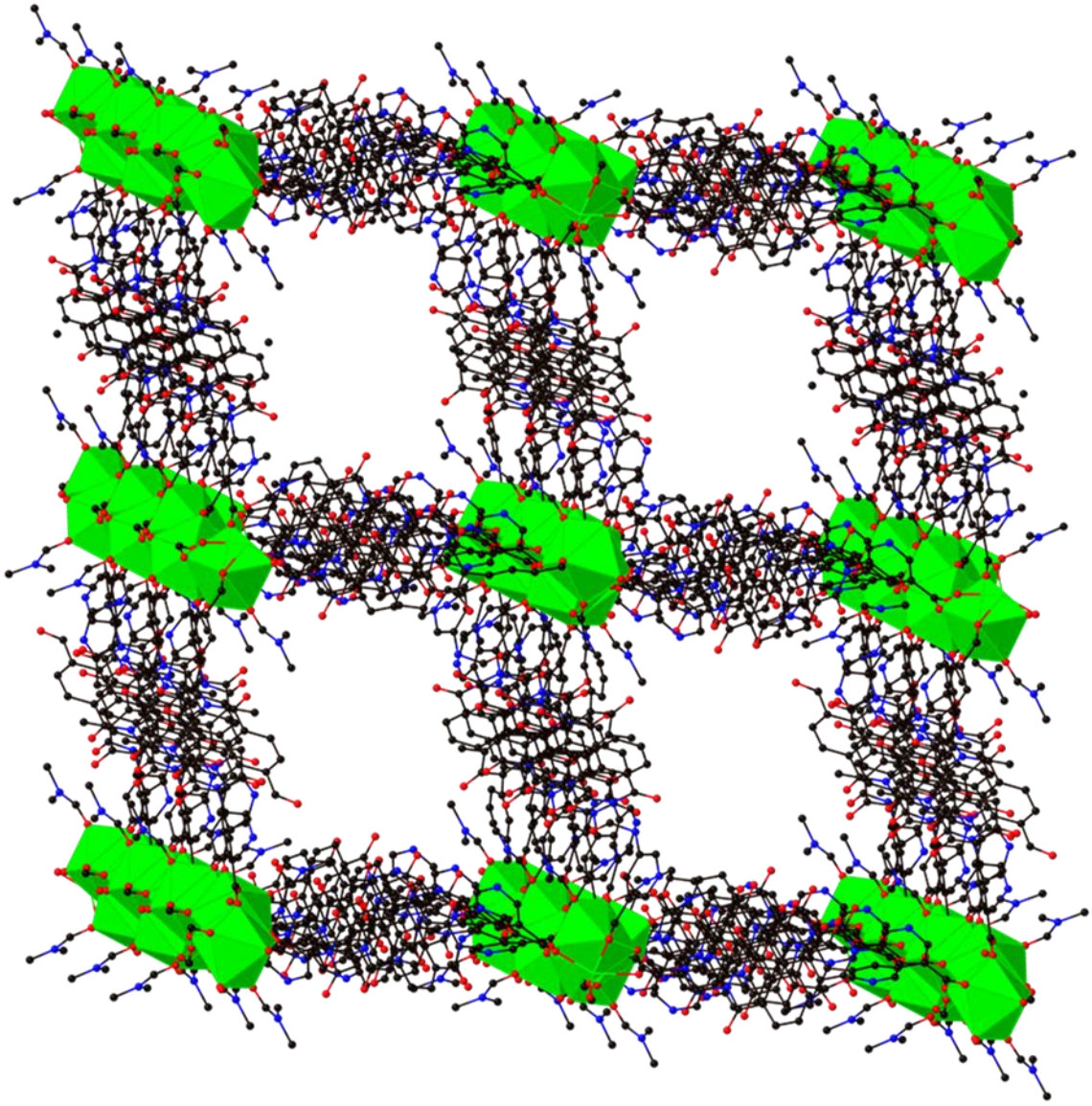

Appendix III: TGA data for five lanthanide MOFs

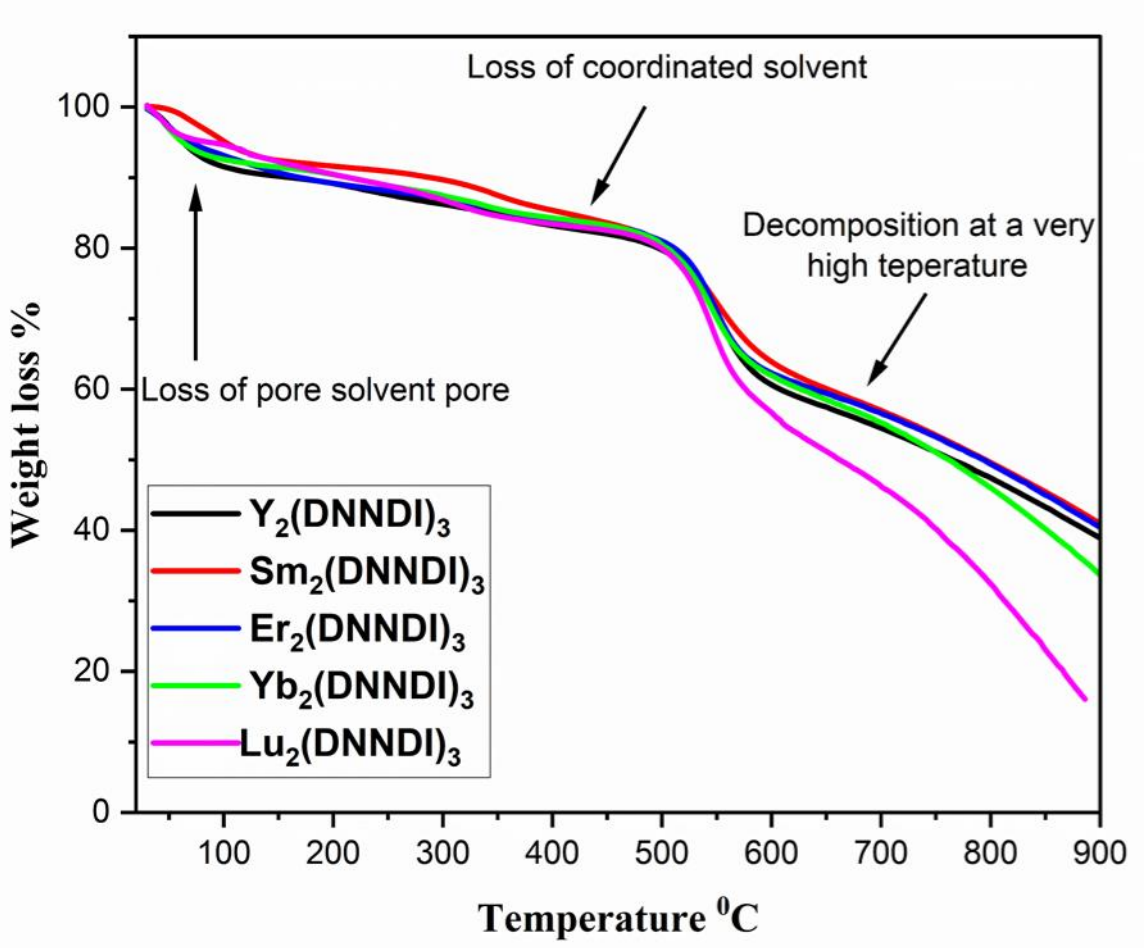

Appendix IV: EDX Metal ratio for mixed MOF

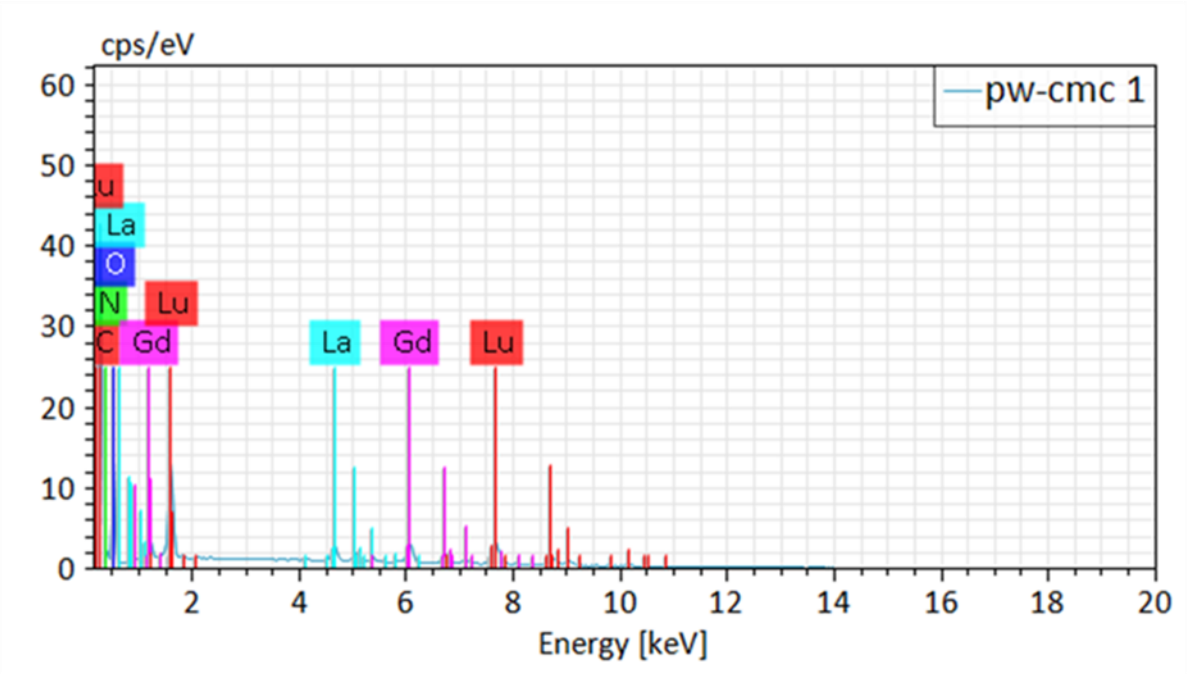

Spectrum	Carbon	Nitrogen	Oxygen	Lanthanum	Gadolinium	Lutetium	Sum
pw-cmc 1	40.30	8.22	18.74	3.08	5.52	11.56	87.43

Appendix V: BET data for three lanthanide MOFs

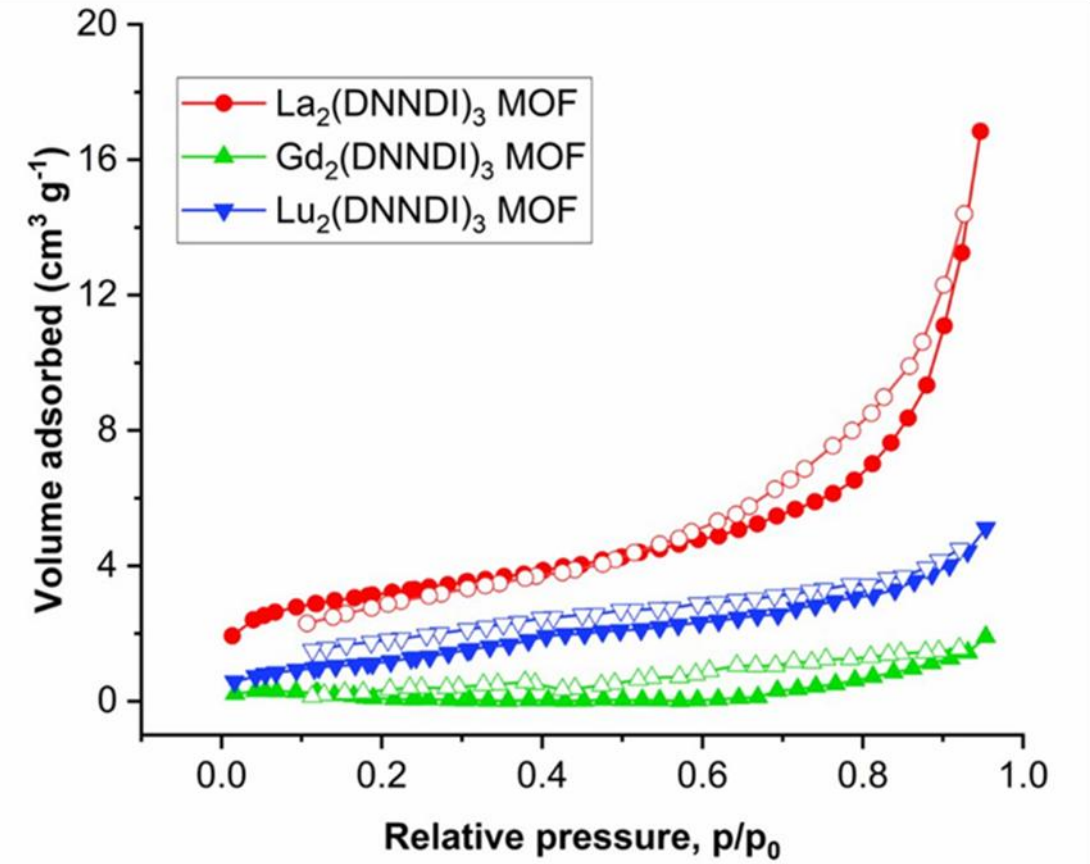

Appendix VI: Crystal data for $Yb_2(DNNDI)_3$ MOF